Molecular and metabolic determinants of metastasis development and progression

DISSERTATION

zur Erlangung des akademishen Grades

Doctor rerum naturalium

(Dr. rer. nat.)

eingereicht an der Lebenswissenschaftlichen Fakultät der Humboldt-Universität zu Berlin

von

MSc Molecular Biosciences Inna Zaimenko

Präsident der Humboldt-Universität zu Berlin

Prof. Dr.-Ing. Dr. Sabine Kunst

Dekan der Lebenswissenschaftlichen Fakultät

Prof. Bernhard Grimm

Gutachter: 1. Prof. Dr. Ulrike Stein

2. Prof. Dr. Claus Scheidereit

3. Dr. Matthias König

Tag der mündlichen Prüfung: 19 March, 2018

Erklärung über die selbstständige Abfassung meiner Dissertation

Hiermit erkläre ich, Inna Zaimenko, Matrikel-Nr: 571543, dass ich die vorliegende Dissertation selbstständig und ohne Benutzung anderer als der angegebenen Hilfsmittel angefertigt habe.
Die aus fremden Quellen direkt oder indirekt übernommenen Gedanken sind als solche kenntlich gemacht.
Die Dissertation wurde bisher in gleicher oder ähnlicher Form keiner anderen Prüfungsbehörde vorgelegt oder veröffentlicht.

Berlin, den……

Unterschrift ……

This study was conducted at the Max-Delbrück-Centrum for Molecular Medicine Berlin-Buch in the research group of Prof. Dr. Ulrike Stein.

INDEX OF CONTENTS

ABBREVIATIONS

5-FU	5-fluorouracil
28S	28S ribosomal RNA
^{18}F-FDG	^{18}F-fluorodeoxyglucose
^{18}F-Gln	^{18}F-(2S,4R)4-fluoroglutamine
^{18}F-Glu	^{18}F-fluoroglutamate
AA	Antimycin A
AJCC	American Joint Commission on Cancer
AMPK	AMP-activated protein kinase
ANOVA	Analysis of variance
Ap1	Activator protein 1
APC	Adenomatous-polyposis-coli
ATCC	American Type Culture Collection
ATP	Adenosine triphosphate
BAX	Bcl-2-associated X protein
BRAF	B-Raf Proto-Oncogene
CDC4	Cell division control protein 4
cEBP	CCAAT/enhancer binding proteins
CIMP	CpG island methylator phenotype
CIN	chromosomal instability
cPEPCK	Cytoplasmic phosphoenolpyruvate carboxykinase
CRC	Colorectal cancer
CT	Computer tomography
CV	Cross-validation
DACHS	Darmkrebs: Chancen der Verhütung durch Screening; Colorectal cancer: chances for prevention through screening
DCC	Deleted in colorectal carcinoma
DMEM	Dulbecco's Modified Eagle's medium
DMSO	Dimethylsulfoxide
DNA	Deoxyribonucleic acid
dNTP	Deoxynucleosidetriphosphate
DON	6-Diazo-5-oxo-L-norleucine
DT	Decision tree
ECAR	Extracellular acidification rate
EGFR	Epidermal growth factor receptor
ERK	Extracellular-signal Regulated Kinase
FACS	Fluorescence-activated cell sorting
FASN	Fatty acid synthase
FBP	fructose-1,6-bisphosphate
FBS	Fetal bovine serum
FCCP	Cyanide-4-(trifluoromethoxy)phenylhydrazone
FDG	^{18}F-fluorodeoxyglucose
FITC	Fluorescein isothiocyanate
FSC	Forward scatter
G6PD	Glucose-6-phosphate-dehydrogenase
GC/LC-MS	Gas/liquid chromatography coupled to mass spectrometry

GDP	Guanosine diphosphate
GLS	Glutaminase
GLUD	Glutamate dehydrogenase
GLUT	Glucose transporter
GOT	Glutamic-oxaloacetic transaminase
GTP	Guanosine triphosphate
GTPase	GTP hydrolase
HER2	Human epidermal growth factor receptor 2
HGF	Hepatocyte growth factor
HIF-1	Hypoxia-inducible factor 1
HK	Hexokinase
HRP	Horseradish Peroxidase
IDH	Isocitrate dehydrogenase
IGF2R	Insulin-like growth factor 2 receptor
KRAS	Kirsten rat sarcoma viral oncogene homolog
LDH	Lactate dehydrogenase
LOH	Loss-of-heterozygosity
mABs	Monoclonal antibodies
MACC1	Metastasis-associated in colon cancer 1
MCT	Monocarboxylate transporter
MDH	Malate dehydrogenase
ME	Malic enzyme
MEK	Mitogen-activated protein kinase kinase
MET	Hepatocyte growth factor receptor
MET	Metachronously metastasized
MFI	Median fluorescence intensity
MLH1	MutL Homolog 1
MMR	Mismatch repair
MOPS	3-(N-Morpholino)propansulfone acid
MRI	Magnetic resonance imaging
MSH	MutS Homolog
MSI	Microsatellite instability
mTOR	Mammalian target of rapamycin
MTT	3-(4,5-Dimethylthiazol-2-yl)-2,5-Diphenyltetrazolium Bromide
MuLV	Moloney murine leukemia virus
MUTYH	MutY Homolog
NADPH	Nicotinamide adenine dinucleotide phosphate
NEAA	Non-essential amino acids
NHE1	Na(+) /H(+) exchanger-1
NON	Non-metastasized
NRAS	Neuroblastoma RAS viral oncogene homolog
OCR	Oxygen consumption rate
Oligo	Oligomycin
OXPHOS	Oxidative phosphorylation
PC	Pyruvate carboxylase
PDK	Pyruvate dehydrogenase kinase
PEG	Polyethylene glycol
PEP	phosphoenolpyruvate
PFA	Paraformaldehyde

PFKFB2	6-phosphofructo-2-kinase/fructose 2, 6 bisphosphatase
PI3K	Phosphoinositide 3-kinase
PKM2	Pyruvate kinase isoform M2
PMS2	PMS1 homolog 2
RIPA	Radioimmunoprecipitation assay buffer
RNA	Ribonucleic acid
ROS	Reactive oxygen species
Rot	Rotenone
RPMI	Roswell Park Memorial Institute
SASH	SAM And SH3 domain containing
SDS-PAGE	Sodium dodecyl sulfate polyacrylamide gel electrophoresis
SEM	Standard error of mean
SLC2A	Solute carrier family 2 member
SMAD4	SMAD family member 4
SNPs	single nucleotide polymorphisms
Sp1	Specificity Protein 1
SSC	Side scatter
STR	short tandem repeat
SVM	Support vector machine
TCA	Tricarboxylic acid
TGFBR2	Transforming Growth Factor Beta Receptor 2
TGFβ	Transforming Growth Factor Beta 1
TNM	Tumor Lymph nodes Metastasis
TP53	Tumor Protein P53
TXNIP	Thioredoxin Interacting Protein
UICC	Union for International Cancer Control
VEGF	Vascular endothelial growth factor
VHL	Von Hippel-Lindau protein
Wnt	Wingless-type

ABSTRACT

MACC1, a master regulator of metastasis, is involved in most hallmarks of cancer, including deregulated metabolism. Yet, fragmentary data on its role in cancer metabolism exist. Here, a systematic analysis of MACC1-driven metabolic networks by elucidation of cell nutrient preferences, environment dependent alterations of nutrient utilization, metabolic pathway functionality and metabolic tracing using ^{13}C-labeled metabolic substrates had been performed. In this context, the impact of MACC1 to the utilization of glucose, glutamine, pyruvate, lactate and palmitate was investigated. MACC1 was found to support context-dependently utilization of glucose, glutamine and pyruvate through their increased depletion or altered distribution within metabolic pathways. In particular, with respect to glucose, MACC1 enhanced surface GLUT1 thus leading to increased glucose depletion, glucose flux and hence increased cell proliferation. With respect to glutamine, MACC1 enhanced glutamine depletion in nutrient depleted conditions and reduced glutamine flux independent of nutrient availability. With respect to pyruvate, MACC1 enhanced pyruvate depletion in glucose depleted conditions, while having minor effects on pyruvate flux. In xenograft tumor model of colorectal cancer (CRC) MACC1 had proven to increase the uptake of ^{18}F-FDG and ^{18}F-glutamate *in vivo*. Taken together, these results demonstrate that MACC1 is a novel regulator of cancer metabolism, and its targeting will affect metabolic pathways thus leading to homeostatic imbalance and reduced cell survival.

Metastasis is the main cause of death from CRC. Fifteen to twenty percent of stage II CRC patients develop metastasis during the course of disease. Chemotherapy treatment is effective in metastasis prevention, but clinical criteria of likely benefitting patients remain imprecise. To assess the potential of plasma metabolites to serve as biomarkers for stratification of stage II CRC patients according to metastasis risk metabolic profiles of non-metastasized and metachronously metastasized stage II CRC patients were retrospectively compared. To identify metabolic biomarkers distinguishing non-metastasized from metachronously metastasized stage II CRC patients robust supervised classifications using decision trees and support vector machines were performed. Metabolic profiles were found to be distinct between non-metastasized vs metachronously metastasized stage II CRC patients. Classification models from decision trees and support vector machines with 10-fold cross-validation gave average accuracy of 0.75 and 0.82, respectively, correctly predicting metachronous metastasis in stage II CRC patients. Importantly, a low number of metabolites was generally sufficient to achieve this accuracy.

Together, these results demonstrate that plasma metabolites have the potential to non-invasively stratify stage II CRC patients according to their metastasis risk.

ZUSAMMENFASSUNG

MACC1, ein Hauptregulator von Metastasen, ist an zahlreichen Kennzeichen von Krebs beteiligt, einschließlich dereguliertem Metabolismus. Dennoch ist seine Rolle im Krebsstoffwechsel unklar. In der vorliegenden Arbeit wurde eine systematische Analyse von MACC1-getriebenen metabolischen Netzwerken durch Aufklärung von Zellnährstoffpräferenzen, kontextabhängigen Veränderungen der Nährstoffverwendung, Stoffwechselfunktionalität, metabolisches Tracing mit ^{13}C-markierten metabolischen Substraten und *in vivo* Studien durchgeführt. In diesem Kontext wurde die Beziehung von MACC1 zur Verwendung von Glukose, Glutamin, Pyruvat, Laktat und Palmitat untersucht. Es wurde gefunden, dass MACC1 die kontextabhängige Verwendung von Glucose, Glutamin und Pyruvat durch ihre verstärkte Anreicherung oder veränderte Verteilung innerhalb von Stoffwechselwegen unterstützt. In Bezug auf Glukose erhöhte MACC1 die GLUT1 auf Zellmembrane, was zu einer erhöhten Glukoseanreicherung, einem erhöhten Glukosefluss und somit zu einer erhöhten Zellproliferation führte. In Bezug auf Glutamin erhöhte MACC1 die Glutaminanreicherung in Nährstoffdeponierten Bedingungen und verringerte den Glutaminfluss unabhängig von der Nährstoffverfügbarkeit. In Bezug auf Pyruvat verstärkte MACC1 die Pyruvatanreicherung unter Glucose-limitierten Bedingungen, während es geringfügige Auswirkungen auf den Pyruvatfluss hatte. Im Xenograft Tumormodell hatte MACC1 nachweislich die Anreicherung von ^{18}F-FDG und ^{18}F-Glutamat *in vivo* erhöht. Zusammen zeigen diese Ergebnisse, dass MACC1 ein neuer Regulator des Krebsstoffwechsels ist und dass sein Targeting Stoffwechselwege beeinflussen wird, was zu einem homöostatischen Ungleichgewicht und einer verringerten Zellüberlebensrate führt.

Metastasen sind die Haupttodesursache bei Darmkrebs (CRC). Fünfzehn bis zwanzig Prozent der Patienten mit einem Stadium-II-CRC entwickeln im Verlauf der Erkrankung Metastasen. Die Chemotherapie ist wirksam bei der Prävention von Metastasen, aber die etablierten klinischen Kriterien sind zu ungenau, um die Wahrscheinlichkeit zu bestimmen, mit welcher die Patienten profitieren werden. Um das Potenzial von Plasmametaboliten als Biomarker für die Stratifizierung von Patienten im Stadium II nach metastasiertem Risiko zu bewerten, wurden metabolische Profile von Plasmaproben von nicht metastasierten und metachron metastasierten CRC-Patienten im Stadium II retrospektiv verglichen. Um metabolische Biomarker zu identifizieren, die nicht-metastasierten von metachronisch-metastasierten Stadiun II CRC Patienten unterscheiden, wurden robuste überwachte Klassifizierungen unter Verwendung von Entscheidungsbäumen und Support-Vektor-Maschinen durchgeführt.

Metabolische Profile unterschieden sich zwischen nicht-metastasierten und metachron-metastasierten Stadium II CRC Patienten. Klassifikationsmodelle aus Entscheidungsbäumen und Support-Vektor-Maschinen mit 10-facher Kreuzvalidierung ergaben eine durchschnittliche Genauigkeit von 0,75 beziehungsweise 0,82, die metachrone Metastasen bei Patienten im Stadium II CRC korrekt voraussagte. Wichtig ist, dass eine geringe Anzahl von Metaboliten im Allgemeinen ausreicht, um diese Genauigkeit zu erreichen. Zusammengenommen zeigen diese Ergebnisse, dass Plasmametaboliten das Potenzial haben, Patienten im Stadium II CRC gemäß ihrem Metastasenrisiko nicht-invasiv zu stratifizieren.

1. INTRODUCTION

1.1 Colorectal cancer: incidence and epidemiology

Colorectal cancer (CRC) is the third most common cancer in men and the second in women worldwide, accounting for about 1.4 million new cases and 700 000 deaths in 2012. Its incidence is higher in males than females (25% difference between sexes) with estimated rates of variability up to 10-fold worldwide. The highest incidence rate is observed in Australia and New Zealand, while the lowest incidence rate is in Western Africa. Mortality rate is the highest in Central and Eastern Europe and the lowest in Western Africa. In general, high incidence and mortality rates are attributed to more developed regions and are associated with "westernization" [1]. In Germany, as reported by German Cancer register database in 2012 there was more than 62.000 new CRC cases, including 25.000 deaths [2].

The risk factors to develop CRC are multiple, where most of them are associated with western lifestyle [3]. The most common risk factor is age. More than half of new CRC cases occur in subjects older than 70 years, and only 10 percent of CRC cases occur in subjects younger than age of 55. However, there is a trend of increased number of cases which occur in younger patients [4]. The other risk factors, besides age, include obesity, smoking, heavy alcohol consumption, type 2 diabetes, family history of CRC, genetical predisposition, inflammatory bowel disease such as Crohn's disease and ulcerative colitis [5]. Seventy percent of all CRC cases are preventable and can be modulated through healthy diet rich in fiber, cereals, by regular intake of fruits and vegetables, reduced consumption of red and processed meat, physical exercise and refuse from smoking. Interestingly, serum vitamin D3 concentration and aspirin intake show opposite correlation with risk of CRC development [6,7]. The rest thirty percent of CRC cases are sporadic or occur due to genetical predisposition.

1.2 Screening and diagnosis

In the last 10 years, the mortality rates due to cancer screening programs, removal of polyps, earlier diagnosis and availability of more effective therapies had been reduced on 20% [2,8]. The aim of the screening is to identify polyps or pre-cancerous lesions, which can be immediately removed, thus preventing further progression to CRC. At the age of 50-54 years it is recommended to perform yearly a diagnostics test on the presence of blood cells in the stool samples. From age of 55 years colonoscopy testing is recommended. During this check-up the colon polyps can be removed on-site. In case if no polyps was found the colonoscopy should be repeated in 10 years. As an alternative, subjects of age of 55 years and older can undergo blood testing in stool samples every 2 years, and in case of positive testing the colonoscopy can be performed [2].

Because colorectal cancer develops slowly over many years at early stages the disease is asymptomatic. The unspecific symptoms appear with disease progression and depend on a tumor location. They include general or localized abdominal pain, weight loss, weakness, iron deficiency and anemia. The CRC is diagnosed histologically from the tissue biopsy taken during endoscopy, which is the main diagnostics technique and which can be carried out either by sigmoidoscopy or total colonoscopy procedure. In case of cancerous lesions and depending on tumor clinico-pathological features further examination for the presence of metastases by magnetic resonance imaging (MRI) or computer tomography (CT) is recommended [6,8].

1.3 Staging and treatment

CRC is staged according to the American Joint Commission on Cancer (AJCC)/Union for International Cancer Control (UICC) TNM system. This includes staging according to depth of tumor invasion, regional lymph node involvement and presence of distance metastasis. Staging defines type and modality of prescribed treatment.

Stage 0 is characterized by intraepithelial carcinoma *in situ* or by invasion of *lamina propria.* The usual treatment involves local excision, polypectomy or segmentary en-bloc resection depending on the size of the lesion. At stages I and II submucosa and *muscularis propria* layers, respectively, are invaded. The treatment for both stage I and II tumors includes wide surgical resection and anastomosis without adjuvant chemotherapy. In case of high-risk stage II patients, who possess at least one of the poor clinico-pathological features such as lymph node sampling <12, pT4 tumor, poorly differentiated tumor, vascular or lymphatic or perineural invasion and tumor obstruction adjuvant chemotherapy is recommended. Stage III is characterized by tumor invasion through the *muscularis propria* into pericolorectal tissues. The standard treatment options are surgery and chemotherapy, where depending on patient state various combinations of 5-fluorouracil (5-FU) with other cytostatics like oxaliplatin, leucovorin, capecitabine and fluoropyrimidine [8] are prescribed. Stage IV is characterized by a spread of a primary tumor to distant organs with formation of metastatic masses. Here, the optimal treatment strategy should be discussed by a multidisciplinary expert team. Because the majority of stage IV patients are not suitable for resection combinational chemotherapy is applied to shrink the size of the lesions with the purpose of their further resection. In case of clearly unresectable metastatic CRC an optimal treatment strategy aimed at prolongation of survival, cure, improving tumor-related symptoms, stopping tumor progression and/or maintaining quality of life should be selected. The systemic treatment includes cytotoxic agents and biologicals, where the latter are subdivided on anti-VEGF, anti-EGFR or multikinase inhibitor agents [9].

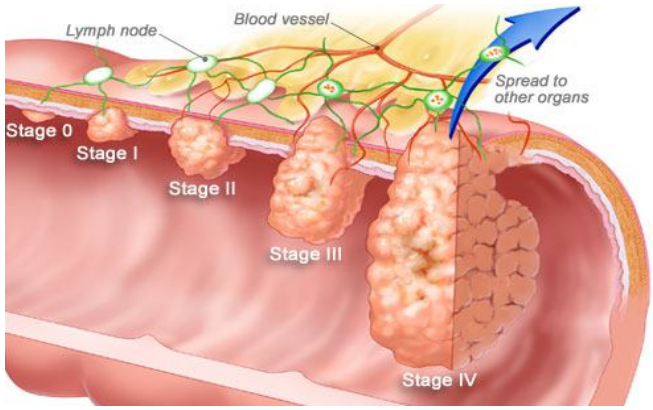

Fig. 1 Illustration of CRC stages with grade of tissue penetration. Stage 0 is intraepithelial carcinoma *in situ* or with invasion of *lamina propria*. Stage I tumors invade submucosa; stage II tumors invade *muscularis propria*; stage III tumors invade through the *muscularis propria* into pericolorectal tissues; and stage IV tumors invade to distant organs. Adopted from [10].

Prognosis and patient survival rate strongly depend on a stage of the disease. The 5-year survival rate for stages 0-I patients is 85-95%, for stage II patients – 60-80%, for stage III patients – 30-60%, while for stage IV patients – 10% only. The high variation in survival rate for stages II and III patients is mostly due to a difference in survival rates for substaged stages II and III such as stage IIA, IIB, IIC and stage IIIA, IIIB and IIIC [11].

1.4 Molecular pathogenesis

In CRC, most of the cases are sporadic while those which occur due to inherited mutations in cancer-related genes account only for 5-10%. There are several models of possible mechanisms for sporadic CRCs: adenoma-carcinoma sequence, chromosomal instability (CIN) and microsatellite instability (MSI).

Adenoma-carcinoma sequence was first proposed by Fearon and Vogelstein in their seminal work in which it was postulated that CRC occurs as a result of subsequent mutations in APC, KRAS, SMAD4 and TP53 genes, what transforms benign polyps into invasive carcinoma (Fig. 2) [12]. However, other investigators have described a different route of CRC development through serrated polyps [13]. Another proposed model of CRC carcinogenesis is chromosomal instability (CIN). The CIN pathway is more common and is found in around 65-70% of CRC patients. It is characterized by the presence of multiple structural and numerical abnormalities in chromosomes, leading to aneuploidy karyotype, loss-of-heterozygosity (LOH) at tumor suppressor loci and chromosomal rearrangements. The third model of sporadic CRCs is microsatellite instability (MSI). The MSI is present in 10-15% of sporadic CRC patients and is caused by dysfunction of MMR genes. MSI generally occurs due to aberrant promoter

hypermethylation of mismatch repair (MMR) genes (in sporadic CRCs) or mutation in MLH1, MSH2, MSH6 and PMS2 genes (in hereditary CRCs) [14]. Silencing of MSH1 gene is the most frequent in the majority of MSI-high (MSH-H) cases [15]. Besides three described above pathways of CRC carcinogenesis researchers distinguish also CpG island methylator phenotype (CIMP) characterized by a widespread CpG island methylation [16]. This phenotype is present in both CIN and sporadic MSI tumors, but is uncommon in Lynch syndrome patients [17].

Genetical predisposition to CRC is found in the minority of CRC patients and includes familial adenomatous polyposis coli and its variants (APC syndrome, 1%), Lynch-associated syndromes (hereditary non-polyposis colon cancer, 3-5%), Turcot-, Peutz-Jeghers- and MUTYH-associated polyposis syndromes [8].

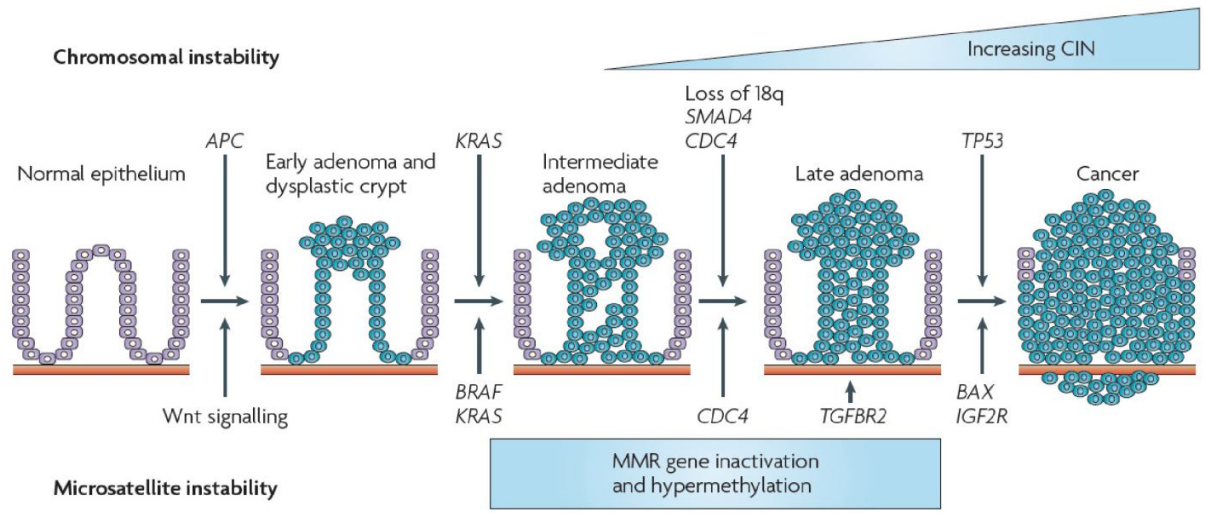

Fig. 2 Mechanisms of colorectal carcinogenesis. According to adenoma-carcinoma sequence, sequential mutations in APC, KRAS, SMAD4 and TP53 genes lead to transformation of normal colon epithelium to adenoma and cancer. Because APC is a crucial part of Wnt signaling, this pathway is thought to be involved in the initial step of carcinogenesis. Mutations in BRAF are mutually exclusive with KRAS, and either one or the other is present. According to chromosomal instability (CIN) model additional events which lead to cancer include loss of long arm of chromosome 18 (18q), mutations in CDC4. Microsatellite instability is caused by mismatch deficiency (MMR) due to promoter methylation or mutations in MMR genes. Positive selection of tumor cells occurs for mutations affecting TGFBR2, IGF2R and BAX genes. Adapted from [18].

1.5 Prognostic and predictive markers

Prognostic marker is a marker which informs about patient potential survival rate. Predictive marker informs whether patient will benefit from certain treatment option. In general, multiple prognostic and predictive markers had been reported for CRC, however only few of them are in clinical use.

1.5.1 KRAS

KRAS is a GTPase which acts downstream of EGFR receptor-tyrosine kinase in RAS/RAF/MEK/ERK kinase cascade, and regulates processes of cell proliferation, growth, apoptosis and metastasis. Mutations in KRAS exon 2 (codons 12 and 13) and in exon 3 (codon 61) had been reported to be associated with poor outcome [19]. Mutations in described above codons lead to constitutive KRAS activation because of inability of GTPase activating proteins to effect the inactivating hydrolysis of GTP to GDP bound to RAS. This gene is mutated in 30-50% of CRC cases [20] and has stronger impact on prognosis in distal compared to proximal CRC [21]. KRAS is one of the best established markers used in the clinics for patient prognosis. It is also a predictive marker in treatment with anti-EGFR mABs like cetuximab or panitumumab. Owing to convergence of EGFR and KRAS pathways KRAS mutated tumors are significantly less responsive to anti-EGFR therapy compared to KRAS wild type tumors [22,23]. There is evidence that in case if KRAS mutational status is negative, NRAS mutations at exons 2, 3 and 4 have to be tested, because mutations in NRAS had been also reported to predict anti-EGFR treatment failure [24,25].

1.5.2 BRAF

BRAF is a serine-threonine kinase acting downstream of KRAS and is found to be mutated (V600E) in around 8% of CRC cases [26]. In CRC, BRAF mutation is mutually exclusive with KRAS or NRAS mutations. Due to pathway convergence BRAF V600E mutation predicts unresponsiveness to anti-EGFR treatment, thus being a predictive marker to EGFR-specific therapies [24]. In a metastatic setting BRAF V600E mutation is associated with poorer prognosis compared to BRAF wild type tumors [27–30]. In contrast to melanoma [31] BRAF V600E mutation in CRC is associated with resistance to anti-BRAF therapy with vemurafenib [32]. This resistance is caused by EGFR activation when BRAF is inhibited. Therefore, clinical trials investigating combinations of BRAF inhibitors with EGFR or MEK were initialized [33]. In a recent study, combination of BRAF inhibition together with MEK/ERK inhibitors had been reported to have a modest activity in metastatic CRC patients [34].

1.5.3 Microsatellite instability (MSI)

MSI is widely used in the clinics to predict CRC patient prognosis and to stratify stage II patients for chemotherapy treatment [8]. Classification of tumors on MSI-high (MSI-H) or MSI-low (MSI-L) is based on

altered size of nucleotide repeats such as BAT25, BAT26, D2S123, D5S346 and D17S250. These nucleotide repeat sequences constitute so called Bethesda panel [35,36]. MSH-H is defined if at least two out of five microsatellite markers are instable [18]. MSI-H patients have better prognosis compared to MSI-L patients and are less likely to benefit from chemotherapy treatment [37,38]. Because inactivation of MMR genes results in accumulation of DNA replication errors this leads to formation of aberrant peptides. The presence of aberrant peptides, in turn, promotes immune response and is associated with increased number of tumor infiltrating lymphocytes, thus explaining better prognosis in patients bearing MSH-H CRC tumors [39–41].

1.5.4 MACC1

MACC1 acts as a transcription factor, which binds MET promoter thereby enhancing MET transcription and HGF-MET signaling [42]. Originally being discovered as a prognostic marker in CRC MACC1 had been shown to have a prognostic value in multiple cancers, including gastrointestinal [43], breast [44], non-small cell lung [45], glioma [46], ovarian [47], cervical [48], renal cell [49], Klatskin [50] and renal pelvis [51] cancers. In CRC, single nucleotide polymorphisms (SNPs) in the coding region of MACC1 had shown no improved prediction value for distant metastasis compared to MACC1 expression alone [52], while SNPs in non-coding region (G-allele of SNP rs1990172) was associated with decreased overall survival [53]. In HER2-positive breast cancer, G-allele of SNP rs1990172 was associated with increased risk for disease progression or patient death, T-allele of SNP rs975263 had an adverse effect on cancer prognosis, while rare C-allele of SNP rs3735615 showed a protective effect on event-free and overall survival [54].

Overall survival rate of MACC1 low stage I-III CRC patients is as high as 80%, whereas if patients are MACC1 high their survival rate drops to as low as 15% only [42]. MACC1 expression stratifies MSH-L patients according to disease recurrence, where MSH-L/MACC1-low tumors have similar favorable prognosis as MSI-H patients, and therefore have to be left untreated [55]. Combined analysis of MSI status, KRAS exon 2 and BRAF exon 15 mutations, gene expression analysis of osteopontin, SASH1 and MACC1 in stage II CRC patients revealed that MACC1 outperforms the other markers in prediction of distant metastasis [56]. Besides having a prognostic value MACC1 was demonstrated to be a predictive marker in several tumor entities. In gastric cancer, increased MACC1 expression is associated with resistance to trastuzumab, which is modulated by PI3K/Akt signaling [57]. In glioma and ovarian cancers, silencing of MACC1 was reported to increase sensitivity to cisplatin treatment [58–60]. In gastric cancer, MACC1 mediated sensitivity to 5-FU and cisplatin via increased MCT1 expression, whereas inhibition of monocarboxylate transporter 1 (MCT1) restored the sensitivity to chemotherapy [61].

1.5.5 Other markers: APC, β-catenin, TP53, 18q locus

Other genomic events are characteristic for CRC but they have lower prognostic value due to their frequent occurrence. These events include germline or somatic mutations in APC gene, its promoter hypermethylation, β-catenin overexpression, loss or mutations of p53 gene and loss of long arm of chromosome 18 (18q). Dysfunction/inactivation of APC gene or mutations in β-catenin lead to increased Wnt signaling. Changes in this pathway account for more than 90% of CRC cases [62] and, therefore, have no role in clinical practice. TP53 is a tumor suppressor and is either lost due to loss of heterozygosity at chromosome 17p or mutated resulting in a dysfunctional protein with an abnormally long half-life [63,64]. P53 had been investigated as both prognostic and predictive marker, however in various studies the results are contradicting [65,66]. Loss of 18q is the most common cytogenetic abnormality in CRC and is associated with poor prognosis [67]. In this region deleted in colorectal carcinoma (DCC) and SMAD4, a member of TGFβ signaling, are located. However, there is a discrepancy between studies, where not all of them found a clear link between 18q loss and SMAD4 expression [68], thus questioning the impact of genes located on 18q to patient prognosis.

1.6 Metabolism related functions of MACC1

MACC1 possesses multiple effects on metabolism of gastric and hepatocellular cancers. In these cancer types, it enhances the Warburg effect through increased expression of key glycolytic enzymes [69,70], and the increase in Warburg effect is associated with trastuzumab resistance due to enhanced PI3K/AKT signaling [57]. MACC1 expression had been shown to positively correlate with 6-phosphofructo-2-kinase/fructose 2, 6 bisphosphatase (PFKFB2) and with fatty acid synthase (FASN) in hepatocellular carcinoma [71] and in gastric cancer [72], respectively. There is evidence that MACC1 affects the expression of plasma membrane transporters such as Na(+) /H(+) exchanger-1 (NHE1) [73] and MCT1 [61].

1.7 Cancer metabolism

Cancer metabolism represents one of the most complex systems wired to satisfy ever growing cell demands for building blocks to enable continuous cell proliferation and at those times when nutrient supply becomes insufficient to ensure cell survival. Since the discovery by Otto Warburg that tumor metabolism is distinct from that of normal tissue [74,75] there is a growing number of publications uncovering metabolic substrate flexibility and bypass mechanisms which cancer cells use in order to overcome nutrient stress and to adapt to unfavorable environment [76–82].

Metabolism by definition is a sum of anabolism and catabolism [83], i.e. if biosynthetic reactions predominate over degradation reactions the object grows, if the degradation occurs faster than biosynthesis the object dies, and if the rate of degradation equals the rate of biosynthesis the object remains in stable conditions thus only surviving. Though this is a simplistic view, it well describes the net balance of incoming sources and outgoing results - cell propagation, death or survival. Hence, most of the studies about cancer metabolism are focused on elucidation which nutrients are preferred by cells in a context dependent manner and how those nutrients are used to produce new molecules like nucleic acids, proteins, carbohydrates and lipids to maintain cell propagation and survival.

The nutrient preferences of cancer cells are heterogeneous within a given tumor, its metastases, and between different tumor types. Depending on tumor tissue-of-origin, tumor microenvironment, mutational landscape and transcriptional profiles cancer cells prefer to burn particular metabolic substrates [84–87]. Therefore, studies of metabolic preferences of cancer cells represent a promising area of research, which can help developing a new generation of drugs able to restrict tumor growth. Below, detailed overview of nutrients and their downstream metabolic pathways utilized by cancer cells as well as impact of oncogenes on rewiring of metabolism (Fig. 3) will be described.

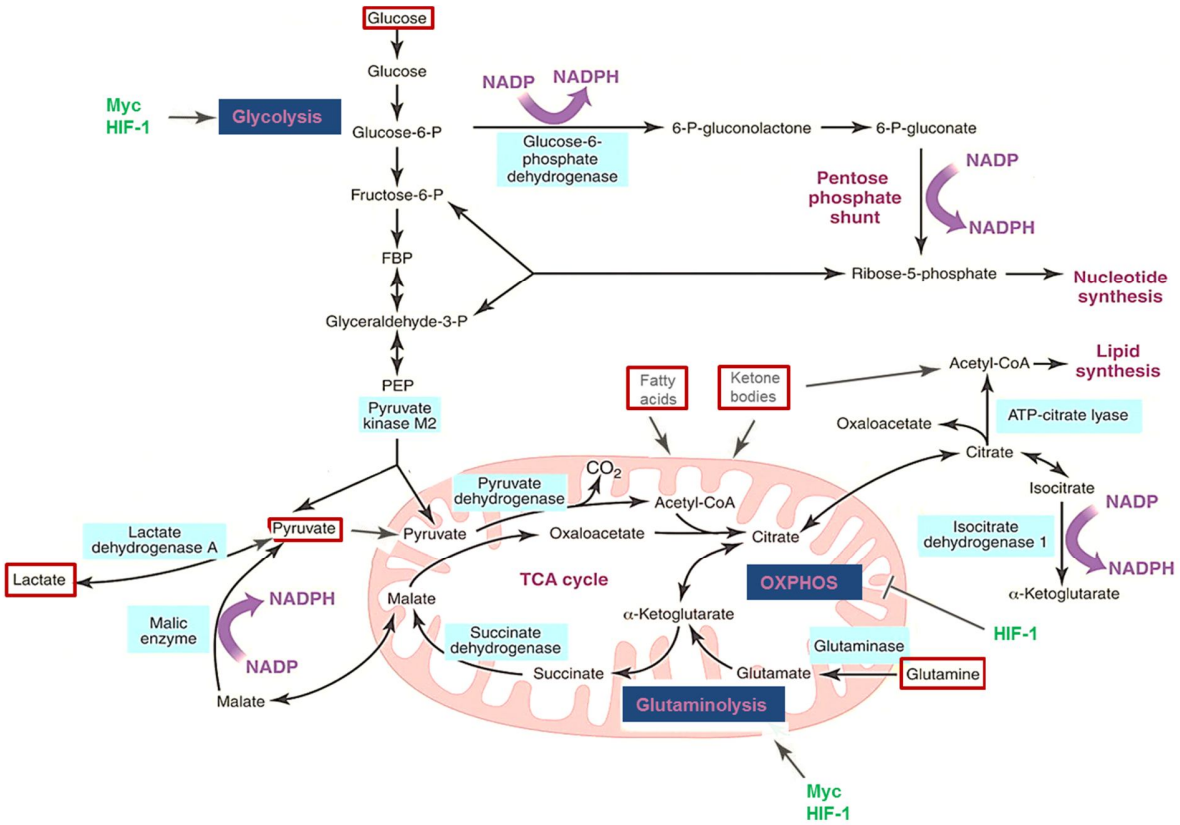

Fig.3 Scheme of cancer metabolic rewiring. In red boxes nutrients differentially used by cancer cells compared to normal cells are shown. Glucose undergoes glycolysis, providing glucose-6-phosphate as a substrate for pentose phosphate pathway, which generates riboses for nucleotide synthesis, and NADPH equivalents for redox maintenance. The last reaction of glycolysis produces pyruvate which is used in the TCA cycle and is converted to lactate. Upon glucose depletion lactate can be converted to pyruvate, thus feeding the TCA cycle. The use of citrate for lipid synthesis depletes its mitochondrial pool, which is reconstituted through glutamine derived α-ketoglutarate which can undergo both oxidative and reductive carboxylation, thus feeding the TCA cycle. Fatty acids undergo β-oxidation resulting in acetyl-CoA generation that is subsequently used in the TCA cycle. Ketone bodies serve as substrates for both TCA cycle and lipid synthesis. Myc and HIF-1 oncogenes induce glycolysis and glutaminolysis and HIF-1 in addition blocks OXPHOS. FBP: fructose-1,6-bisphosphate; PEP: phosphoenolpyruvate; NADP(H): nicotinamide adenine dinucleotide phosphate (hydrogen); OXPHOS: oxidative phosphorylation. Adopted from [88] with modifications.

1.7.1 Glucose

Glucose is the main nutrient to support cell proliferation, growth, survival, facilitate invasion and metastasis. There are 14 glucose transporters in the cells, out of which GLUT1, GLUT2, GLUT3 and GLUT4 are glucose-specific while the rest of transporters can also transport other sugars [89]. In normal untransformed cells, glucose is usually burned through oxidative phosphorylation in mitochondria, whereas in cancer cells it is preferably utilized through glycolysis irrespectively of oxygen availability, phenomenon called the Warburg effect. Burning of 1 molecule of glucose can produce in total 38 molecules of ATP, where 36 ATP molecules are derived from oxidative phosphorylation and 2 ATP molecules from glycolysis [83]. Despite low energy yield when burning glucose through glycolysis this pathway gives cancer cells several advantages. First, the rate of glucose metabolism through aerobic glycolysis is 10-100 times faster than complete glucose oxidation in mitochondria. This means that the increased speed of glucose utilization through glycolysis compared to oxidative phosphorylation provides cells flexibility to rapidly adapt to changed metabolic environment, giving thereby selective advantage when ATP production has to be rapidly tuned to support the energetic demands [90]. Second, rapid depletion of glucose from microenvironment by cancer cells limits its availability to tumor infiltrating lymphocytes, which require glucose for their expansion and effector functions, thus explaining their reduced ability to recognize and eliminate tumor cells [91]. Third, glycolysis provides important precursors for a pentose phosphate pathway such as glucose-6-phosphate out of which NADPH and riboses for nucleotide synthesis are generated. 3-phosphoglycerate is a precursor for synthesis of serine,

a non-essential amino acid important for one-carbon folate metabolism [92]. Fourth, acidification of surrounding microenvironment by lactate efflux facilitates extracellular matrix destruction, thus facilitating invasion and metastasis. One way to cope with decreased pH cancer cells evolved to express carbonic anhydrase IX, which neutralizes low pH by conversion of CO_2 and H_2O to HCO_3^- bicarbonate [93].

Pyruvate kinase isoform M2 (PKM2) is an important role in regulation of glycolysis. This enzyme catalyzes the last reaction of glycolysis (conversion of phosphoenolpyruvate to pyruvate) and slows down the entering of phosphoenolpyruvate to TCA cycle, thereby enabling synthesis of nucleotides, amino acids and lipids from glycolytic precursors [94].

Increased glucose uptake by cancer cells compared to normal cells had been a basis of tumor tissue imaging by ^{18}F-fluorodeoxyglucose (FDG) positron emission/computer tomography (PET/CT) [95]. However, FDG PET/CT is not always objectively detects tumor area due to variability in glucose transporters, nutrient availability and cancer cell nutrient preferences. So, in prostate [96,97], breast [98] and gastric [99] cancers FDG PET/CT fails to objectively determine either tumor mass or its spread.

The concentration of glucose in the blood is 4-6 mM [100], what is much lower than normally used in cell culture conditions. The concentration of glucose in ovarian tumor had been shown to be extremely low (0-1 mM) [101], meaning that its availability is either limited or it is rapidly converted into downstream metabolites. The scarceness of glucose and the leakiness of tumor blood vessels suggest that cancer cells have to find alternative metabolic fuels to sustain proliferation and survival. Such alternative metabolic fuels reported to be used in increased rates by cancer cells compared to normal cells include glutamine, lactate, pyruvate, fatty acids and ketone bodies [82].

1.7.2 Glutamine

Glutamine is the second most important nutrient used by cancer cells to maintain cell homeostasis. Glutamine can be delivered to cancer cells by blood supply, be derived from nearby muscle tissue by its destruction releasing in addition other amino acids [102], be *de novo* synthesized by cancer cells [103] or by stromal cells such as fibroblasts [77]. Glutamine once uptaken is converted to glutamate, a reaction which is catalyzed by glutaminase with a release of ammonia. Glutamate is a precursor for glutathione synthesis, an important ROS scavenger, and it undergoes conversion to α-ketoglutarate by glutamate dehydrogenase. Glutamate, besides, can be used as an exchange shuttle in reactions of conversion of pyruvate to alanine or oxaloacetate to aspartate. Both reactions are important, one for extracellular acidification (alanine production and its release into environment) and the other for regeneration of NADH equivalents (malate-aspartate shuttle). Glutamate derived α-ketoglutarate immediately enters

TCA cycle, where it can undergo both reductive or oxidative carboxylation and thus be used for fatty acid synthesis from citrate precursor or be used down into TCA cycle. Depending on cell transcriptional landscape glutamate can be *de novo* synthesized in cells from precursors such as α-ketoglutarate and aspartate together with other non-essential amino acids [84,104]. Utilization of glutamine by cancer cells allows to overcome temporary glucose restriction and to maintain ROS scavenging, thus supporting cell survival.

Glutamine is one of the most abundant amino acids in the blood whose concentration in human tumors ranges from 0.5 mM to 1 mM [105,106]. In patients with advanced-stage cancers blood glutamine levels are increased [107], hinting that glutamine is actively used by tumor cells. ^{18}F-(2S,4R)4-fluoroglutamine (^{18}F-Gln) and ^{18}F-glutamate (^{18}F-Glu) PET/CT are informative in visualizing glutamine avid cancers, including glioma [108]. ^{18}F-Gln has been used for assessment of the glutamine pool in breast [109] and lung [110] cancers, and for prediction of response to BRAF inhibitors in colon cancer [111].

1.7.3 Lactate

Lactate initially thought to be a waste product of glycolysis is now considered to be a metabolic substrate utilized by glucose deprived cancer cells to satisfy their energy demands. Indeed, the concentration of lactate within tumors ranges within 5-10 mM [112,113], while glucose concentrations are extremely low (0-1 mM), supporting the idea of lactate utilization by cancer cells. There is an emerging concept of so called metabolic symbiosis, according to which cells exposed to favorable glucose rich environment run glycolysis and produce lactate, which is exported and uptaken by nearby starving cells which will burn it through oxidative phosphorylation. There is evidence that resistance to anti-angiogenic therapies is mediated by metabolic symbiosis, whereas its disruption by e.g. glycolysis inhibitors enhances the efficacy of anti-angiogenic drugs [114,115]. In breast cancer, lactate had been shown to support cell proliferation in glucose low and glucose depleted conditions being utilized through TCA cycle [116].

Besides acidification and nutrient functions lactate triggers inflammatory response resulting in the release of cytokines which promote tumor progression [117]. Increased lactate concentration is associated with metastasis and short overall survival of cancer patients [118,119]. Lactate is also a substrate for alanine and glutamate production. As demonstrated by ^{14}C labeled lactate its uptake seems to occur specifically in regions rich on oxygen or having active mitochondrial metabolism [120]. The key determinants in lactate shuttling are monocarboxylate transporters (MCTs) – MCT4, which exports lactate from glycolytic cells, and MCT1 and MCT2, which are responsible for lactate uptake [121].

1.7.4 Pyruvate

Pyruvate is another alternative metabolic fuel used by cancer cells. It can be generated through glycolysis or be imported from microenvironment. Pyruvate can be utilized through two pathways – gluconeogenesis or oxidative phosphorylation. Similarly to lactate, pyruvate is imported through MCT1 and MCT2 transporters [121]. In breast cancer pyruvate-mediated increase in mitochondrial metabolism had been shown to correlate with increased cell proliferation and tumor aggressiveness [78]. The presence of pyruvate in cancer cell microenvironment is associated with resistance to metformin treatment *in vitro* [122]. Interestingly, inhibition of MCT1 in glycolytic breast cancer cells which co-express MCT1 and MCT4 leads to decreased pyruvate but not lactate export, suggesting that besides lactate glycolytic cells also export pyruvate, thereby feeding starving nearby cells [123].

1.7.5 Fatty acids and ketone bodies

Fatty acids are substrates for mitochondrial oxidation and contribute to energy generation under glucose low or glucose depleted conditions. However, some cancer cells preferably utilize fatty acids even in nutrient rich environment [124]. The production of ATP from 1 molecule of fatty acid is 2.5 times higher than from complete glucose oxidation. Fatty acid derived acetyl-CoA is a substrate for generation of TCA cycle intermediates, which are further used in oxidative phosphorylation [83]. Cancer cells derive fatty acids through two mechanisms: autophagy or self-eating and through adjacent non-cancerous cells, like adipocytes for example [125,126]. It had been shown that co-culture of ovarian cancer cells with adipocytes leads to direct transfer of lipids from adipocytes to cancer cells promoting tumor growth *in vitro* and *in vivo* [80]. This suggests that adipocyte-derived fatty acids act as an energy source to maintain cancer cell activity.

Ketone bodies, which include acetate, β-hydroxybutyrate and acetoacetate, are another source of energy for cancer cells. Hypoxia and nutrient stress had been shown to increase dependence of cells on ketone bodies consumption [79]. Autophagy and gut microbiota are two sources of ketone bodies generation. Altered gut microbiota as a result of Western diet or the use of antibiotics had been suggested as a contributing factor to the increased incidence of colon cancer [127,128]. Acetate is an important energy source in human tumors, especially in glioblastoma and prostate cancer [129,130]. The ^{11}C-acetate radioactive tracer, which informs about the state of lipid membrane metabolism and *de novo* fatty acid biosynthesis has been widely used to image prostate cancer [131].

1.8 Impact of oncogenes on metabolic reprograming

1.8.1 Myc

Myc is a master transcription factor that controls 15% of the human genome and is deregulated in many cancer types. Quantitative analysis of Myc target expression and function in a system where Myc was temporally and physiologically regulated revealed that Myc is not an on-off specifier of gene activity, but acts universally at active genes as a non-linear amplifier of their expression [132]. However, regulation of cell growth by Myc requires coordinate expression of growth involved genes in addition to ensuring sufficient number of ribosomes to maintain efficient protein translation [133]. Myc stimulates virtually all glycolytic genes as well as those involved in glutamine metabolism both at transcriptional and posttranslational levels [134,135]. Myc had been shown to mediate increased synthesis of nucleotides and lipids through enhanced uptake of glucose and glutamine [136,137], which serve as precursors for most molecules in a cell. In addition, Myc overexpressing cells show enhanced one-carbon metabolism and mitochondrial biogenesis [138–140]. Its high protein expression is associated with tumor aggressiveness and poor survival in cancer patients [141,142].

1.8.2 HIF-1

HIF-1 is a transcription factor, which consists of HIF-1α and HIF-1β subunits. HIF-1β subunit is constantly expressed while HIFα under normoxic conditions is hydroxylated what inhibits its transactivation and targets for proteasomal degradation mediated by von Hippel-Lindau protein (VHL) complex. Under hypoxia, the HIFα subunit is stabilized and accumulates in the nucleus where it binds to HIF-1β, thus allowing activation of transcriptional target genes [143]. In mammalian cells, there are three types of alpha subunit - HIF-1α, HIF-2α and HIF-3α [144–146]. Each of the alpha subunits differs in transcriptional target genes. HIF-1α regulates the activation of glycolytic genes and inhibits genes involved in oxidative phosphorylation [147], thus controlling the switch from mitochondrial respiration to anaerobic glycolysis under hypoxic conditions. It had been shown that by activation of HIF-1 under hypoxia renal cells almost exclusively relied on reductive carboxylation of glutamine-derived α-ketoglutarate for *de novo* lipogenesis [148]. This suggests that HIF-1 controls glutaminolysis under hypoxic conditions. HIF-2α induces the expression of genes involved in angiogenesis and maintenance of stem cell property [149]. HIF-3α possesses distinct characteristics from HIF-1α and HIF-2α, and acts as a negative regulator of HIF-1α [150]. The best studied hypoxia-induced transcription factor is HIF-1, however its role in the tumors is controversial: in some cells it acts as an oncogene being expressed in multiple tumors, whereas some reports have demonstrated that it can act as a tumor suppressor and its role in the cells is context-specific [151–153].

2. AIM OF THE STUDY

MACC1, initially identified as a prognostic marker and a transcription factor in CRC, had been proven to be a master regulator of metastasis in multiple tumor entities. Its increased expression is associated with most of the hallmarks of cancer, including deregulated cancer metabolism. In gastric cancer and hepatocellular carcinoma MACC1 had been shown to enhance the Warburg effect, however its role in metabolism of CRC remains unknown.

For stage II CRC patients multiple treatment options are available, including by observation only, participation in clinical trials or prescription of adjuvant chemotherapy regimens. Identification of high-risk for metastasis stage II CRC patients would allow to treat them with chemotherapy earlier, thereby restricting metachronous metastasis and improving patient outcome. To approach the central goal of tailored stage II CRC patient stratification for metastasis risk, it was hypothesized that metabolic features of a localized tumor that will not metastasize are different from those of an equally localized tumor prone to develop distant metastasis, and that these changes can be detected non-invasively in a liquid blood biopsy.

This thesis consists of two projects:

I. Elucidation of MACC1 role in CRC metabolism.
II. Identification of metabolic prognostic biomarkers for metachronous metastasis formation in the plasma of stage II CRC patients.

The aims of the first project were:

1. To identify MACC1-dependent metabolic processes *in vitro* with particular focus on context-dependent nutrient utilization. This included investigation of MACC1-dependent metabolic processes with respect to glucose, glutamine, pyruvate, lactate and palmitate metabolic substrates.
2. To investigate MACC1-dependent flux *in vitro* by application of stable isotope labeled metabolic substrates.
3. To confirm *in vitro* findings in mouse model system *in vivo*.

The aims of the second project were:

1. To retrospectively analyze plasma metabolic profiles of non-metastasized vs metachronously metastasized stage II CRC patients on the subject of identification of potential prognostic markers able to distinguish the analyzed groups.
2. To find a metabolic signature distinguishing non-metastasized from metachronously metastasized stage II CRC patients and to build a classifier which can predict formation of distant metachronous metastases.

3. MATERIALS AND METHODS

PROJECT I: Elucidation of MACC1 role in CRC metabolism

3.1 Cell culture

All used human CRC cell lines were from American Type Culture Collection (ATCC). The list of used cell lines is shown in Table 3.1. Cell culture reagents including cell culture media, phosphate-buffered saline (PBS) and Trypsin/EDTA were obtained from Life Technologies. Cell culture plastic ware was obtained from TPP, BD Biosciences or Greiner BioOne. SW620, HCT116, HT29, HCT15 were grown in Dulbecco's Modified Eagle Medium (DMEM) no glucose, no glutamine, no phenol red (Gibco) supplemented with 10 mM glucose (Sigma), 2 mM glutamine (Gibco) and 10% fetal bovine serum (Bio&Sell). SW480 were grown in Roswell Park Memorial Institute-1640 (RPMI-1640 from Gibco) supplemented with 10% fetal bovine serum (Bio&Sell). All cell lines were maintained in a humidified incubator at 37°C with 5% carbon dioxide. Cells were splitted at 1:8 ratio every 3-4 days. All cell lines were regularly tested for mycoplasma using MycoAlert® Mycoplasma detection kit (Lonza) and were maintained mycoplasma-free. Authentication of the cell lines was performed by short tandem repeat (STR) genotyping at the Leibniz-Institute DSMZ (Braunschweig, Germany). The STR genotypes were in accordance with published genotypes for used cell lines.

Table 3.1 CRC cell lines used in this study

Cell line	ATCC number
SW620	CCL-227
SW480	CCL-228
HCT116	CCL-247
HCT15	CCL-225
HT29	HTB-38

3.2 Derivative cell lines

SW620 cells with stable knockdown of MACC1 were obtained by transduction with lentiviral vectors expressing shcntl (SW620 shcntl) or shMACC1 (SW620 shMACC1) constructs as described in [42].

HCT116 cells with stable knockdown of MACC1 were obtained by transfection with plasmid expressing shcntl (HCT116 shcntl) or shMACC1 (HCT116 shMACC1) construct as described in [154]. SW480 cells overexpressing MACC1 were obtained by transfection with plasmid expressing empty vector (SW480 ev) or MACC1 construct (SW480 MACC1). SW620 cells with MACC1 knockdown and luciferase co-expression were obtained by 2-step transfection: first, cells were transfected with the firefly luciferase reporter vector generating SW620/luc cells and second, with plasmids expressing shcntl or shMACC1 constructs generating SW620/luc shcntl and SW620/luc shMACC1 cells as described in [155].

3.3 Promoter activity

To measure activity of MACC1 wild type (MACC1 wt) promoter construct and of MACC1 promoter construct with mutated binding sites for Sp1 (Sp1 mut), Ap1 (Ap1 mut) and cEBP (cEBP1 mut) transcription factors HCT116 cells were transfected with corresponding constructs as described in [156]. Briefly, HCT116 cells were seeded at density $7*10^4$ cells/well on a 24-well plate with complete DMEM no glucose, no glutamine, no phenol red (Gibco) supplemented with 10 mM glucose (Sigma), 2mM glutamine (Gibco) and 10% FBS (Bio&Sell) in duplicates. Twelve hours after cell seeding cells were washed with PBS and medium was changed on DMEM supplemented with 0 mM glucose, 2 mM glucose or 10 mM glucose (Sigma), respectively, and 10% FBS (Bio&Sell). Twelve hours later cells were transfected with 500 ng of corresponding firefly construct (MACC1 wt, Sp1 mut, Ap1 mut, cEBP mut or empty vector) together with 50 ng of Renilla construct using TransIT-2020 transfection reagent (MirusBio). Fourty eight hours after cell transfection cells were analyzed by dual luciferase reporter assay system (Promega). Briefly, cells were lysed with 100 µL passive lysis buffer and shaked gently at room temperature for 15 minutes. 100 µL luciferase assay reagent followed by 20 µL of cell lysate was added to a white 96-well plate. The plate was mixed briefly and the luminescence was measured with plate reader (Tecan infinite 200 PRO). The firefly luciferase values were normalized by Renilla values which accounted for variation in cell seeding number and transfection efficiency.

3.4 RNA isolation and reverse transcription

RNA was isolated from cells using Roboklon RNA extraction kit (Roboklon) according to manufacturer's protocol. The RNA was quantified using NanoDrop1000 spectrophotometer (PEQLAB). For cDNA synthesis 1 µg of total RNA was used. The reaction was performed in total volume of 20 µL. The reaction mixture contained 1 µg of total RNA (up to 4 µL), 4 µL 25 mM $MgCl_2$ (Roche), 1 µL 50 µM hexamer random primer (Applied Biosystems) and 4 µL 10 mM dNTP mix (Applied Biosystems). RNA and hexamer random primer were denatured at 65°C for 5 minutes. Then, 2 µL 10x PCR buffer II (Applied Biosystems), 1 µL 200 U/µL RNase inhibitor (Applied Biosystems) and 4 µL 50U/µL MuLV reverse transcriptase

(Applied Biosystems) were added to the denatured RNA mixture. The parameters of cDNA synthesis were as follows: 25°C for 5 minutes, 50°C for 50 minutes, 95°C for 5 minutes and 4°C for cooling. The synthesized cDNA was stored at -20°C.

3.5 Quantitative polymerase chain reaction (qPCR)

For qPCR 10 ng of cDNA was used. The cDNA template was amplified with specific primers in total volume of 20 µL. All primers, except for MACC1 and human microsatellite DNA, were pre-designed KiCqStart® SYBR® Green Primers (Sigma). The primers for MACC1 and human microsatellite DNA were synthesized by BioTeZ. Primer characteristics, including sequences and final concentrations used in the reaction are listed in Table 3.2. GoTag® qPCR Master Mix (Promega), which included all reaction components except cDNA, primers and water was used. Parameters of amplification were as follows: pre-incubation at 95°C for 3 minutes; amplification: denaturation at 95°C for 30 seconds, annealing at 60°C for 30 seconds, extension at 72°C for 30 seconds repeated for 40 cycles; cooling at 40°C for 30 seconds. For amplification of 28S rRNA the parameters were same as above except annealing at 67°C. Each reaction was analyzed in duplicates. Water blank was used as a negative control. All mRNA expression values for genes of interest were normalized by 28S rRNA and analyzed by $2^{-\Delta\Delta CT}$ method.

Table 3.2 Primers used in this study

Name	Sequence	Working concentration	Company
MACC1 fw1	TTCTTT TGATTC CTCCGGTGA	0.5 µM	BioTeZ
MACC1 rw1	ACTCTGATGGGCATGTGCTG	0.5 µM	BioTeZ
SLC2A1 fw1	ACCTCAAATTTCATTGTGGG	0.4 µM	Sigma
SLC2A1 rw1	GAAGATGAAGAACAGAACCAG	0.4 µM	Sigma
SLC2A2 fw1	ATGAGTGGGATGTTTGTTTG	0.4 µM	Sigma
SLC2A2 rw 1	TCCTTGACTGAAAAACTCAG	0.4 µM	Sigma
SLC2A3 fw1	GGATAACTATAATGGGATGAGC	0.4 µM	Sigma
SLC2A3 rw1	CCACAATAAACCAGGGAATG	0.4 µM	Sigma
SLC2A4 fw1	CCATTGTTATCGGCATTCTG	0.4 µM	Sigma
SLC2A4 rw 1	ATTCTGGATGATGTAGAGGTAG	0.4 µM	Sigma
GLUD2 fw2	CCCTGCAACCATGTGCTGA	0.4 µM	Sigma
GLUD2 rw2	GCTGTAACGGATACCTCCCTTG	0.4 µM	Sigma
GLUD1 fw3 Lin	GGTTGTGCCATACTCATGACC	0.4 µM	Sigma

GLUD1 rw3 Lin	CAGATAGGACATCCAGGGTAGC	0.4 µM	Sigma
GOT1 fw1	CAAGAACACACCTGTCTATG	0.4 µM	Sigma
GOT1 rw1	TTCTCCAGATCATTCAGGAAG	0.4 µM	Sigma
GOT2 fw1	CAAGAACATGGGCTTATATGG	0.4 µM	Sigma
GOT2 rw1	CATTGTTTTCGCAAATCTGG	0.4 µM	Sigma
MDH1 fw1	GAGAATTTGTCACGACTGTG	0.4 µM	Sigma
MDH1 rw1	GAGTAGAGCAGATCATCAGG	0.4 µM	Sigma
GLS fw1	TTGAGTTTGATGCATTCCTG	0.4 µM	Sigma
GLS rw1	ACAAGATCGTGACAAAAGTG	0.4 µM	Sigma
HK1 fw1	AGGTATGAGAAGATGATCAGTG	0.4 µM	Sigma
HK1 rw1	GAGAAACTTGGTCTCAAAGATG	0.4 µM	Sigma
G6PD fw1	AAGGTCAAGGTGTTGAAATG	0.4 µM	Sigma
G6PD rw1	TCTCATTCTCCACATAGAGG	0.4 µM	Sigma
PFKM fw1	AGGACCAGACAGATTTTGAG	0.4 µM	Sigma
PFKM rw1	GATCAGGTAATCTATTCCCCTC	0.4 µM	Sigma
ME1 fw1	CTACGGCAGAGAAGAGTAAG	0.4 µM	Sigma
ME1 rw1	GCCATACTTGGAAGAAACTG	0.4 µM	Sigma
IDH1 fw1	TCAGGAGATATATGACAAGCAG	0.4 µM	Sigma
IDH1 rw1	CATAGTTTTTACAGGCCCAG	0.4 µM	Sigma
IDH2 fw1	GAGTTCAAGCTGAAGAAGATG	0.4 µM	Sigma
IDH2 rw1	GATGTTTTTGCAGATGATGG	0.4 µM	Sigma
MDH1B fw1	GACAGTGAGTGGGTAAAAAG	0.4 µM	Sigma
MDH1B rw1	TTCCTAAAGATACAATCTCCCC	0.4 µM	Sigma
IDH3a fw1	CACCCATCTATGAATTTACTGC	0.4 µM	Sigma
IDH3a rw1	AATCACATGCTCAATTCCAC	0.4 µM	Sigma
LDHa fw1	CACCATGATTAAGGGTCTTTAC	0.4 µM	Sigma
LDHa rw1	AGGTCTGAGATTCCATTCTG	0.4 µM	Sigma
LDHb fw1	CAACAATGGTAAAGGGGATG	0.4 µM	Sigma
LDHb rw1	TCACTAGTCACAGGTCTTTTAG	0.4 µM	Sigma
LDHc fw1	GATTCTAGTGTGCCCTTATG	0.4 µM	Sigma
LDHc rw1	CCAGTGTTCCTTATCTGAATC	0.4 µM	Sigma
PDK1 fw1	ATGATGTCATTCCCACAATG	0.4 µM	Sigma

PDK1 rw1	AAGAGTGCTGATTGAGTAAC	0.4 µM	Sigma
PDK2 fw1	TCTGTCCATCAAGATGAGTG	0.4 µM	Sigma
PDK2 rw1	TACATGTAGCTGAAGAGTCG	0.4 µM	Sigma
PDK3 fw1	ATGCATATGAAACAGCCAAG	0.4 µM	Sigma
PDK3 rw1	GCTTTGGCATTGAATTCTTC	0.4 µM	Sigma
PDK4 fw1	CTTGGGAAAAGAAGACCTTAC	0.4 µM	Sigma
PDK4 rw1	GTGCAGTGGAGTATGTATAAC	0.4 µM	Sigma
PKM2 fw1	ATGTTGATATGGTGTTTGCG	0.4 µM	Sigma
PKM2 rw1	ATTTCATCAAACCTCCGAAC	0.4 µM	Sigma
HK2 fw1	GAAAGCAACTGTTTGAGAAG	0.4 µM	Sigma
HK2 rw1	CAATGTCTGAGATGTCTTTGG	0.4 µM	Sigma
PC fw1	TTATGGTGCAGAATGGATTG	0.4 µM	Sigma
PC rw1	TCAGTACCTTAGAGCGAAAG	0.4 µM	Sigma
MYC FH1	TGAGGAGGAACAAGAAGATG	0.4 µM	Sigma
MYC RH1	ATCCAGACTCTGACCTTTTG	0.4 µM	Sigma
28S Lin fw1	GTTCACCCACTAATAGGGAACGTGA	0.4 µM	Sigma
28S Lin rw1	GGATTCTGACTTAGAGGCGTTCAGT	0.4 µM	Sigma
Human microsatellite DNA fw1	GGGATAATTTCAGCTGACTAAACAG	0.5 µM	BioTeZ
Human microsatellite DNA fw1	AAACGTCCACTTGCAGATTCTAG	0.5 µM	BioTeZ

3.6 Western blotting

For Western blotting cells were lysed with RIPA buffer (50 mM Tris–HCl pH 7.5, 150 mM NaCl, 1% Nonidet P-40) containing PhosSTOP phosphatase and cOmplete protease inhibitors (Roche) and incubated at 4°C for 30 minutes at rotation platform. Cell lysate was centrifuged at 11,000 g at 4°C for 20 minutes. Supernatant was removed and stored at -20°C or used immediately to determine protein concentration. Protein concentration was determined by Bradford assay. 5 µL of bovine serum albumin (BSA from Pierce) standard or sample was mixed with 250 µL of Coomassie Reagent and the mixture was incubated for 10 minutes at room temperature. Each sample was processed in quadruplicates. The

absorbance was measured at 595 nm using plate reader (Tecan infinite 200 PRO). Values for blank samples were subtracted from all the standards and samples. Standard curve was plotted as blank-corrected standard values against standard concentration in µg/mL. Protein concentration was determined from the slope of the standard curve. 10 µg of protein samples was mixed with NuPAGE® loading buffer (Life Technologies) in a ratio sample:buffer as 1:4, and with DTT (Applichem) in a ratio sample:DTT as 1:10. Protein samples were resolved by sodium dodecyl sulphate-polyacrylamide gel electrophoresis (SDS-PAGE) using pre-casted 4-12% SDS-PAGE gels (Bio-Rad). Protein samples were resolved in 1x 3-(N-morpholino) propanesulfonic acid (MOPS) running buffer (0.02 M MOPS free acid, 2 mM $C_2H_3NaO_2$, 1 mM Na_2EDTA, pH 7.0) at 140 V for 1 hour in XCellSureLock™ Mini Cell System (Thermo Fisher). To determine the protein size pre-stained Spectra™ Multicolor broad Range Protein Ladder (Fermentas) was used. The proteins were transferred to nitrocellulose membrane (Amersham Protran 0.45 µm) by semi-dry electrotransfer in blotting buffer (25 mM Tris-HCl, 200 mM glycin, 0,1 % SDS, 20 % methanol, pH 7.5) at 25 V for 10 minutes in the Trans-Blot® Turbo™ Blotting System (Bio-Rad). The membrane was washed in TBST (50 mM Tris-HCl, 150 mM NaCl, 0.05 % Tween 20, pH 7.5) and blocked in blocking buffer (6% skim milk powder in TBST) for 1 hour at the rotation platform at room temperature. Membrane was incubated with primary antibodies overnight at 4°C. After incubation with primary antibodies membrane was washed with TBST and secondary HRP-conjugated antibodies were added. The list of used antibodies and their characteristics are provided in Table 3.3. The membrane was incubated with secondary antibodies for 1 hour at room temperature. Both primary and secondary antibodies were diluted in TBST with 5% BSA. The membrane was washed and incubated with WesternBright™ Enhanced Chemiluminescent HRP substrate (Advansta Biozym) to visualize proteins of interest. Chemiluminescence, which is proportional to the amount of protein of interest, was detected by exposure to X-ray film (Fujifilm). As a protein loading control β-actin was used.

Table 3.3 Antibodies used for Western blotting

	Target	Dilution	Antibody	Company and catalogue number
Primary antibodies	Anti-MACC1	1:1000	Rabbit polyclonal	Sigma (HPA020103)
	Anti- β-actin	1:10000	Mouse monoclonal	Sigma (A19778)
	Anti-GLUT1	1:6000	Rabbit monoclonal	Abcam (ab115730)
Secondary antibodies	Anti-rabbit	1:10000	HRP conjugated	Promega (W401)
	Anti-mouse	1:10000	HRP conjugated	Pierce (31430)

3.7 Cell viability

For both nutrient related and upon drug treatment cell viability assays, SW620 shcntl and shMACC1 cells as well as HCT116 shcntl and shMACC1 cells were seeded in duplicates at density $0.3*10^6$ cells/well on a 6-well plate with DMEM no glucose, no glutamine, no phenol red (Gibco) supplemented with 10 mM glucose (Sigma), 2mM glutamine (Gibco) and 10% FBS (Bio&Sell). For assessment of SW480 ev and MACC1 cell viability cells were seeded in duplicates at density $0.1*10^6$ cells/well on a 6-well plate with RPMI-1640 (Gibco) supplemented with 10% FBS (Bio&Sell). For nutrient related cell viability assays, twelve hours after cell seeding cells were washed with PBS and the medium was changed on the corresponding medium. The types of media used in nutrient related cell viability assays are listed in Table 3.4. For assessment of cell viability upon drug treatment, twelve hours after cell seeding cells were washed with PBS and were treated with the corresponding drug. The drugs used in this work and their characteristics and treatment conditions are presented in detail in chapter 3.7.2. For both nutrient related and upon drug treatment cell viability assays, fourty eight hours after either medium change or drug treatment cells were washed with PBS, trypsinized and manually counted using Neubauer hemocytometer chamber (Celeromics).

3.7.1 Medium supplementation with metabolic substrates

Medium used to assess the effect of MACC1 on nutrient utilization differed in supplementation with various metabolic substrates, including glucose (Sigma), glutamine (Gibco), pyruvate (Gibco), lactate (Sigma), palmitate (Sigma), α-ketoglutarate (Sigma) and non-essential amino acids (NEAA: serine, proline, aspartate, asparagine, alanine and glycine 0.1 mM each – all from Sigma), and their concentrations. All types of media used in this work were supplemented with 10% FBS (Bio&Sell). The types of media and their supplementation with metabolic substrates are presented in detail in Table 3.4.

Table 3.4 Types of medium supplementation with metabolic substrates used in this study

Application	Supplements and their concentrations						
	Glucose (mM)	Glutamine (mM)	Pyruvate (mM)	Lactate (mM)	Palmitate (µM)	α-ketoglutarate (mM)	NEAA (mM)
Basal medium (both DMEM and RPMI)	10	2	-	-	-	-	-
Glucose utilization	0	2	-	-	-	-	-
	2	2	-	-	-	-	-
	10	2	-	-	-	-	-
Glutamine utilization	10	0	-	-	-	-	-
	10	1	-	-	-	-	-
	10	2	-	-	-	-	-
	2	0	-	-	-	-	-
	2	1	-	-	-	-	-
	2	2	-	-	-	-	-
	0	0	-	-	-	-	-
	0	0.5	-	-	-	-	-
	0	1	-	-	-	-	-
	0	2	-	-	-	-	-
De novo glutamate synthesis	2	2	-	-	-	-	-
	2	0	-	-	-	-	-
	2	0	-	-	-	2	-
	2	0	-	-	-	-	0.1
	2	0	-	-	-	2	0.1
	0	2	-	-	-	-	-
	0	0	-	-	-	-	-
	0	0	-	-	-	2	-
	0	0	-	-	-	-	0.1
	0	0	-	-	-	2	0.1
Pyruvate utilization	2	2	0	-	-	-	-
	2	2	5	-	-	-	-

	2	2	10	-	-	-	-
	0	2	0	-	-	-	-
	0	2	5	-	-	-	-
	0	2	10	-	-	-	-
Lactate utilization	2	2	-	0	-	-	-
	2	2	-	5	-	-	-
	2	2	-	10	-	-	-
	0	2	-	0	-	-	-
	0	2	-	5	-	-	-
	0	2	-	10	-	-	-
Palmitate utilization	2	2	-	-	0	-	-
	2	2	-	-	25	-	-
	2	2	-	-	50	-	-
	0	2	-	-	0	-	-
	0	2	-	-	25	-	-
	0	2	-	-	50	-	-

3.7.2 Drug treatment

SW620 shcntl and shMACC1 cells were seeded at density $0.3*10^6$ cells/well on a 6-well plate with DMEM no glucose, no glutamine, no phenol red (Gibco) supplemented with 10 mM glucose (Sigma), 2mM glutamine (Gibco) and 10% FBS (Bio&Sell). SW480 ev and MACC1 cells were seeded at density $0.1*10^6$ cells/well on a 6-well plate with RPMI-1640 (Gibco) supplemented with 10% FBS (Bio&Sell). Cells were treated with the following drugs: WZB117 (Millipore), 6-Diazo-5-oxo-L-norleucin (DON from Sigma), cPEPCK inhibitor (Axon Medchem) and rotenone (Sigma). All drugs were tested in a range of concentrations on their effect on cell viability. This included testing of at least two drug concentrations with further selection of an optimal concentration.

WZB117 was diluted in dimethylsulfoxid (DMSO) (Sigma) to prepare 10 mM stock solution. The stock solution was stored at -20°C light protected. WZB117 after being dissolved in DMSO was used within three days from the day of preparation. The final concentration of WZB117 used in this work was 10 µM.

DON was diluted in DMEM medium no glucose, no glutamine, no phenol red (Gibco) supplemented with 10 mM glucose (Sigma), 2 mM glutamine (Sigma) and 10% FBS (Bio&Sell) to prepare 25 mM stock

solution. DON was freshly prepared each time. The final concentration of DON used in this work was 0.25 mM.

cPEPCK was diluted in DMSO (Sigma) to prepare 10 mM stock solution. The stock solution was stored at -20°C. The final concentration of cPEPCK inhibitor used in this work was 10 µM.

Rotenone was diluted in DMEM no glucose, no glutamine, no phenol red (Gibco) supplemented with 10 mM glucose (Sigma), 2 mM glutamine (Sigma) and 10% FBS (Bio&Sell) to prepare 100 mM stock solution. Rotenone was freshly prepared each time. The final concentration of rotenone used in this work was 50 nM.

For details regarding drug treatment of cells during measurement of oxygen consumption and extracellular acidification rates please see chapter 3.12.

3.8 Conjugation of palmitate to BSA

For conjugation of palmitate (Sigma) to BSA (Sigma), 20 mL 150 mM NaCl solution was autoclaved and 538.4 mg ultra low fatty acid BSA was diluted in 12 mL of warm (37°C) 150 mM NaCl followed by incubation at 37°C till the BSA is dissolved. Then, 9.18 mg palmitate was diluted in 6.6 mL of warm 150 mM NaCl and the solution was heated at 70°C with stirring till the solution was clear. After that, 8.25 mL warm BSA solution was transferred in a new tube and palmitate solution was added slowly by portions to BSA solution. The conjugate of palmitate to BSA was stirred at 37°C for 1 hour. After incubation, 1.65 mL 150 mM NaCl solution was added to the conjugate. The pH was adjusted to 7.4 with 1 M NaOH. The conjugate solution was aliquoted and stored at -20°C. BSA vehicle was prepared by mixing 3 mL BSA solution with 3 mL 150 mM NaCl. BSA vehicle was aliquoted and stored at -20°C. The molar ratio of conjugated palmitate:BSA was as 6:1. Before treatment of cells with palmitate:BSA conjugate both BSA and palmitate were thawed at 37°C for 10 minutes prior being added to the medium.

3.9 Preparation of stock solution of non-essential amino acids (NEAA)

Powdered non-essential amino acids such as serine, proline, aspartate, asparagine, alanine and glycine (all from Sigma) were combined as 100 mM of each and dissolved in a sterile grade water (Gibco) to prepare 100 mM stock solution. To dissolve the powder solution was warmed up at 37°C for 30 minutes and vortexed well. The NEAA solution was stored at 2-8°C.

3.10 Gas/liquid chromatography coupled to mass spectrometry (GC/LC-MS)

3.10.1 Metabolomics using $^{13}C_6$ glucose

SW620 shcntl and shMACC1 cells were seeded at density $0.25*10^6$ cells/well on a 6-well plate with DMEM no glucose, no glutamine, no phenol red (Gibco) supplemented with 10 mM glucose (Sigma), 2mM glutamine (Gibco) and 10% FBS (Bio&Sell) in 5 replicates. Twenty four hours after cell seeding cells were washed with PBS and medium was changed on DMEM no glucose, no glutamine, no phenol red (Gibco) supplemented with 10 mM $^{13}C_6$ glucose (Sigma), 2mM glutamine (Gibco) and 10% FBS (Bio&Sell). Cells were allowed to grow in the presence of $^{13}C_6$ glucose (Sigma) for 24 hours. After that, medium was taken from each well into separate tube and stored at -80°C till further use. Cells were washed with PBS and 150 µL of -20°C cold methanol (Sigma) was added followed by 5 minutes incubation at room temperature. Then, 150 µL of sterile distilled water (Gibco) was added. Cells were scraped and transferred to a 2 mL tube, and 1.3 mL of chloroform (Sigma) was added. The lysate was vortexed and placed on ice for 30 minutes. After that, 300 µL of sterile distilled water (Gibco) was added and the mixture was centrifuged at 3000 g at 4°C for 20 minutes. The aqueous phase was transferred into a new tube and stored at -80°C till further use. The samples were evaporated at SpeedVac® vacuum concentrator (VWR) and derivatized with 15 µL Methoxylamine HCl (MeOX)-pyridine (Sigma) and 60 µL N-Trimethylsilyl-N-methyl trifluoroacetamide (MSTFA, Sigma). As retention index markers fatty acid methyl esters (FAMEs, Sigma) were spiked in total volume of 2 µL to the derivatization mixture. The samples were processed automatically with a pipetting robot and 1 µL of a sample with split ratio of 1:100 was run at GC-EI-TOF-MS 7890 from Agilent and Pegasus III Leco. The analysis of peaks was performed with self-written software (R packages: APCIFlux, MetabolomicsHelpers, CorrectOverloadedPeaks and InterpretMSSpectrum). Each peak for metabolites in a in-house library (57 metabolites in total) was checked manually and in case of a significant retention time (RT) shift, the RT was adjusted manually or in case of a co-elution a different fragment was selected.

3.10.2 Metabolomics using $^{13}C_5$ glutamine

Metabolomics using $^{13}C_5$ glutamine was performed in 10 mM glucose/2 mM glutamine (basal) and 0 mM glucose/1 mM glutamine (glucose depleted) conditions. For metabolomics in basal conditions, SW620 shcntl and shMACC1 cells were seeded at density $0.25*10^6$ cells/well on a 6-well plate with DMEM no glucose, no glutamine, no phenol red (Gibco) supplemented with 10 mM glucose (Sigma), 2mM glutamine (Gibco) and 10% FBS (Bio&Sell) in 5 replicates. Twenty four hours after cell seeding cells were washed with PBS and medium was changed on DMEM no glucose, no glutamine, no phenol red (Gibco) supplemented with 10 mM glucose (Sigma), 2 mM $^{13}C_5$ glutamine (Sigma) and 10% FBS (Bio&Sell). Cells

were allowed to grow in the presence of $^{13}C_5$ glutamine (Sigma) for 24 hours. After that, medium was taken from each well into separate tube and stored at -80°C till further use. Cells were washed with PBS and 150 µL of -20°C cold methanol (Sigma) was added followed by 5 minutes incubation at room temperature. Then, 150 µL of sterile distilled water (Gibco) was added. Cells were scraped and transferred to a 2 mL tube, and 1.3 mL of chloroform (Sigma) was added. The lysate was vortexed and placed on ice for 30 minutes. After that, 300 µL of sterile distilled water (Gibco) was added and the mixture was centrifuged at 3000 g at 4°C for 20 minutes. The aqueous phase was transferred into a new tube and stored at -80°C. The samples were evaporated at SpeedVac® vacuum concentrator (VWR) and derivatized with 15 µL Methoxylamine HCl (MeOX)-pyridine (Sigma) and 60 µL N-Trimethylsilyl-N-methyl trifluoroacetamide (MSTFA, Sigma). As retention index markers fatty acid methyl esters (FAMEs, Sigma) were spiked in total volume of 2 µL to the derivatization mixture. The samples were processed automatically with a pipetting robot and 1 µL of a sample with split ratio of 1:100 was run at GC-EI-TOF-MS 7890 from Agilent and Pegasus III Leco. The analysis of peaks was performed with self-written software (R packages: APCIFlux, MetabolomicsHelpers, CorrectOverloadedPeaks and InterpretMSSpectrum). Each peak for metabolites in a in-house library (57 metabolites in total) was checked manually and in case of a significant retention time (RT) shift, the RT was adjusted manually or in case of a co-elution a different fragment was selected.

For metabolomics in glucose depleted conditions, SW620 shcntl and shMACC1 cells were seeded at density $3*10^6$ cells per 10-cm dish with DMEM no glucose, no glutamine, no phenol red (Gibco) supplemented with 10 mM glucose (Sigma), 2 mM glutamine (Gibco) and 10% FBS (Bio&Sell) in 5 replicates. Twelve hours after cell seeding cells were washed with PBS and medium was changed on DMEM no glucose, no glutamine, no phenol red (Gibco) supplemented with 1 mM glutamine (Gibco) and 10% FBS (Bio&Sell). Cells were cultivated for 24 hours. After that, cells were washed with PBS and medium was changed on DMEM no glucose, no glutamine, no phenol red (Gibco) supplemented with 1 mM $^{13}C_6$ glutamine (Sigma) and 10% FBS (Bio&Sell). Cells were incubated in the presence of $^{13}C_6$ glutamine (Sigma) for 24 hours. Medium was taken from each dish into a separate tube and stored at -80°C till further use. Cells were washed with PBS and 750 µL of -20°C cold methanol (Sigma) was added followed by 5 minutes incubation at room temperature. Then, 750 µL of sterile distilled water (Gibco) was added. Cells were scraped and transferred to a 15 mL tube, and 6.5 mL of chloroform (Sigma) was added. The lysate was vortexed and placed on ice for 30 minutes. After that, 300 µL of sterile distilled water (Gibco) was added and the mixture was centrifuged at 3000 g at 4°C for 20 minutes. The aqueous phase was transferred into a new tube and stored at -80°C. Because in glucose depleted conditions cell

viability of SW620 shcntl cells was 15 times higher compared to shMACC1 cells and, therefore, ion intensity from shcntl and shMACC1 samples was not comparable, the volume of extracted metabolites from shcntl cells was taken 10 times smaller compared to such one from shMACC1 cells. In this way, extracted metabolites were normalized by cell number.

The samples were evaporated at SpeedVac® vacuum concentrator (VWR) and derivatized with 15 µL Methoxylamine HCl (MeOX)-pyridine (Sigma) and 60 µL N-Trimethylsilyl-N-methyl trifluoroacetamide (MSTFA, Sigma). As retention index markers fatty acid methyl esters (FAMEs, Sigma) were spiked in total volume of 2 µL to the derivatization mixture. The samples were processed automatically with a pipetting robot and 1 µL of a sample with split ratio of 1:100 was run at GC-EI-TOF-MS 7890 from Agilent and Pegasus III Leco. The analysis of peaks was performed with self-written software (R packages: APCIFlux, MetabolomicsHelpers, CorrectOverloadedPeaks and InterpretMSSpectrum). Each peak for metabolites in a in-house library (57 metabolites in total) was checked manually and in case of a significant retention time (RT) shift, the RT was adjusted manually or in case of a co-elution a different fragment was selected.

3.10.3 Metabolomics using $^{13}C_3$ pyruvate

SW620 shcntl and shMACC1 cells were seeded at density $0.25*10^6$ cells/well on a 6-well plate with DMEM no glucose, no glutamine, no phenol red (Gibco) supplemented with 10 mM glucose (Sigma), 2 mM glutamine (Gibco) and 10% FBS (Bio&Sell) in 5 replicates. Twelve hours after cell seeding cells were washed with PBS and medium was changed on DMEM no glucose, no glutamine, no phenol red (Gibco) supplemented with 2 mM glutamine (Gibco), 10 mM pyruvate (Gibco) and 10% FBS (Bio&Sell). Cells were cultivated for 24 hours. After that, cells were washed with PBS and medium was changed on DMEM no glucose, no glutamine, no phenol red (Gibco) supplemented with 2 mM glutamine (Sigma), 10 mM $^{13}C_3$ pyruvate (Sigma) and 10% FBS (Bio&Sell). Cells were incubated in the presence of $^{13}C_3$ pyruvate (Sigma) for 24 hours. Medium was taken from each well into separate tube and stored at -80°C till further use. Cells were washed with PBS and 150 µL of -20°C cold methanol (Sigma) was added followed by 5 minutes incubation at room temperature. Then, 150 µL of sterile distilled water (Gibco) was added. Cells were scraped and transferred to a 2 mL tube, and 1.3 mL of chloroform (Sigma) was added. The lysate was vortexed and placed on ice for 30 minutes. After that, 300 µL of sterile distilled water (Gibco) was added and the mixture was centrifuged at 3000 g at 4°C for 20 minutes. The aqueous phase was transferred into a new tube and stored at -80°C. The samples were evaporated at SpeedVac® vacuum concentrator (VWR) and derivatized with 15 µL Methoxylamine HCl (MeOX)-pyridine (Sigma) and 60 µL N-Trimethylsilyl-N-methyl trifluoroacetamide (MSTFA, Sigma). As retention index markers fatty acid methyl esters (FAMEs, Sigma) were spiked in total volume of 2 µL to the derivatization mixture. The samples

were processed automatically with a pipetting robot and 1 µL of a sample with split ratio of 1:100 was run at GC-EI-TOF-MS 7890 from Agilent and Pegasus III Leco. The analysis of peaks was performed with self-written software (R packages: APCIFlux, MetabolomicsHelpers, CorrectOverloadedPeaks and InterpretMSSpectrum). Each peak for metabolites in a in-house library (57 metabolites in total) was checked manually and in case of a significant retention time (RT) shift, the RT was adjusted manually or in case of a co-elution a different fragment was selected.

3.11 Flow cytometry

SW620 shcntl and shMACC1 and SW480 ev and MACC1 cells were detached with 1x TrypLE™ Express enzyme no phenol red (Gibco) and counted with Neubauer chamber (Celeromics). Cells at density $0.5*10^6$/tube were placed in a 5 mL falcon tube with strainer cap (Biolab). Cells were fixed with 100 µL 4% paraformaldehyde (PFA, from Sigma) for 10 minutes at room temperature and spun down at 400 g for 5 minutes. Then, cells were stained with 5 µL of mouse IgG2B isotype fluorescein isothiocyanate (FITC) conjugated antibody (RnD Systems) or primary anti-GLUT1 mouse antibody (RnD Systems) diluted in 100 µL PBS supplemented with 5% FBS. The staining occurred for 30 minutes at room temperature in the dark. The cells were washed twice with PBS supplemented with 5% FBS and resuspended in 300 µL PBS supplemented with 5% FBS. Flow cytometry was performed at BD LSRFortessa™ cell analyzer (BD Biosciences) at FACS Core Facility at Max-Delbrück-Centrum for Molecular Medicine. The cell acquiring parameters were set by plotting side scatter area (SSC-A) against forward scatter area (FSC-A). The doublets were excluded by plotting forward scatter width (FSC-W) against forward scatter area (FSC-A) and SSC-W against SSC-A. To define FITC-positive cell population the gating at SSC-A against FITC-A was set using negative isotype control. The signal was acquired from 10,000 cells. The measurement data from flow cytometry standard files was further analyzed with FlowJo® software (FLOWJO, LLC) with the license owned by FACS Core Facility at Max-Delbrück-Centrum for Molecular Medicine. The data was presented as a net mean fluorescence intensity (net MFI) depicted as the number of FITC-positive cells multiplied by FITC geometric mean.

3.12 Oxygen consumption (OCR) and extracellular acidification rate (ECAR)

Cell metabolic phenotype was assessed with Seahorse XFp Cell Energy Phenotype Test kit (Agilent). Mitochondrial functionality was assessed with Seahorse XFp Cell Mito Stress Test Kit (Agilent). For metabolic phenotype assessment, on the day prior to assay SW620 shcntl and shMACC1 at density 8*104/well and SW480 ev and MACC1 at density 3*104/well were seeded with DMEM no glucose, no glutamine, no phenol red (Gibco) supplemented with 10 mM glucose (Sigma), 2mM glutamine (Gibco) supplemented with 10% FBS (Bio&Sell); or with RPMI (Gibco) supplemented with 10% FBS (Bio&Sell),

respectively, on a 96-well Seahorse XF Cell Culture Microplate provided within Seahorse XFe96 FluxPaks (Agilent) in 5-8 replicates in total volume of 200 µL. For all cell lines at least three different cell densities were tested prior experiments. An optimal cell density was selected by mitochondrial respiration values and by differences in respiration between SW620 shcntl and shMACC1, and between SW480 ev and MACC1. Seahorse XFe96 Analyzer (Agilent) was warmed up overnight at 37°C. Seahorse XFe96 Sensor Cartridge provided within Seahorse XFe96 FluxPaks (Agilent) was hydrated with 200 µL Seahorse XF Calibrant (Agilent) in a non-CO_2 incubator at 37°C overnight. On the day of the assay, assay medium was prepared. The medium components included XF Base Medium Minimal DMEM (Agilent), 10 mM glucose (Sigma), 1 mM pyruvate (Gibco) and 2 mM glutamine (Gibco). The medium was warmed up to 37°C, and pH was adjusted to 7.4 with NaOH. The medium was kept at 37°C till use. The medium from the Seahorse XF Cell Culture Microplate with seeded cells was removed by tapping the plate at paper towels followed by washing with prepared warm assay medium. After final washing step 180 µL assay medium was added to each well. The cells were placed in a non-CO_2 incubator at 37°C for 1 hour. Oligomycin and carbonyl cyanide-4-(trifluoromethoxy)phenylhydrazone (FCCP) provided within Seahorse XFp Cell Energy Phenotype Test kit (Agilent) were reconstituted by adding 630 µL and 720 µL of assay medium, respectively, to prepare 100 µM stock. Equal volumes of oligomycin and FCCP drug solution were mixed and further diluted with assay medium in a ratio drug:medium as 1:10. Final concentration of oligomycin and FCCP in the assay reaction was 1 µM. 20 µL of mixed drugs was loaded into port A of a hydrated Seahorse XFe96 Sensor Cartridge (Agilent). The Seahorse XFe96 Sensor Cartridge (Agilent) was placed without lid into Seahorse XFe96 Analyzer (Agilent) for calibration. Once calibration was finished Seahorse XFe96 Sensor Cartridge was placed into Seahorse XF Cell Culture Microplate (Agilent) and the assay was run using Seahorse XFe96 Analyzer (Agilent). All measurement data were processed with Seahorse Wave software (Agilent). All measurements were normalized by protein content. Briefly, medium was removed from Seahorse XF Cell Culture Microplate by tapping at paper towels and cells were washed with PBS. 20 µL of RIPA buffer was added to each assay well. The Seahorse XF Cell Culture Microplate was placed on ice for 20 minutes. 400 µL Coomassie reagent was added to each well and the absorbance was measured at 595 nm using plate reader (Tecan infinite 200 PRO). The absorbance values were uploaded into each measurement in Seahorse Wave software (Agilent) and the normalization of measurement values was done automatically by the software.

For assessment of mitochondrial functionality, similar procedures as described above for metabolic phenotype assay were applied with the exception that, besides oligomycin and FCCP, a mixture of rotenone/antimycin A provided within Seahorse XFp Cell Mito Stress Test Kit (Agilent) was used and the

drugs were not mixed. The rotenone/antimycin A was reconstituted in 540 µL assay medium to prepare 50 µM stock solution. Each drug solution was further diluted with assay medium in a ratio as 1:10. Final concentration of oligomycin, FCCP and rotenone/antimycin A in the assay reaction was 1 µM, 1 µM and 0.5 µM, respectively. 20 µL of oligomycin was loaded into port A, 22 µL of FCCP was loaded into port B and 25 µL of rotenone/antimycin A was loaded into port C of Seahorse XFe96 Sensor Cartridge (Agilent). The rest of the procedures was same as described above for metabolic phenotype assay. All measurement data were processed with Seahorse Wave software (Agilent). All measurements were normalized by protein content as described above.

3.13 ATP measurements

Measurements of mitochondrial ATP were extrapolated from OCR values upon oligomycin and FCCP treatments, which reflect mitochondrial functionality. Because oligomycin inhibits ATP synthase and FCCP uncouples mitochondria subtraction of OCR values at the time of oligomycin treatment from OCR values at the time of FCCP treatment provides relative rate of mitochondrial ATP production. Detailed description of read-outs of mitochondrial functionality based on specific mitochondria-related drug treatment is described in Fig.4.

Measurements of total ATP was performed with CellTiter-Glo® Luminescent cell viability assay (Promega). Briefly, SW620 shcntl and shMACC1 and SW480 ev and MACC1 cells were trypsinized and counted with Neubauer hemocytometer chamber (Celeromics). SW620 shcntl and shMACC1 cells at density $5*10^4$ cells/well, and SW480 ev and MACC1 cells at density $3*10^4$ cells/well were placed into white 96-well plate in total volume of 100 µL. 25 µL of CellTiter-Glo® reagent (Promega) was added to each well followed by intense mixing for 3 minutes at shaker platform. Plate was removed from shaker platform and incubated for 10 minutes at room temperature. The luminescence was measured with plate reader (Tecan infinite 200 PRO). Luminescence was normalized by blank wells containing medium without cells.

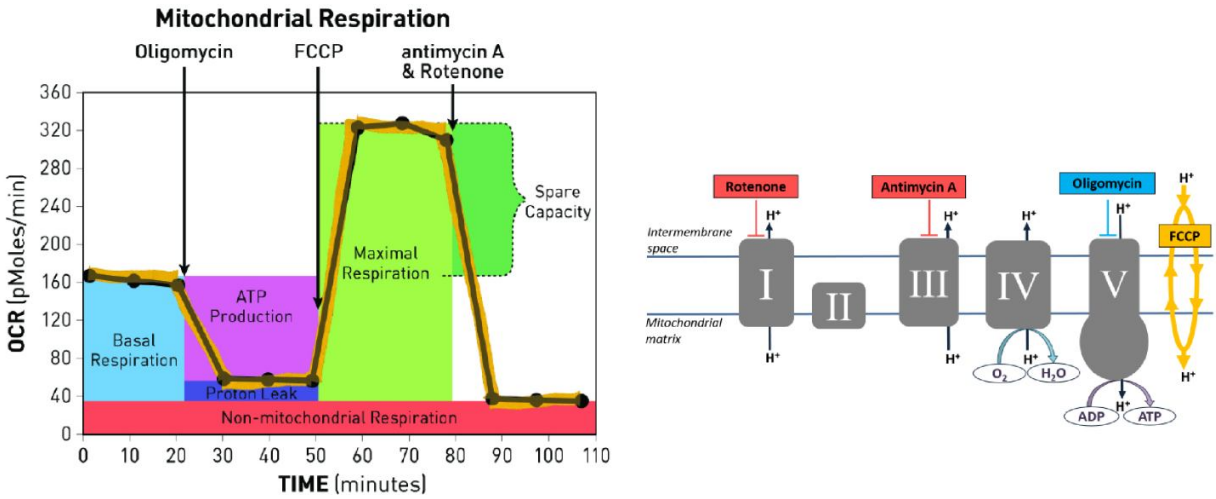

Fig.4 Mitochondrial respiratory profile based on treatment with drugs affecting mitochondrial function. Mitochondrial functionality is determined by measurement of oxygen consumption rate (OCR) upon treatment with oligomycin, FCCP and rotenone/antimycin A. First, basal respiration is measured. Then oligomycin, which is an inhibitor of mitochondrial complex V ATP synthase, is added. Because ATP synthase is blocked oxygen consumption, which is coupled to ATP production, gradually decreases. Upon treatment with FCCP, which collapses the proton gradient and disrupts mitochondrial membrane potential, respiration increases gradually reflecting maximal respiration uncoupled from ATP synthesis. Treatment with rotenone and antimycin A, inhibitors of mitochondrial complex I and III, respectively, shunts down respiration. The difference between OCR at basal level and maximal respiration is indicative of mitochondrial spare respiratory capacity. Because treatment with rotenone/antimycin A completely shuts down mitochondrial respiration the remaining OCR shows non-mitochondrial respiration driven by the processes outside of mitochondria like respiration mediated by the activity of cytosolic NADPH oxidase. The difference between the OCR upon oligomycin treatment and the OCR upon rotenone/antimycin A treatment correlates with proton leak. Adopted from [157].

3.14 Nutrient depletion

3.14.1 Gas chromatography coupled to mass spectrometry (GC-MS) screening

SW620 shcntl and shMACC1 cells were seeded at density $0.3*10^5$ cells/well with DMEM no glucose, no glutamine, no phenol red (Gibco) supplemented with 10 mM glucose (Sigma), 2 mM glutamine (Gibco) and 10% FBS (Bio&Sell) on 6-well plate in 6 replicates. Twelve hours after cell seeding was considered as timepoint 0. At timepoint 0, day 2, day 4 and day 5 12 µL of medium was taken and stored at -80°C till

further use. Before metabolite extraction all samples were randomized. 12 µL of medium sample from each timepoint was extracted with 1.5 ml of methanol (Sigma)/chloromethane (Sigma)/water in a ratio as 1:2:1, respectively. The 150 µl aliquots of the resulting polar phase were dried down and were derivatized with trimethylchlorsilane. Measurements were performed on gas chromatography-electron impact ionization-time-of-flight-mass spectrometry (GC-EI-TOF-MS 7890 from Agilent and Pegasus III Leco).

3.14.2 Measurement of nutrient depletion using enzymatic assays

Glutamine concentration in cell growth medium was determined with EnzyChrom™ glutamine assay kit (EnzyChrom). Briefly, SW620 shcntl and shMACC1 cells were seeded at density $0.3*10^6$ cells/well on a 6-well plate with DMEM no glucose, no glutamine, no phenol red (Gibco) supplemented with 10 mM glucose (Sigma), 2 mM glutamine (Gibco) and 10% FBS (Bio&Sell) in duplicates. Twelve hours after cell seeding cells were washed with PBS and medium was changed on DMEM no glucose, no glutamine, no phenol red (Gibco) supplemented with 1mM glutamine (Gibco) and 10% FBS (Bio&Sell). This timepoint was considered as timepoint 0. Medium in total volume of 50 µL was taken every 12 hours in total for 48 hours. DMEM no glucose, no glutamine, no phenol red (Gibco) supplemented with 2 mM glutamine (Gibco) and 10% FBS (Bio&Sell) was used to prepare glutamine standard curve, which ranged from 0 mM to 2 mM glutamine. 20 µL of standards or samples and 80 µL of working reagent were added per well on a transparent 96-well plate. The working reagent contained 65 µL assay buffer, 1 µL enzyme A, 1 µL enzyme B, 2.5 µL nicotinamide adenine dinucleotide (NAD) and 14 µL 3-(4,5-dimethylthiazol-2-yl)-2,5-diphenyltetrazolium bromide (MTT). The plate was mixed briefly by tapping and incubated for 40 minutes at room temperature. 100 µL stop reagent was added to each assay well (all reagents were provided within EnzyChrom™ glutamine assay kit, EnzyChrom) and the absorbance was measured at 565 nm with plate reader (Tecan infinite 200 PRO). Blank values were subtracted from values for standards and samples. Glutamine concentration was determined from the slope of a standard curve.

Pyruvate concentration in cell growth medium was determined with EnzyChrom™ pyruvate assay kit (EnzyChrom). SW620 shcntl and shMACC1 cells were seeded at density $0.3*10^6$ cells/well on a 6-well plate with DMEM no glucose, no glutamine, no phenol red (Gibco) supplemented with 10 mM glucose (Sigma), 2mM glutamine (Gibco) and 10% FBS (Bio&Sell) in duplicates. Twelve hours after cell seeding cells were washed with PBS and medium was changed on DMEM no glucose, no glutamine, no phenol red (Gibco) supplemented with 2 mM glutamine (Gibco), 10 mM pyruvate (Gibco) and 10% FBS (Bio&Sell). This timepoint was considered as timepoint 0. Medium in total volume of 50 µL was taken every 12 hours in total for 48 hours. DMEM no glucose, no glutamine, no phenol red (Gibco)

supplemented with 2 mM glutamine (Gibco), 10 mM pyruvate (Gibco) and 10% FBS (Bio&Sell) was used to prepare pyruvate standard curve, which ranged from 0 mM to 0.5 mM pyruvate. Samples were diluted with water in a ratio sample:water as 1:20. 10 µL of standards or samples and 90 µL of working reagent were added per well on a transparent 96-well plate. The working reagent contained 94 µL enzyme mix and 1 µL dye reagent. All reagents were provided within EnzyChrom™ pyruvate assay kit (EnzyChrom). The plate was mixed briefly by tapping and incubated for 30 minutes at room temperature. The absorbance was measured at 565 nm with plate reader (Tecan infinite 200 PRO). Blank values were subtracted from values for standards and samples. Pyruvate concentration was determined from the slope of a standard curve.

Lactate concentration in cell growth medium was determined with EnzyChrom™ lactate assay kit (EnzyChrom). SW620 shcntl and shMACC1 cells were seeded at density $0.3*10^6$ cells/well on a 6-well plate with DMEM no glucose, no glutamine, no phenol red (Gibco) supplemented with 10 mM glucose (Sigma), 2mM glutamine (Gibco) and 10% FBS (Bio&Sell) in duplicates. Twelve hours after cell seeding cells were washed with PBS and medium was changed on DMEM no glucose, no glutamine, no phenol red (Gibco) supplemented with 2 mM glutamine (Gibco), 10 mM lactate (Sigma) and 10% FBS (Bio&Sell). This timepoint was considered as timepoint 0. Medium in total volume of 50 µL was taken every 12 hours in total for 48 hours. DMEM no glucose, no glutamine, no phenol red (Gibco) supplemented with 2 mM glutamine (Gibco), 10 mM lactate (Sigma) and 10% FBS (Bio&Sell) was used to prepare lactate standard curve, which ranged from 0 mM to 2 mM lactate. Samples were diluted with water in a ratio sample:water as 1:10. 20 µL of standards or samples and 80 µL of working reagent were added per well on a transparent 96-well plate. The working reagent contained 60 µL assay buffer, 1 µL enzyme A, 1 µL enzyme B, 10 µL NAD and 14 µL MTT. All reagents were provided within EnzyChrom™ lactate assay kit (EnzyChrom). The plate was mixed briefly by tapping and the absorbance was measured at 565 nm with plate reader (Tecan infinite 200 PRO) at time 0 and after 20 minutes of incubation at room temperature. Values at time 0 were subtracted from values at time 20 minutes for standards and samples. Lactate concentration was determined from the slope of a standard curve.

3.15 Animal experiments

All experiments were performed in accordance with the United Kingdom Co-ordinated Committee on Cancer Research (UKCCCR) guidelines and approved by the responsible local authorities (State Office of Health and Social Affairs, Berlin, Germany).

3.15.1 Intrasplenal injection of cancer cells

For intrasplenal injection 6-8-week old SCID/beige female mice (Charles River, Wilmington, MA) at epo GmbH were used. Mice were anesthetized with 35 mg/kg Hypnomidate® (Jassen-Cilag) and the peritoneum was opened. SW620/luc shcntl and SW620/luc shMACC1 cells were injected ($3*10^6$ cells) into the spleen in PBS in total volume of 30 µL. After the injection, peritoneum was closed with Surgicryl® absorbable suture and the skin was clamped twice. The tumor was allowed to form for 28 days before imaging with PET/CT (for details see 3.15.3).

3.15.2 *In vivo* bioluminescence imaging

Tumor growth and metastasis formation were monitored by bioluminescence imaging using NightOWL LB 981 imaging system (Berthold Technologies, Bad Wildbad, Germany). For bioluminescence imaging, mice were anesthetized with isoflurane gas and received intraperitoneally 150 mg/kg D-luciferin (Biosynth, Staad, Switzerland). Tumor growth and metastasis formation was imaged and quantified by WinLight (Berthold Technologies) and ImageJ 1.48v.

3.15.3 Positron emission/magnetic resonance imaging (PET/MRI)

Five female SW620/sh-control and four female SW620/sh-MACC1 SCID/beige mice were brought to the animal husbandry at the Berlin Experimental Radionuclide Imaging Center (BERIC) of the Charité for imaging. Tomographic imaging was performed using the dedicated small animal 1 Tesla nanoScan PET/MRI (Mediso, Hungary). With isoflurane anaesthetized mice were injected into the tail vein either with 80 µl contrast agent Primovist™ (1:5 diluted with 0.9% sodium chloride) for contrast-enhanced magnetic resonance imaging (MRI) or 200 µl of ^{18}F-fluorofluor-deoxyglucose (^{18}F-FDG, 6.5-15.6 MBq) for positron emission computed tomography (PET). In addition to the ^{18}F-FDG-PET two SW620-control and two SW620/sh-MACC1 mice were injected with 3.5-5.0 MBq ^{18}F-fluorofluor-glutamate after 48 h. Anatomic MRI scans were acquired using a T1-weighted 3D spoiled Gradient Echo sequence (T1 GRE 3D) with the following parameters: coronal as well as transverse sequentially, matrix 256x256x42 with dimensions 0.23x0.23x0.5 mm³, TR: 15 ms, TE: 2.9 ms, and a flip angle of 25°. PET scans with ^{18}F-FDG as well as ^{18}F-glutamate were performed for 20 min starting 1 hour after injection of the tracer. The uptake of ^{18}F-FDG as well as ^{18}F-glutamate in the tumor tissue of the liver and spleen was determined by manual contouring of a volume-of-interest (VOI) of the PET image using PMOD 3.5 (PMOD Technologies Ltd., Switzerland). Furthermore, the uptake in the thigh muscle of the hind limb was taken as reference value to assess differences in tracer distribution volume between animals. An average standardized uptake value (SUV) was computed from the 10 hottest voxels regardless of their location within the FDG- and glutamate positive lesions (SUVmax10), which is not influenced by heterogenous tracer uptake within

the tumor. Additionally, the SUVmax10 of the tumor lesions was normalized to the uptake of the thigh muscle according to the formula: SUVratio = SUVmax10 tumor / SUVmax10 muscle. This served as cross-check to correct for changes in the distribution volume e.g. animal size or reduced renal function in mice, which influences tumor SUVmax10.

3.15.4 Animal tissue analyses

After sacrifice of animals, the spleen (the tumor implantation site) and the liver (the metastasis target organ) were removed, shock frozen in liquid nitrogen, and 10 µm-think cryosections (for DNA and RNA extraction) or 5 µm-thick cryosections (for immunohistochemistry - IHC) using ThermoScientific CryoStar NX50 microtome were performed. The cryosections were stored at -20°C till further use. For isolation of genomic DNA and total RNA 15-20 sections were used. Genomic DNA and total RNA were extracted using DNA/RNA/Protein extraction kit (Roboklon) according to manufacturer's instructions. After the extraction genomic DNA and RNA were stored at -20°C.

3.15.5 IHC

For IHC staining cryosections were thawed and circled with a Dako Pen (Agilent) and allowed to dry out for 30 minutes. The cryosections were washed with PBS and fixed with 4% paraformaldehyde in PBS for 10 minutes at room temperature. After fixation the cryosections were washed with PBS and quenched with 0.1 M glycin in PBS for 20 minutes. After the quenching the cryosections were washed with PBS and blocked for endogenous peroxidase with 3% H_2O_2 for 10 minutes. Then, the cryosections were again washed with PBS three times and permeabilized with 0.2% Triton-100 in PBS for 2 minutes, followed by blocking with 5% IgG-free albumin (Roth) for 1 hr at room temperature. After that anti-human CK-19 primary antibodies (see table 3.5) diluted 1:200 in 2.5% blocking buffer (IgG-free albumin in PBS) were added to cryosections and incubated in a humid chamber overnight at +4°C. After incubation with primary antibodies, cryosections were washed with PBS five times and secondary anti-rabbit antibodies diluted 1:500 in 2.5% blocking buffer were added. The cryosections were incubated with secondary antibodies for 1 hr at room temperature. After that the cryosections were washed with PBS ten times and stained with Dako DAB liquid (Agilent) for 2 minutes at room temperature. The cryosections were washed with distilled water and counterstained with hematoxylin (Roth) for 1 minute, followed by washing under running water. The slides were covered Dako Glycergel mounting medium (Agilent) and let to dry out overnight at room temperature. The tissue sections were imaged with Zeiss Axioplan2 microscope and analysed with AxioVision® software.

Table 3.5 List of antibodies used for IHC

	Target	Dilution	Antibody	Company and catalogue number
Primary antibodies	Anti- CK19	1:300	Rabbit polyclonal	OriGene (TA336845)
Secondary antibodies	Anti-rabbit	1:500	HRP conjugated	Promega (W401)

3.16 Statistical analysis

All statistical analyses were performed with GraphPad Prism version 6.01. The statistical analyses were performed using two-sided, two-tailed Student's t-test. The p values of less than 0.05 were defined as statistically significant.

PROJECT II: Identification of metabolic prognostic biomarkers for metachronous metastasis formation in the plasma of stage II CRC patients

3.17 Patient samples

Plasma samples were analyzed from patients who had no distant metastasis at the time of blood drawing and who were not treated with (neo)adjuvant therapy. Plasma was prepared within 2 hours of blood drawing according to a standard protocol. In the initial study plasma samples and tumor tissues were obtained from databank of Charité Comprehensive Cancer Center (CCCC) in Berlin. Fresh frozen tumor tissues were used. In total 9 plasma samples of non-metastasized (n=9) and 3 samples from metachronously metastasized (measured in triplicates n=9) CRC patients were analyzed. For tumor tissues 4 samples from non-metastasized and 5 samples from metachronously metastasized CRC patients were analyzed. In Colorectal cancer: chances for prevention through screening (Darmkrebs: Chancen der Verhütung durch Screening) (DACHS) study plasma samples were received from DACHS study initiated at German Cancer Research Center (DKFZ) in Heidelberg. In total 92 plasma samples of non-metastasized (n=50) and metachronously metastasized (n=42) stage II CRC patients were analyzed. All patients at both Berlin and Heidelberg sites gave written informed consent for their sample acquisition. No samples were excluded from analysis.

3.18 Metabolite extraction and raw data processing

In both initial and DACHS studies all samples were processed in a randomized order. In the initial study samples were processed as outlined in [158]. Briefly, samples in total volume of 100 µl each were extracted in 1.5 ml of methanol/chlormethane/water (1:2:1) (all from Sigma) and aliquots of the polar phase (150 µl and 450 µl for gas or liquid chromatography, respectively, coupled to mass spectrometry – GC-MS or LC-MS) and non-polar phase (450 µl) were evaporated and subjected for derivatization (for GC-MS) or re-suspended in a solvent (for LC-MS). GC-MS measurements were performed on GC-EI-TOF-MS, while LC-MS measurements were performed on LC-ESI-MS (Aquity, Waters, USA coupled to Exactive, Thermo, USA). In DACHS study samples in total volume of 50 µl each were mixed with 150 µL of methanol/methyl-tert-butylether (1:1) (all from Sigma), and subjected to protein precipitation at -20 °C for 20 minutes. The supernatant was mixed with 70 µL chloroform (Sigma), yielding polar and lipid fractions which were subjected to high resolution mass spectrometry. This subsequently resulted in four LC derived data sets – lipid polar (lp), lipid non-polar (ln), polar positive (pp) and polar negative (pn) data sets.

To combine measurement signals into spectra and to remove redundancies, including adducts, fragments and isotopes the measurement spectra was evaluated using xcms/CAMERA tool as described in [159,160]. Preliminary annotation of spectra was achieved using in-house software as reported in [161]. Batch and run order effects were removed using analysis of variance (ANOVA) based normalization [162]. The base peak ion of each spectrum was retained to build the raw data matrix, which was the basis for further statistical analyses. Vast missing values, which comprise less than 4% of the final data matrix, were treated as NA in all algorithms capable of handling missing values or were substituted using a PCA based approach as described in [163].

3.19 Statistical methods and classification

All analyses were conducted in the R statistical software framework [164] using various packages and self-written scripts. Significant differences between analyzed groups were visualized and identified using PCA (package 'pcaMethods') and ANOVA (package 'stats'). Decision tree (package 'rpart'[165]) and support vector machine (package 'e1071'[166]) models were computed using the respective packages according to the recommendations within the package documentation. Cross validation and sampling of replications was achieved using custom wrapper functions for the aforementioned packages. The statistical significance for metastasis-free and overall patient survival was calculated in GraphPad version 6.01 using Student's t-test. The p value of less than 0.05 was considered to be statistically significant.

4. RESULTS

PROJECT I: Elucidation of MACC1 role in CRC metabolism

4.1 MACC1 enhances surface GLUT1

4.1.1 MACC1 expression is upregulated by glucose

In gastric cancer, MACC1 had been shown to be upregulated by glucose depletion *in vitro,* while *in vivo* MACC1 led to increased ^{18}F-fluorodeoxyglucose (^{18}F-FDG) uptake. These contradicting findings prompted to check what is the effect of glucose on MACC1 expression in CRC. To begin with, MACC1 promoter activities using MACC1 wild type (wt) promoter construct or promoter constructs with Sp1, Ap1 or cEBP1 mutated binding sites were analyzed in HCT116 cells upon treatment with 0 mM, 2 mM and 10 mM glucose. Promoter activity of MACC1 wt construct was upregulated by increasing glucose concentrations (Fig.1, A). And this upregulation of MACC1 promoter activity was mediated by Sp1 binding site, but not by Ap1 or cEBP1 binding sites (Fig. 1, A).

Observation that MACC1 promoter activity was increased by glucose prompted to ask whether MACC1 mRNA and protein expression were also affected by glucose. To address this question, SW620, HCT116, HT29 and HCT15 cells were treated with 0 mM, 2 mM and 10 mM glucose and MACC1 mRNA and protein expression were analyzed. Increased concentration of glucose led to both increased MACC1 mRNA and protein expression in SW620, HCT116, HT-29 and HCT15 cell lines (Fig. 1, B).

4.1.2 MACC1 enhances cell proliferation in glucose replete conditions

Because MACC1 expression was the highest in SW620 cells and because this cell line was derived from lymph node metastatic site these cells were taken as a model system to study further MACC1-dependent metabolic processes unless other indicated.

The upregulation of MACC1 expression by glucose is not an exclusive effect of glucose since it is a well-known stimulus of expression of many genes, thereby increasing cell proliferation. It was questioned whether MACC1 once being upregulated by glucose can further increase cell proliferation. To address this question, lentiviral small hairpin (sh)RNA-mediated knockdown of MACC1 was performed in SW620 cells generating MACC1 wt (shcntl) and MACC1 knockdown (shMACC1) cells. SW620 shcntl and shMACC1 cells were treated with 0 mM, 2 mM and 10 mM glucose and cell proliferation was analyzed. In 0 mM glucose, MACC1 had no effect on cell proliferation, while in the presence of glucose (2 mM and 10 mM glucose) MACC1 enhanced cell proliferation (Fig. 1, C).

4.1.3 MACC1 enhances glucose depletion from cell growth medium

MACC1 mediated increase in cell proliferation in glucose replete conditions indicates that MACC1 wt cells may deplete nutrients, including glucose, faster compared to their counterparts. To check this, gas chromatography coupled to mass spectrometry (GC-MS) screening of metabolites of cell growth medium of SW620 shcntl and shMACC1 cells cultivated over 5 days was performed. It was assumed that those metabolites, which are supposed to enhance cell proliferation should be depleted over time. By GC-MS both uptaken and secreted metabolites were found. The top hits were defined by cut-off of fold change>2 and $p<0.05$. This cut-off was applied to a ratio of metabolite ion intensity at day 5 divided by day 0. In this way, among top uptaken metabolites glucose was identified. There were also top differentially secreted metabolites, such as citric acid, alanine beta and cysteine (Fig. 1, D). Gradual depletion of glucose in SW620 shcntl and shMACC1 cells from growth medium over 5 days of culture is shown on Fig. 1, E. These findings are in line with data published in [57,69], where authors found that MACC1 enhanced glucose uptake in gastric and hepatocellular cancers.

4.1.4 MACC1 does not alter basal GLUT1 expression

Increased depletion of glucose from cell growth medium by MACC1 wt cells prompted to check the expression of glucose transporters. In the cells 14 glucose transporters are distinguished, out of which only four transporters (GLUT1, GLUT2, GLUT3 and GLUT4) are known to transport specifically glucose, while the rest of the transporters transport other sugars or are not expressed in colon. GLUT1 is the most abundant glucose transporter and is ubiquitously expressed in many tissue types. In cancer, GLUT1 is recognized to be upregulated with the disease progression and is associated with poor patient survival.

In this context, the mRNA levels of GLUT1, GLUT2, GLUT3 and GLUT4 were assessed in SW620 shcntl and shMACC1 cells. GLUT1 and GLUT3 expressions were not found to be different between SW620 shcntl and shMACC1 cells; GLUT2 was not expressed in SW620; and GLUT4 was increased in shMACC1 cells, however its expression was three magnitudes smaller compared to GLUT1 or GLUT3 (Fig. 1, F). Because GLUT1 expression was the highest among tested transporters and because it is the most abundant glucose transporter, it was taken for further work. GLUT1 protein expression was assessed and it was found that on protein level there was no difference in GLUT1 expression between SW620 shcntl and shMACC1 cells (Fig. 1, G). These findings demonstrate that overall GLUT1 basal expression is not altered by MACC1.

4.1.5 MACC1 increases surface GLUT1

Considering that GLUT1 transporters reside within endosomal pool and therefore their basal expression is not representative of the amount of transporters incorporated into plasma membrane staining for surface GLUT1 was performed. MACC1 knockdown in SW620 cells led to reduced surface GLUT1 (Fig. 1, H), while overexpression of MACC1 in endogenously low MACC1 SW480 cells led to increase in surface GLUT1 (Fig. 1, K).

4.1.6 Increased surface GLUT1 is a vulnerability of MACC1 expressing cells

Because surface GLUT1 level positively correlated with MACC1 expression further functionality of this association needed to be investigated. For that, GLUT1 inhibitor WZB117 was applied to SW620 shcntl and shMACC1 cells and cell proliferation was assessed. The effect of GLUT1 inhibition was much stronger in MACC1 wt compared to MACC1 knockdown cells (Fig. 1, I). Similar effect was observed in SW480 cells, where treatment with WZB117 reduced cell proliferation of MACC1 overexpressing cells to a greater extent compared to their counterparts (Fig. 1, L).

4.1.7 GLUT1 inhibitor WZB117 reduces MACC1 expression

Because reduction of glucose concentration in cell growth medium as shown on Fig. 1, A-B led also to reduced MACC1 expression treatment with GLUT1 inhibitor WZB117 was hypothesized to reduce MACC1 expression. Indeed, treatment with GLUT1 inhibitor WZB117 led to reduced MACC1 expression in SW620 cells (Fig.1, J), but not in SW480 cells (Fig. 1, M), possibly because MACC1 overexpressing construct was lacking Sp1 binding site, which was shown to mediate glucose-dependent increase in MACC1 promoter activity (Fig .1, A).

Taken together, these results demonstrate the presence of positive feedback loop, where MACC1 once being upregulated by glucose enhances surface GLUT1 leading thereby to increased glucose consumption and thus increased proliferation. And, importantly, targeting of GLUT1 in MACC1 expressing cells yields stronger effect on cell proliferation thus representing MACC1-mediated metabolic vulnerability of CRC cells.

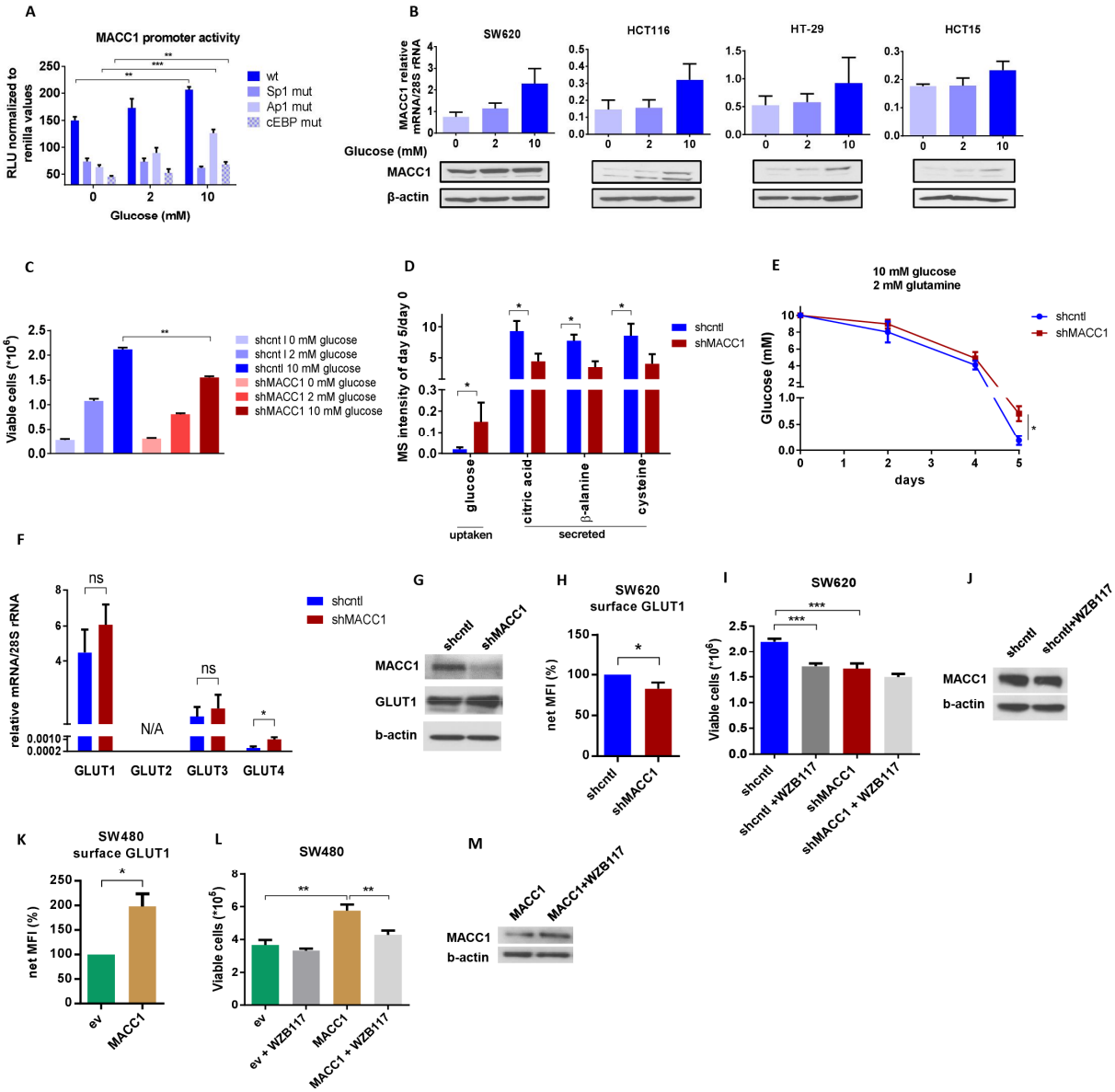

Fig. 1 MACC1 enhances surface GLUT1. (A) Promoter activity of MACC1 wt construct or with indicated mutated binding sites was measured in HCT116 cells treated with 0 mM, 2 mM and 10 mM of glucose. (B) MACC1 mRNA and protein expression in SW620, HCT116, HT29 and HCT15 cells treated with 0 mM, 2 mM and 10 mM of glucose. (C) Cell viability of SW620 wt (shcntl) and MACC1 knockdown (shMACC1) cells treated with 0 mM, 2 mM and 10 mM of glucose. (D-E) GC-MS screening of growth medium metabolites after 5 days of culture of SW620 shcntl and shMACC1 cells grown in nutrient-replete medium (10 mM glucose/2 mM glutamine). (D) Top uptaken and secreted metabolites by SW620 shcntl and shMACC1 cells. (E) Gradual depletion of glucose from (D) over 5 days. (F) MRNA levels of GLUT1, GLUT2, GLUT3 and GLUT4 in SW620 shcntl and shMACC1 cells. (G) GLUT1 total and (H) surface expresssion in SW620 shcntl and shMACC1 cells. (I) Cell viability of SW620 shcntl and shMACC1 cells

treated with GLUT1 inhibitor WZB117. (J) MACC1 expression of SW620 shcntl cells treated with WZB117. (K) GLUT1 surface expression in SW480 empty vector (ev) and MACC1 overexpressing (MACC1) cells. (L) Cell viability of SW480 ev and MACC1 cells treated with WZB117. (M) MACC1 expression of SW480 MACC1 cells treated with WZB117. *, $p<0.05$; **, $p<0.001$; ***, $p<0.0001$. Data are representative of a mean ±SEM of at least three independent experiments, for GC-MS screening n=3 technical replicates.

4.2 MACC1 increases glucose flux throughout glycolysis, pentose phosphate pathway (PPP) and TCA

Because MACC1 enhanced glucose depletion from cell growth medium thereby increasing cell proliferation it was of interest to check whether MACC1 also altered glucose distribution within the metabolic pathways. To address this question uniformly labeled $^{13}C_6$ glucose was introduced to SW620 shcntl and shMACC1 cells and GC-MS-based metabolic profiling of cells and cell growth medium after 24 hr of incubation with $^{13}C_6$-labeled glucose was performed. To check whether MACC1 affected glucose distribution within the metabolic pathways the comparison of metabolite labeling patterns between the SW620 shcntl and shMACC1 cells was performed. In this and further ^{13}C metabolomics experiments (chapters 4.7 and 4.9) the metabolites were considered to be ^{13}C abundant if at least 10% of metabolite isotopomer contained ^{13}C. Overall, the ^{13}C carbon from glucose was found in glycolytic, TCA intermediates, within PPP (ribose), nucleotides and amino acids (Fig. 2, A). The percentage of ^{13}C labeled isotopologues was higher among glycolytic metabolites, citrate, malate, ribose and alanine (Fig.2, A-R). When comparing overall percentage of ^{13}C labeled isotopologues it was higher in shcntl cells for all metabolites compared to shMACC1 cells, what is in line with previous findings of increased glucose uptake by MACC1, thus explaining increased flux from glucose in MACC1 expressing cells. The percentage of ^{13}C labeled isotopologues in the cells correlated with such percentage in cell growth medium, where overall it was also higher in shcntl compared to shMACC1 cells (Fig. 2, A). Glutamate was found to be synthesized from glucose to 20% even in glutamine rich (2 mM) environment (Fig. 2, A). ^{13}C labeled pyruvate, ribose, glutamate, asparagine, glycerate, serine and glutamate were found in cell growth medium possibly because of their secretion or cell disrupture during the cell death (Fig. 2, A).

The TCA intermediates such as α-ketoglutarate, succinate and fumarate were derived from glucose only to 20-30% (Fig. 2, I-K), indicating the presence of other sources of their biosynthesis. Fructose which is supposed to be generated presumably from glucose was labeled to approximately 25-50% (M+5 and M+6) (Fig. 2, C), meaning that it was also produced from other than glucose sources. Probably the most astonishing finding was that ^{13}C-labeled serine was found presumably in shcntl but not in shMACC1 cells (Fig. 2, A and R). While serine is normally present in cell growth medium SW620 shcntl cells produce it

from glucose, while shMACC1 cells synthesize it from other unlabeled substrates. Fig. 2, S summarizes the distribution of $^{13}C_6$ glucose within the metabolic pathways in SW620 cells.

In conclusion, MACC1 increases the flux of glucose-derived glycolytic, TCA intermediates, ribose and amino acids, and exclusively enables serine production from glucose. The $^{13}C_6$ glucose is distributed to 80% within glycolysis and PPP, while to 20% within citrate, which when exported from mitochondria to be used for fatty acid production leaves even less glucose-derived carbon for the TCA, thus bringing a need for glutamine to replenish the lack of carbon in the TCA.

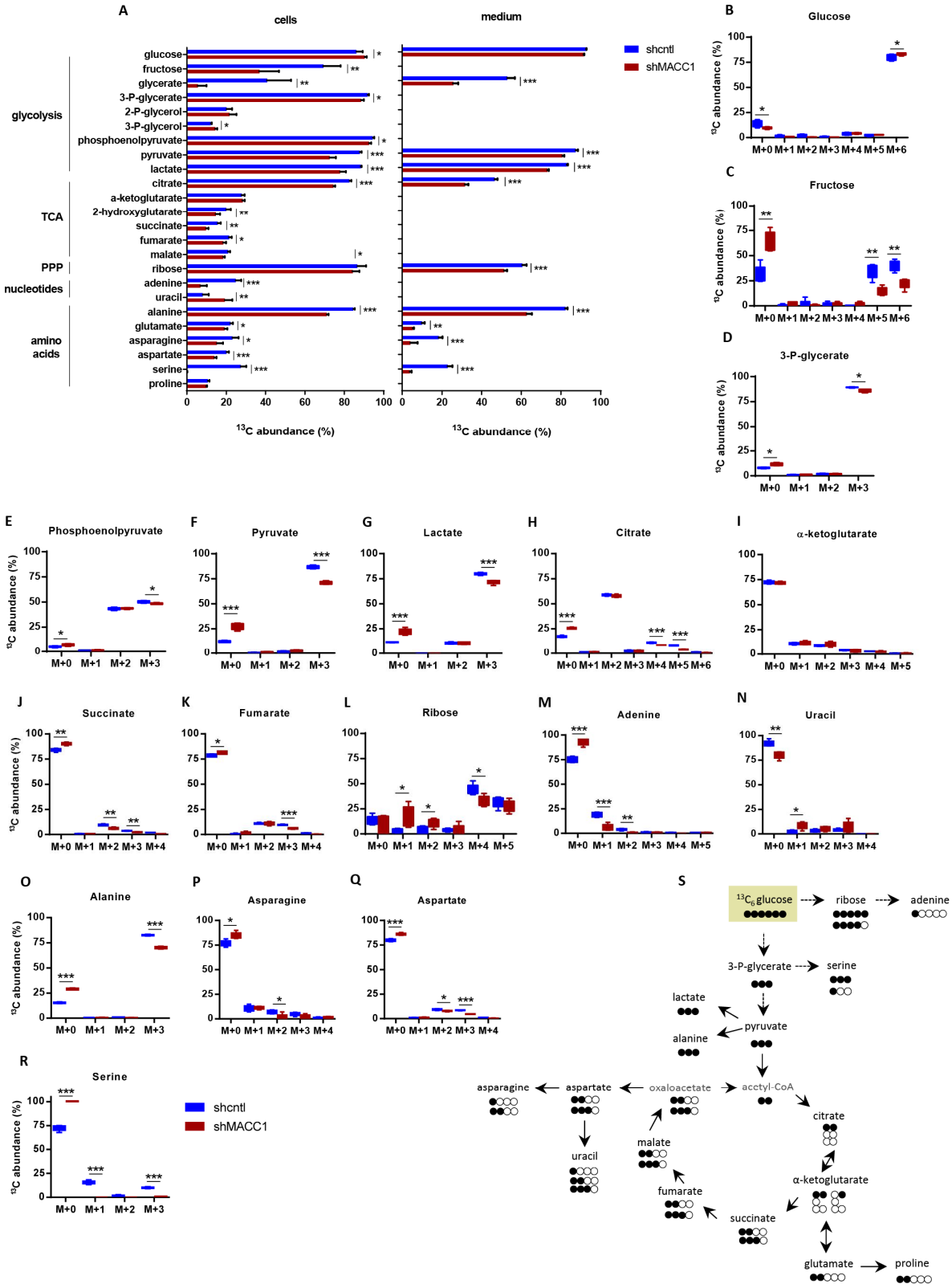
A
cells
medium
shcntl
shMACC1
glycolysis
TCA
PPP
nucleotides
amino acids
glucose
fructose
glycerate
3-P-glycerate
2-P-glycerol
3-P-glycerol
phosphoenolpyruvate
pyruvate
lactate
citrate
a-ketoglutarate
2-hydroxyglutarate
succinate
fumarate
malate
ribose
adenine
uracil
alanine
glutamate
asparagine
aspartate
serine
proline
13C abundance (%)
B
Glucose
C
Fructose
D
3-P-glycerate
E
Phosphoenolpyruvate
F
Pyruvate
G
Lactate
H
Citrate
I
α-ketoglutarate
J
Succinate
K
Fumarate
L
Ribose
M
Adenine
N
Uracil
O
Alanine
P
Asparagine
Q
Aspartate
R
Serine
S
13C6 glucose
ribose
adenine
3-P-glycerate
serine
lactate
pyruvate
alanine
asparagine
aspartate
oxaloacetate
acctyl-CoA
citrate
α-ketoglutarate
malate
uracil
fumarate
succinate
glutamate
proline

Fig. 2 Metabolic tracing of $^{13}C_6$ glucose. SW620 shcntl and shMACC1 cells were maintained in nutrient rich conditions (10 mM glucose/2 mM glutamine) and treated with $^{13}C_6$ glucose for 24 hr. (A) The abundance of ^{13}C isotopologues in cells and cell growth medium. (B-R) Metabolite isotope distribution within (B) glucose, (C) fructose, (D) 3-P-glycerate, (E) phosphoenolpyruvate, (F) pyruvate, (G) lactate, (H) citrate, (I) α-ketoglutarate, (J) succinate, (K) fumarate, (L) ribose, (M) adenine, (N) uracil, (O) alanine, (P) asparagine, (Q) aspartate and (R) serine. M plus consecutive number stands for mass shift on that number of atoms. (S) Scheme summarizing $^{13}C_6$ glucose distribution based on ^{13}C enrichment within the cells. The most abundant ^{13}C isotopologues of metabolites are shown. Each circle represents one carbon. Filled circles: ^{13}C carbon. Unfilled circles: ^{12}C carbon. Oxaloacetate and acetyl-CoA are not detected by GC-MS. *, $p<0.05$; **, $p<0.001$; ***, $p<0.0001$. Data are representative of a mean ±SD, n=5.

4.3 MACC1 reduces mitochondrial respiration and spare respiratory capacity

Because of increased production of glucose-derived metabolites it was hypothesized that the glycolysis and mitochondrial respiration as functional read-outs may be also increased. Measurement of oxygen consumption rate (OCR) and extracellular acidification rate (ECAR) had demonstrated that, surprisingly, SW620 shcntl cells were less energetic compared to shMACC1 cells (Fig. 3, A-B). Application of ATP synthase inhibitor oligomycin and mitochondrial uncoupler FCCP yielded higher increase in respiration in SW620 shMACC1 cells compared to shcntl cells (Fig. 3, A and C). Conversely, overexpression of MACC1 in SW480 cells resulted in reduction of respiration upon oligomycin and FCCP treatment (Fig. 3, D and F). Although, MACC1 knockdown resulted in increased ECAR in SW620 cells (Fig. 3, B), overexpression of MACC1 in SW480 cells could not reverse this effect (Fig. 3, E). One of the reasons of this observation may be that the ECAR should not be treated as pure glycolysis readout because, besides glucose derived lactate, bicarbonate which is produced in high amounts by actively respiring mitochondria can also contribute to ECAR. Therefore, the contribution to ECAR depends on the ratio between glycolytic activity and mitochondrial respiration. If the amount of bicarbonate produced by mitochondria is higher than the amount of lactate contributing to ECAR the cells will show higher ECAR without being glycolytic.

Mitochondrial respiration is coupled to mitochondrial ATP production. In SW620 shMACC1 cells mitochondria derived ATP was increased compared to shcntl cells (Fig. 3, G). Overexpression of MACC1 in SW480 cells reversed this effect leading to a reduction of mitochondria derived ATP (Fig. 3, J). The observation that mitochondria derived ATP was increased in SW620 shMACC1 cells while total ATP remained unchanged between shcntl and shMACC1 cells (Fig. 3, H), and the fact that shcntl cells depleted glucose from cell growth medium faster compared to their counterparts (Fig. 1, D-E) hinted that reduced respiration and hence mitochondrial ATP production may act as a compensation for

increased glucose uptake. Indeed, treatment of SW620 shcntl cells with GLUT1 inhibitor WZB117 led to increased total ATP production (Fig. 3, F). In SW480 cells total ATP was reduced by MACC1 overexpression (Fig. 3, K) and treatment of MACC1 overexpressing cells with WZB117 did not affect total ATP production (Fig. 3, L). This suggests that in SW480 cells MACC1 mediates removal of glucose-derived carbon to other metabolic pathways outside of glycolysis and therefore glucose is not used in reactions of glycolysis which generate ATP. In addition, this hints that TCA is fed almost exclusively by glutamine in MACC1 overexpressing cells.

Taken together, these results demonstrate that MACC1 reduces mitochondrial respiration and mitochondrial ATP production, and as judged by spare respiratory capacity mitochondrial respiration in MACC1 expressing cells is fully turned on ATP production.

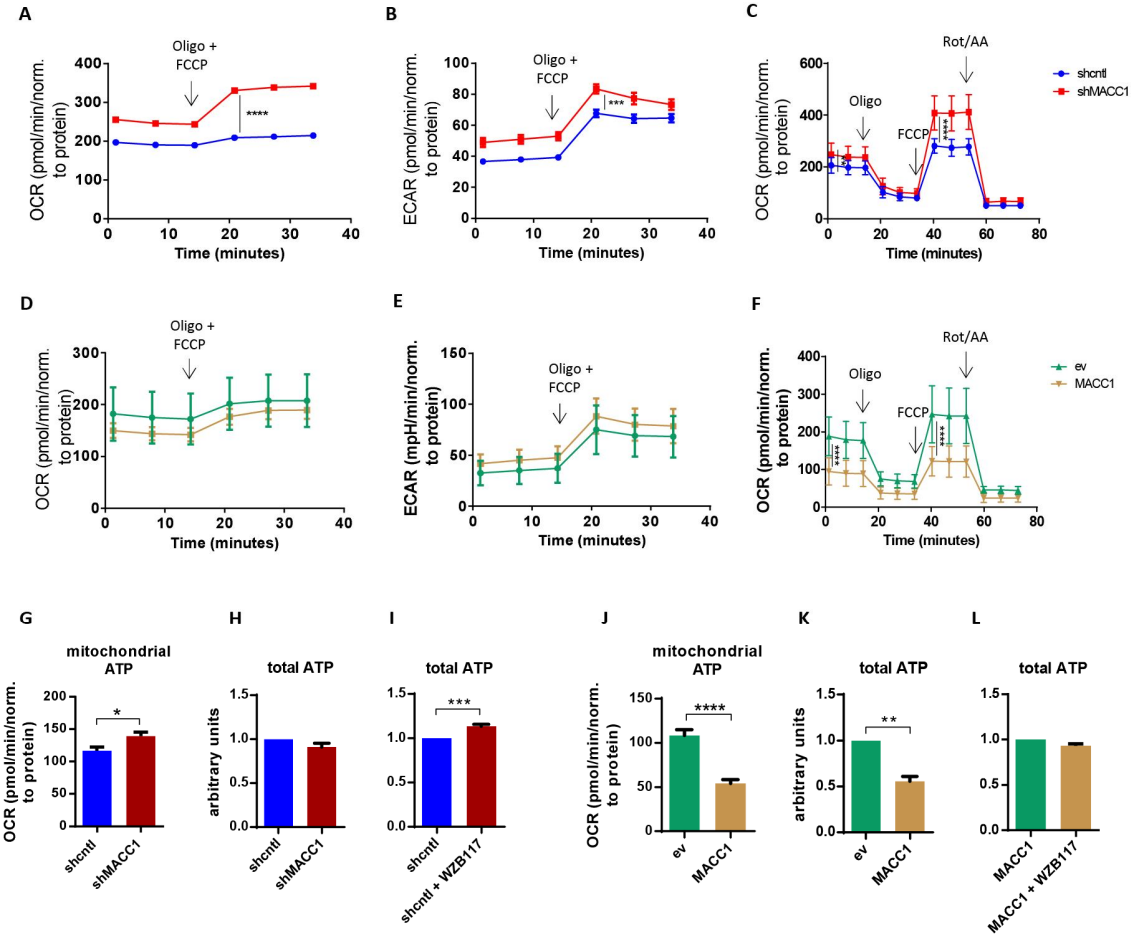

Fig. 3 MACC1 decreases mitochondrial respiration and spare respiratory capacity. (A) Oxygen consumption rate (OCR) and (B) extracellular acidification rate (ECAR) of SW620 shcntl and shMACC1 cells treated with the mixture of oligomycin (Oligo) and FCCP. (C) OCR of cells as in (A-B) treated with oligo, FCCP and rotenone/antimycin A (rot/AA). (D) OCR and (E) ECAR of SW480 empty vector (ev) and MACC1 overexpressing (MACC1) cells treated with the mixture of oligo and FCCP. (F) OCR of cells as in (D-E) treated with oligo, FCCP and rotenone/antimycin A (rot/AA). (G) Mitochondrial and (H) total ATP without or (I) with GLUT1 inhibitor WZB117 in SW620 shcntl and shMACC1 cells. (J) Mitochondrial and (K) total ATP without or (L) with GLUT1 inhibitor WZB117 in SW480 ev and MACC1 cells. *, $p<0.05$; **, $p<0.001$; ***, $p<0.0001$. Data are representative of a mean ±SEM of at least three independent experiments.

4.4 Outline of further metabolic studies

Because cancer metabolic studies are mostly about metabolic flexibility in burning fuels depending on the environmental conditions it was of interest to investigate the effect of MACC1 on utilization of

various metabolic substrates including glutamine, pyruvate, lactate and fatty acids. The outline of further studies is presented on Fig. 4, A. First, MACC1-dependent cell proliferation was assessed in various nutrient conditions. It was assumed that in some conditions MACC1 did not support cell proliferation, and in some conditions MACC1 enhanced cell proliferation. Those conditions in which MACC1 enhanced cell proliferation were considered as positive hits. Then, to find out how MACC1 enhanced utilization of certain nutrients in positive hit conditions nutrient depletion studies and metabolic distribution using ^{13}C labeled metabolic substrates were performed. This was followed by target selection and its drug application in positive hit conditions (Fig. 4, A), followed by animal experiments. Working according to this outline the relation of MACC1 to glutamine utilization was assessed first.

4.5 MACC1 enhances glutamine utilization in glucose depleted conditions partially through enhanced glutamine depletion

4.5.1 MACC1 enhances glutamine utilization in glucose depleted conditions

Glutamine, after glucose, is a second most important nutrient used by cells to build up precursors necessary for cell growth and survival. It was of interest to examine how important is glutamine for MACC1-dependent cell proliferation. Because PIK3CA mutation had been reported to sensitize colon cancer cells to glutamine depletion [167] to rule out the effect of PIK3CA mutation on MACC1-dependent glutamine utilization PIK3CA wild type SW620 cells and PIK3CA mutant HCT116 cells were taken for further work. SW620 shcntl and shMACC1 cells and HCT116 shcntl and shMACC1 were subjected to high glucose (10 mM), low glucose (2 mM) and no glucose (0 mM) environment and treated with various glutamine concentrations. In glucose abundant and glutamine depleted conditions MACC1 had no effect on cell proliferation in both SW620 and HCT116 cells (Fig. 4, B-C, E-F). However, in glucose and glutamine abundant conditions MACC1 supported cell proliferation (Fig. 4, B-C, E). Interestingly, in glucose depleted conditions and with reduced glutamine concentration to physiological range (0.5 – 1 mM) MACC1 supported glutamine utilization as is judged by enhanced cell viability of SW620 shcntl cells and HCT116 shcntl cells compared to their counterparts (Fig. 4, D, G). Out of these cell proliferation/viability studies 10 mM glucose/2 mM glutamine and 0 mM glucose/1 mM glutamine conditions were considered as positive hits.

4.5.2 MACC1 enhances glutamine depletion from cell growth medium in glucose depleted conditions

To find out whether in identified as positive hit conditions MACC1 had an effect on glutamine depletion the latter was assessed in SW620 shcntl and shMACC1 cells. In 10 mM glucose/2 mM glutamine

conditions as demonstrated previously by GC-MS screening MACC1 had no effect on glutamine depletion from cell growth medium (Fig. 4, H), whereas in 0 mM glucose/1 mM glutamine conditions MACC1 enhanced glutamine depletion (Fig. 4, I).

4.5.3 Glutaminase inhibition does not yield MACC1-dependent effect on cell proliferation

Though in 10 mM glucose/2 mM glutamine conditions MACC1 did not alter glutamine uptake (Fig. 4, H), this did not exclude the possibility that MACC1 may affect glutaminolysis in given conditions. To assess the effect of MACC1 on cell viability upon inhibition of glutamine utilizing enzymes SW620 shcntl and shMACC1 cells were treated with DON inhibitor. Upon treatment with DON inhibitor cell viability of both SW620 shcntl and shMACC1 cells was reduced to a similar extent (Fig. 4, J), suggesting that glutamine is important for SW620 cells, however there is no MACC1-dependent effect on cell viability.

Together these findings demonstrate: 1) if both glucose and glutamine are abundant in the environment MACC1 acts as a modulator of glucose and glutamine metabolism; 2) in cases where one of the nutrients either glucose or glutamine is not present in the environment MACC1 does not provide advantage to cell viability to substitute their lack; 3) in glucose depleted conditions MACC1 supports glutaminolysis to increase cell survival partially through enhanced glutamine depletion.

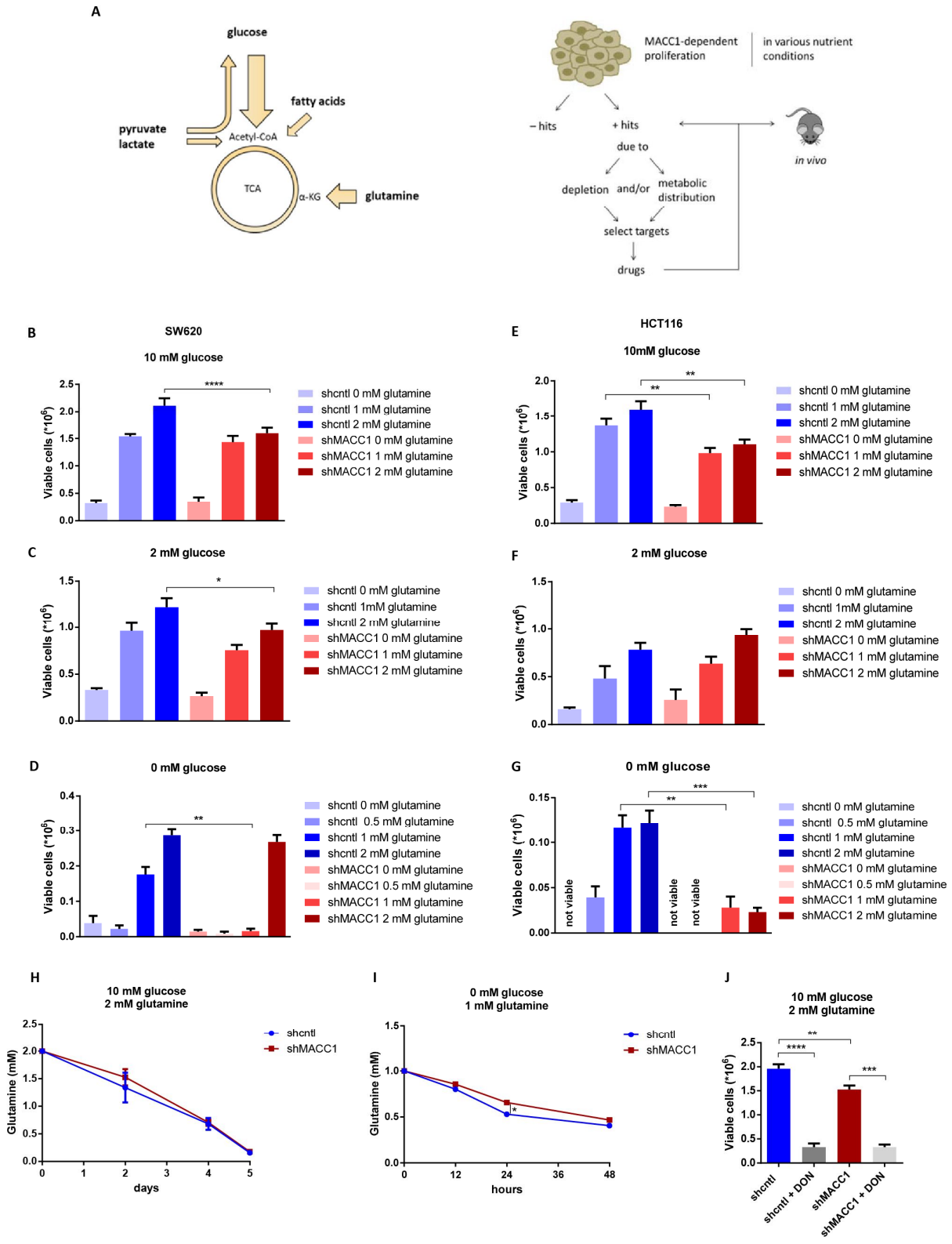

Fig. 4 Impact of MACC1 on glutamine utilization. (A, left) Schematic drawing of metabolic pathways fed by indicated nutrients. (A, right) Outline of workflow to identify MACC1-dependent nutrient conditions

affecting cell proliferation. MACC1-dependent cell proliferation is investigated in various nutrient conditions. Those conditions where MACC1 does not increase proliferation are considered as negative hits, those conditions in which MACC1 supports cell proliferation are considered as positive hits. In positive hit conditions further depletion and metabolic distribution studies are performed. Depending on the results of depletion and metabolic distribution studies targets and their drugs are selected and applied to positive hit conditions, followed by animal experiments. (B-D) Cell viability of SW620 shcntl and shMACC1 cells treated in high (B), low (C) and no glucose (D) conditions with various glutamine concentrations. (E-G) Cell viability of HCT116 shcntl and shMACC1 cells treated in high (E), low (F) and no glucose (G) conditions with various glutamine concentrations. (H) Glutamine depletion from cell growth medium of SW620 shcntl and shMACC1 cells after 5 days of culture in nutrient-replete medium. (I) Glutamine depletion from cell growth medium of SW620 shcntl and shMACC1 cells after 48 hours of culture in indicated conditions. (J) Cell viability of SW620 shcntl and shMACC1 cells grown in basal medium and treated with an inhibitor of glutamine utilizing enzymes DON. *, $p<0.05$; **, $p<0.001$; ***, $p<0.0001$. Data are representative of a mean ±SEM of at least three independent experiments.

4.6 Impact of MACC1 on transcription of metabolism related genes and on *de novo* glutamate synthesis

Because MACC1 had shown to possess multiple effects on CRC metabolism it was of interest to investigate whether those effects were caused by altered transcription of metabolism related genes. On this basis, the mRNA expression of genes involved in glycolysis (pyruvate kinase isoform M2, PKM2; lactate dehydrogenase A, B or C chain, LDHA, LDHB or LDHC; hexokinase 1 or 2, HK1 or HK2; 6-phosphofructokinase, PFKM), glutaminolysis (glutaminase, GLS; glutamate dehydrogenase 1 or 2, GLUD1 or GLUD2), pentose phosphate pathway (glucose-6-phosphate 1-dehydrogenase, G6PD), reactions of transamination (aspartate aminotransferase 1 or 2, GOT1 or GOT2), tricarboxylic acid cycle (isocitrate dehydrogenase 1 or 2, IDH 1or IDH2; isocitrate dehydrogenase subunit alpha, IDH3a), branching points (pyruvate dehydrogenase kinase 1, 2, 3 or 4, PDK1, PDK2, PDK3 or PDK4; pyruvate carboxylase, PC; malic enzyme, ME1), malate-aspartate shuttle (malate dehydrogenase 1 or 1B, MDH1 or MDH1B) and gene involved in regulation of metabolic pathways (Myc proto-oncogene protein, MYC (c-MYC)) were investigated in SW620 shcntl and shMACC1 cells in 10 mM glucose/2 mM glutamine conditions.

Genes involved in malate-aspartate shuttle (MDH1 and MDH1B) and LDHC were not expressed in SW620 cells (Fig. 5, A). MRNA level of c-MYC was increased in SW620 shcntl cells compared to shMACC1 cells; PC was unchanged between the cell lines; while the rest of tested genes were upregulated in shMACC1 cells compared to shcntl cells.

These findings demonstrate that MACC1 does not influence cell metabolism through increased expression of metabolism related genes, at least as tested in nutrient-replete conditions with high glucose and glutamine abundance.

De novo glutamate synthesis had been reported to provide an advantage in cell survival upon treatment with glutaminase inhibitors [84]. The potential of MACC1 to support *de novo* glutamate synthesis in conditions of glutamine depletion was examined in SW620 shcntl and shMACC1 cells and in HCT116 shcntl and shMACC1 cells in low glucose (2 mM) and glucose depleted (0 mM) conditions. Treatment of SW620 shcntl and shMACC1 and HCT116 shcntl and shMACC1 cells with α-ketoglutarate and non-essential amino acids, substrates essential for the *de novo* glutamate synthesis, did not substitute glutamine withdrawal in low glucose conditions as judged by cell viability (Fig. 5, B and D). Similar treatment of SW620 shcntl and shMACC1 cells in glucose depleted conditions resulted in reduced viability of SW620 shcntl cells compared to shMACC1 cells (Fig. 5, C), indicating that in SW620 cells MACC1 restricted *de novo* glutamate synthesis in glucose depleted conditions. Treatment of HCT116 shcntl and shMACC1 cells with α-ketoglutarate and non-essential amino acids in glucose and glutamine depleted conditions did not substitute glutamine withdrawal (Fig. 5, E).

These findings indicate that upon low glucose (2 mM) conditions MACC1 does not influence *de novo* glutamate synthesis, while upon glucose depleted conditions (0 mM) the effect of MACC1 on the *de novo* glutamate synthesis is inconsistent among tested cell lines.

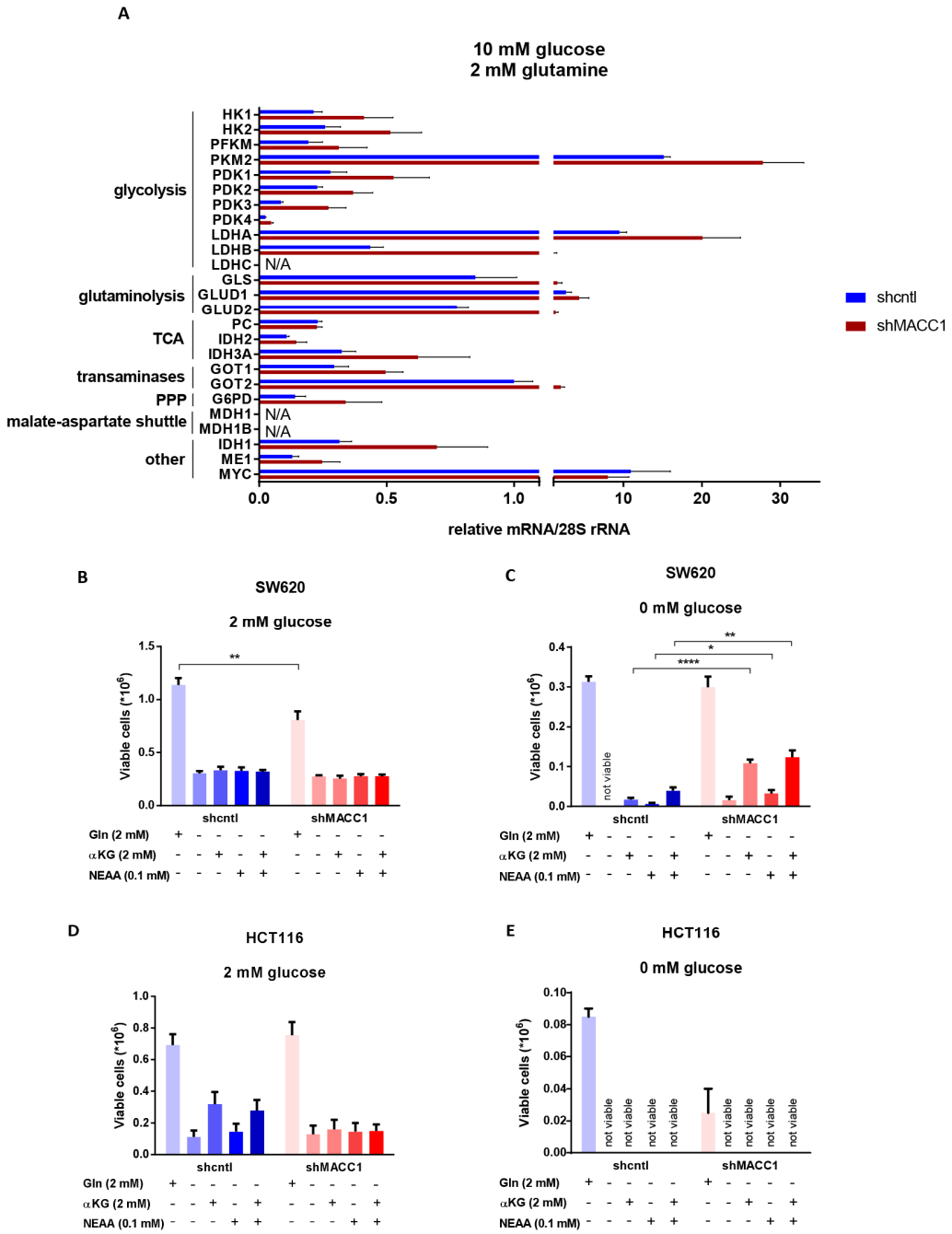

Fig.5 Impact of MACC1 on transcription of metabolism related genes and on *de novo* glutamate synthesis. (A) MRNA expression of indicated genes as determined by RT-qPCR and normalized by 28S rRNA in SW620 shcntl and shMACC1 cells grown in indicated conditions. N/A: gene not expressed. (B-E) Cell viability of (B-C) SW620 shcntl and shMACC1 cells and (D-E) HCT116 shcntl and shMACC1 cells treated as indicated in (B, D) low glucose and (C, E) glucose depleted conditions. *, $p<0.05$; **, $p<0.001$; ***, $p<0.0001$. Data are representative of a mean ±SEM of at least three independent experiments.

4.7 MACC1 reduces glutamine flux independent of nutrient availability

To investigate the effect of MACC1 on glutamine distribution within metabolic pathways uniformly labeled $^{13}C_5$ glutamine was applied to SW620 shcntl and shMACC1 cells grown in nutrient-replete environment (10 mM glucose/2 mM glutamine). Metabolic profiling of cells and growth medium 24 hr after incubation with $^{13}C_5$ glutamine was performed. Glutamine-derived ^{13}C carbon was found within the TCA metabolites and those amino acids, nucleotides and polyamines whose synthesis is related to TCA (Fig. 6, A-B). In the cells overall MACC1 reduced the percentage of ^{13}C labeled isotopologues within glutamate, citrate, fumarate, malate, proline and aspartate (Fig. 6, A). Glutamine-derived metabolites were vastly found in the medium, including *de novo* synthesized asparagine and their percentage in the medium including the ratio between shcntl and shMACC1 cells was comparable to such one within the cells (Fig. 6, A). This indicates that first, glutamine is used to acidify microenvironment by secretion of glutamine-derived acidic TCA intermediates to the medium and second, that those secreted metabolites may potentially be used by nearby starving cells in times when nutrient supply is insufficient. As judged by metabolite isotope distribution MACC1 generally reduced the percentage of ^{13}C labeled isotopologues in most of glutamine-derived metabolites (Fig.6, A-C, F and H-K) with the exception of α-ketoglutarate (M+4), 2-hydroxyglutarate (M+5), citrate (M+5), succinate (M+4), fumarate (M+3), malate (M+3), proline (M+5) and aspartate (M+3), where MACC1 increased their production. Asparagine, uracil and putrescine were not significantly different between the cell lines (Fig. 6, L-N). Schematically glutamine distribution within the metabolic pathways in nutrient-replete conditions is presented on Fig. 6, O.

Further, because of strong differences in cell viability between SW620 shcntl and shMACC1 cells and HCT116 shcntl and shMACC1 cells in 0 mM glucose and 1 mM glutamine conditions defined in chapter 4.5.1 as positive hit conditions (Fig. 4, D and G) it was of interest to investigate whether MACC1 influenced glutamine utilization through altered glutamine flux. To address this question, $^{13}C_5$ glutamine was applied to SW620 shcntl and shMACC1 cells in nutrient deprived (0 mM glucose/1 mM glutamine) conditions. Metabolic profiling of cells and growth medium 24 hr after incubation with $^{13}C_5$ glutamine was performed. Generally, metabolic profile and the effect of MACC1 on it were comparable to nutrient-replete conditions (Fig. 6), where MACC1 reduced the percentage of ^{13}C labeled isotopologues for most of glutamine-derived metabolites (Fig. 7, A). Glutamine-derived metabolites in the medium were found with the ratio between SW620 shcntl and SW620 shMACC1 cells comparable to such one within the cells (Fig. 7, A). The labeling pattern in nutrient deplete conditions was stronger compared to nutrient-replete conditions in terms of differences between SW620 shcntl and SW620 shMACC1 cells (Fig. 7, C-N). MACC1

increased the percentage of ^{13}C labeled isotopologues for glutamate (M+4 and M+5), α-ketoglutarate (M+4 and M+5), fumarate (M+4), malate (M+4) and aspartate (M+4) (Fig. 7, C-D, G-H, K). Interestingly, under nutrient depletion pyruvate and alanine started to be synthesized from glutamine (Fig. 7, A, I-J), demonstrating metabolic rewiring and enhanced need in these metabolites for cell survival.

In conclusion, MACC1 reduced glutamine flux independent of nutrient availability. Upon nutrient repletion glutamine was used to feed TCA cycle, while upon nutrient depletion glutamine in addition served as a precursor of pyruvate and alanine production in SW620 cells.

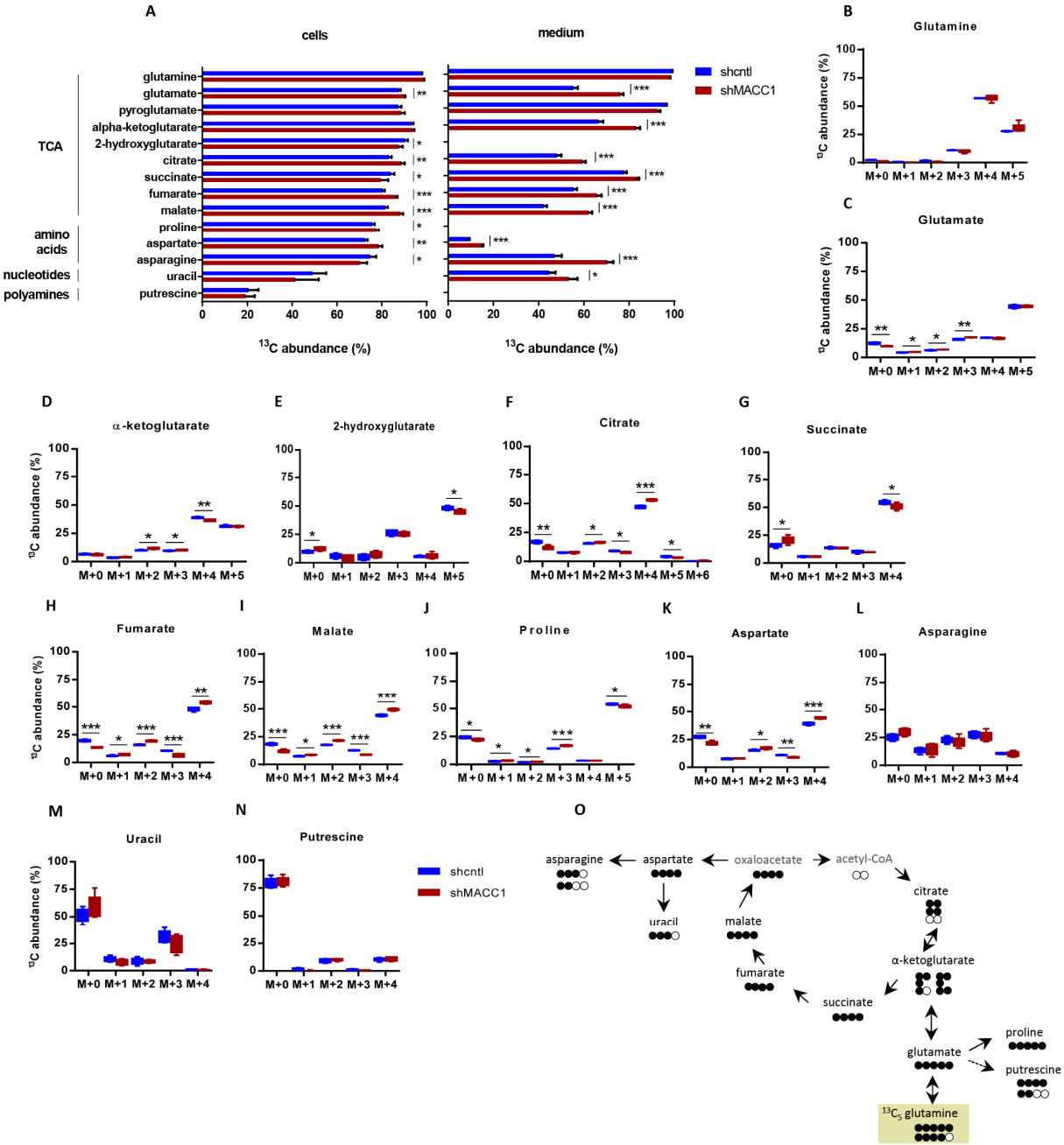

Fig.6 Metabolic tracing of $^{13}C_5$ glutamine in nutrient-replete (10 mM glucose/2 mM glutamine) conditions. SW620 shcntl and shMACC1 cells were grown in nutrient-replete (10 mM glucose/2 mM glutamine) conditions and treated with $^{13}C_5$ glutamine for 24 hr. (A) The abundance of ^{13}C isotopomers in cells and cell growth medium. (B-N) Metabolite isotope distribution within (B) glutamine, (C) glutamate, (D) α-ketoglutarate, (E) 2-hydroxyglutarate, (F) citrate, (G) succinate, (H) fumarate, (I) malate, (J) proline, (K) aspartate, (L) asparagine, (M) uracil and (N) putrescine metabolites measured in the cells. M plus consecutive number stands for mass shift on that number of atoms. (O) Scheme summarizing $^{13}C_5$ glutamine distribution based on ^{13}C abundance within the cells. The most abundant ^{13}C containing

isotopomers are shown. Each circle represents one carbon. Filled circles: ^{13}C carbon. Unfilled circles: ^{12}C carbon. Oxaloacetate and acetyl-CoA are not detected by GC-MS. *, p<0.05; **, p<0.001; ***, p<0.0001. Data are representative of a mean ±SD, n=5.

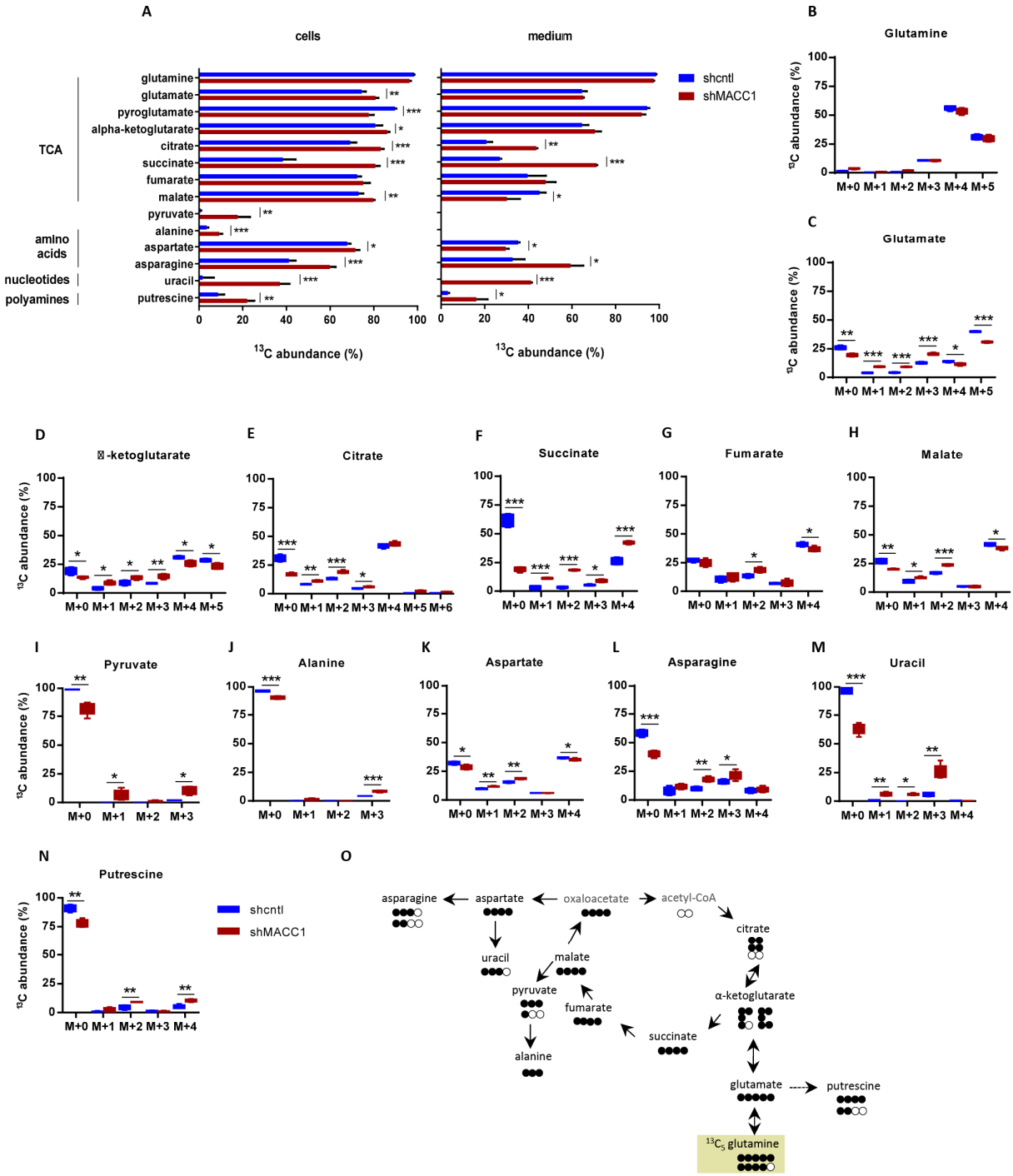

Fig. 7 Metabolic tracing of $^{13}C_5$ glutamine in nutrient depleted (0 mM glucose/1 mM glutamine) conditions. SW620 shcntl and shMACC1 cells were grown in nutrient depleted (0 mM glucose/1 mM glutamine) conditions and treated with $^{13}C_5$ glutamine for 24 hr. (A) The abundance of ^{13}C isotopomers in cells and cell growth medium. (B-N) Metabolite isotope distribution within (B) glutamine, (C) glutamate, (D) α-ketoglutarate, (E) citrate, (F) succinate (G) fumarate (H) malate (I) pyruvate, (J) alanine, (K) aspartate, (L) asparagine, (M) uracil and (N) putrescine metabolites measured in the cells. M plus consecutive number stands for mass shift on that number of atoms. (O) Scheme summarizing $^{13}C_5$ glutamine distribution based on ^{13}C abundance within the cells. The most abundant ^{13}C containing isotopomers are shown. Each circle represents one carbon. Filled circles: ^{13}C carbon. Unfilled circles: ^{12}C carbon. Oxaloacetate and acetyl-CoA are not detected by GC-MS. *, $p<0.05$; **, $p<0.001$; ***, $p<0.0001$. Data are representative of a mean ±SD, n=5.

4.8 MACC1 enhances pyruvate utilization in glucose depleted conditions through enhanced pyruvate depletion

4.8.1 MACC1 promotes pyruvate and restricts lactate utilization in glucose depleted environment

Besides glucose and glutamine, pyruvate, lactate and fatty acids are known to enable cancer cell survival in nutrient stress conditions. In this context, it was examined whether MACC1 can provide advantage in utilization of pyruvate, lactate and palmitate used as alternative metabolic fuels in low (2 mM) glucose and glucose depleted (0 mM) environment in SW620 cells. In low (2 mM) glucose conditions MACC1 did not support any of the assessed alternative metabolic fuels (Fig. 8, A-C). In glucose depleted conditions MACC1 supported pyruvate utilization (Fig. 8, D) and restricted lactate utilization (Fig. 8, E), while having no effect on palmitate utilization (Fig. 8, F). The findings that MACC1 supported pyruvate utilization and restricted lactate utilization were confirmed in SW480 cells, where overexpression of MACC1 led to increased pyruvate and reduced lactate utilization (Fig. 8, G-H). Conditions of 0 mM glucose/2 mM glutamine and 10 mM pyruvate were considered as positive hit and were taken for further work.

4.8.2 MACC1 promotes pyruvate and restricts lactate utilization through altered nutrient depletion

To find whether increased pyruvate utilization by MACC1 was due to altered depletion of pyruvate from cell growth medium pyruvate depletion assay was performed. Although lactate utilization was not supported by MACC1, but strong MACC1-dependent restriction of lactate utilization was observed lactate depletion assay was also performed. Pyruvate depletion was increased in SW620 shcntl cells compared to shMACC1 cells (Fig. 8, I), whereas lactate depletion, surprisingly was not altered by MACC1 instead lactate secretion was increased in SW620 shMACC1 cells compared to shcntl cells (Fig. 8, J).

4.8.3 Effect of MACC1 on inhibition of gluconeogenesis and mitochondrial respiration

As outlined on Fig. 4, A, followed by identification of positive hit conditions pharmacological inhibition of MACC1-dependent targets was aimed to be performed. Pyruvate can undergo two metabolic pathways: serve as a substrate in gluconeogenesis to synthesize glucose and run then glycolysis or be utilized through TCA feeding mitochondrial respiratory chain. To find which pathway is used for pyruvate utilization by SW620 shcntl cells compared to shMACC1 cells gluconeogenic or mitochondrial respiratory chain pathways were inhibited. Treatment of SW620 shcntl and shMACC1 cells with inhibitor of cytoplasmic phosphoenolpyruvate carboxylase, the first enzyme in gluconeogenic pathway, cPEPCK inhibitor had no effect on cell viability (Fig. 8, K), suggesting that either pyruvate did not undergo gluconeogenic pathway or mitochondrial isoform of PEPCK was prevalent. Treatment of cells with mitochondrial complex I inhibitor rotenone reduced cell viability, however to the same extent in both SW620 shcntl and shMACC1 cells (Fig. 8, L). This demonstrates the intrinsic property of mitochondria in SW620 cells, which is MACC1-independent in the context of pyruvate utilization, hinting that a real target is upstream of mitochondrial respiratory chain.

In summary, MACC1 supports pyruvate utilization and restricts lactate utilization in glucose depleted environment through altered nutrient transport, thus defining cell nutrient preferences and providing an advantage to cell survival upon nutrient stress.

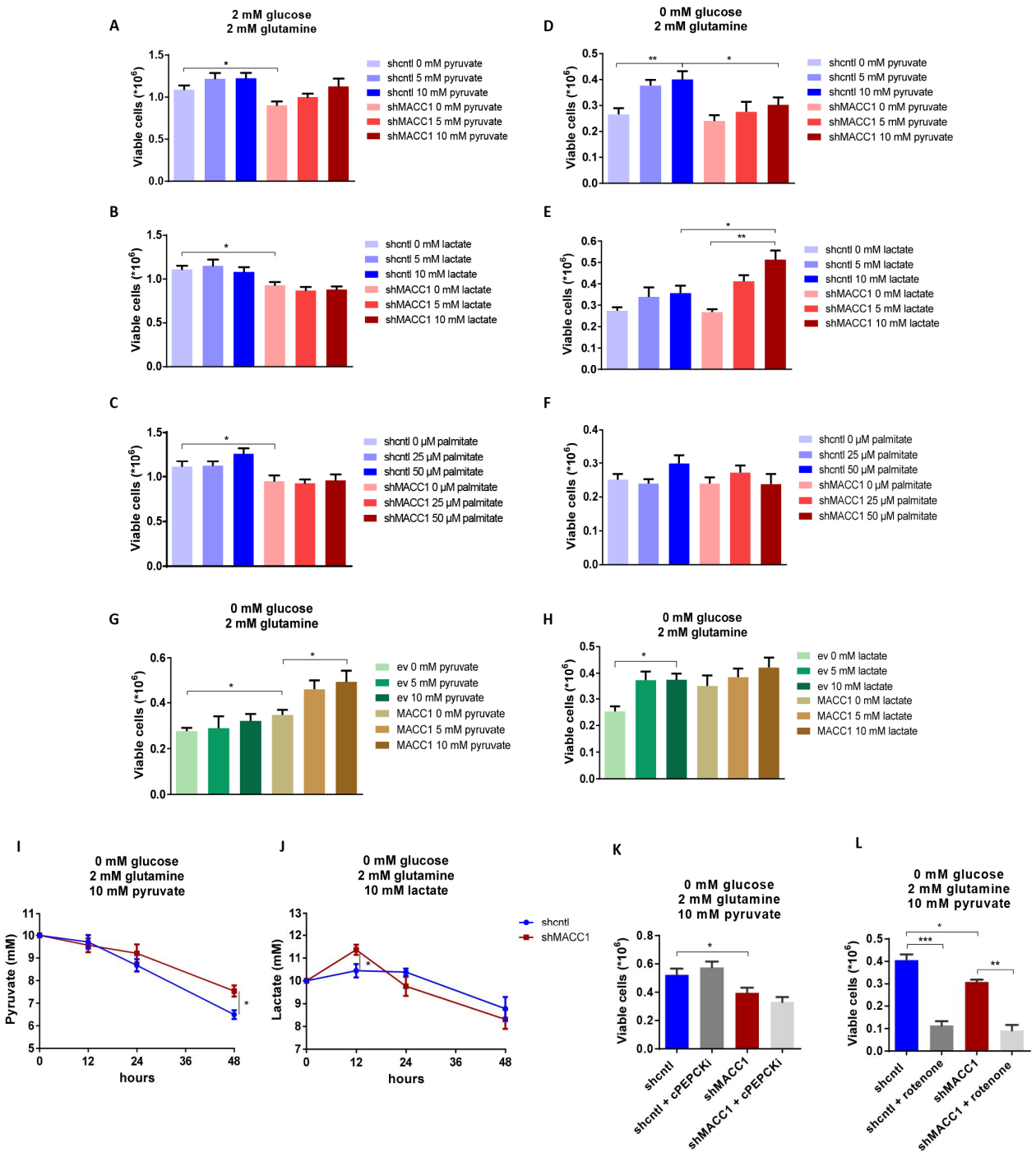

Fig. 8 MACC1 promotes pyruvate and restricts lactate utilization in glucose depleted environment. (A-F) Cell viability of SW620 shcntl and shMACC1 cells treated with pyruvate, lactate and palmitate at indicated concentrations in (A-C) low glucose and (D-F) glucose depleted conditions. (G-H) Cell viability of SW480 ev and MACC1 cells treated as indicated in glucose depleted conditions. (I) Pyruvate and (J) lactate depletion from cell growth medium of SW620 shcntl and shMACC1 cells after 48 hours of culture in indicated conditions. (K) Cell viability of SW620 shcntl and shMACC1 cells treated at indicated

conditions with cytoplasmic PEPCK inhibitor (cPEPCKi) and (L) mitochondrial complex I inhibitor rotenone. *, p<0.05; **, p<0.001; ***, p<0.0001. Data are representative of a mean ±SEM of at least three independent experiments.

4.9 MACC1 has minor effects on pyruvate flux

The findings that MACC1 supports pyruvate utilization as judged by increased cell viability of SW620 shcntl compared to shMACC1 cells (Fig. 9, D), prompted to ask whether MACC1 affects pyruvate distribution and if it is the case whether it drives it towards certain metabolic pathway. To address this question, SW620 shcntl and shMACC1 cells grown in 0 mM glucose/2 mM glutamine/10 mM pyruvate conditions were treated with $^{13}C_3$ pyruvate for 24 hr and GC-MS-based metabolic profiling of cells and cell growth medium was performed. Unlike in $^{13}C_6$ glucose and $^{13}C_5$ glutamine labeling experiments MACC1 was not found to vastly affect the percentage of ^{13}C labeled isotopologues, where only few metabolites were significantly different between MACC1 knockdown and control cells (Fig. 9, A). Metabolic profiling revealed that pyruvate-derived ^{13}C carbon was deposited within metabolites of gluconeogenesis, TCA, amino acids and nucleotides whose production closely related to TCA intermediates (Fig. 9, A). Similarly to $^{13}C_6$ glucose and $^{13}C_5$ glutamine labeling experiments many pyruvate-derived metabolites found in the cells were present in the medium (Fig. 9, A). Interestingly, $^{13}C_3$ labeled pyruvate (Fig. 9, B) was found to be converted to lactate (Fig. 9, C; M+3) and to phosphoenolpyruvate and glycerate (Fig. 9, D-F; M+3), where the latter two metabolites are part of gluconeogenesis pathway. The generated ^{13}C labeled glucose was found in trace amounts, however because of its very low abundance the peak could not be reliably quantified (data not shown). While glutamine feeds a TCA the generation of glycolytic/gluconeogenic intermediates from pyruvate brings additional carbon to those metabolites which are critical for generation of biomass thus compensating lack of glucose and thus explaining the increase in cell viability in the presence of pyruvate.

More than a half of all citrate produced in the cells was derived from $^{13}C_3$ pyruvate (Fig. 9, G), however the other TCA intermediates downstream of citrate had much less ^{13}C carbon (25-30% only) (Fig. 9, H-L), suggesting that citrate is exported to cytoplasm to be used for fatty acid synthesis. MACC1 reduced production of ^{13}C labeled citrate (M+2, M+4, Fig. 8, G) and alanine (M+3, Fig. 9, M), while overall, the distribution of pyruvate-derived ^{13}C within gluconeogenesis related intermediates (Fig. 9, B-F) and most of TCA intermediates (Fig. 9, H-L) was MACC1-independent. Glutamate, asparagine, aspartate, proline

and uracil were also found to contain pyruvate-derived ^{13}C, however they were mostly produced from unlabeled substrates (Fig. 9, N-R).

In conclusion, pyruvate generates important glycolytic/gluconeogenic intermediates which substitute the lack of glucose in glucose depleted conditions and brings additional carbon to the TCA (Fig. 8, S) which contributes to increased cell viability. The effect of MACC1 on pyruvate utilization lays in increased pyruvate uptake (Fig. 8, I) while having minor effects on pyruvate-derived ^{13}C distribution leaving it mostly unchanged.

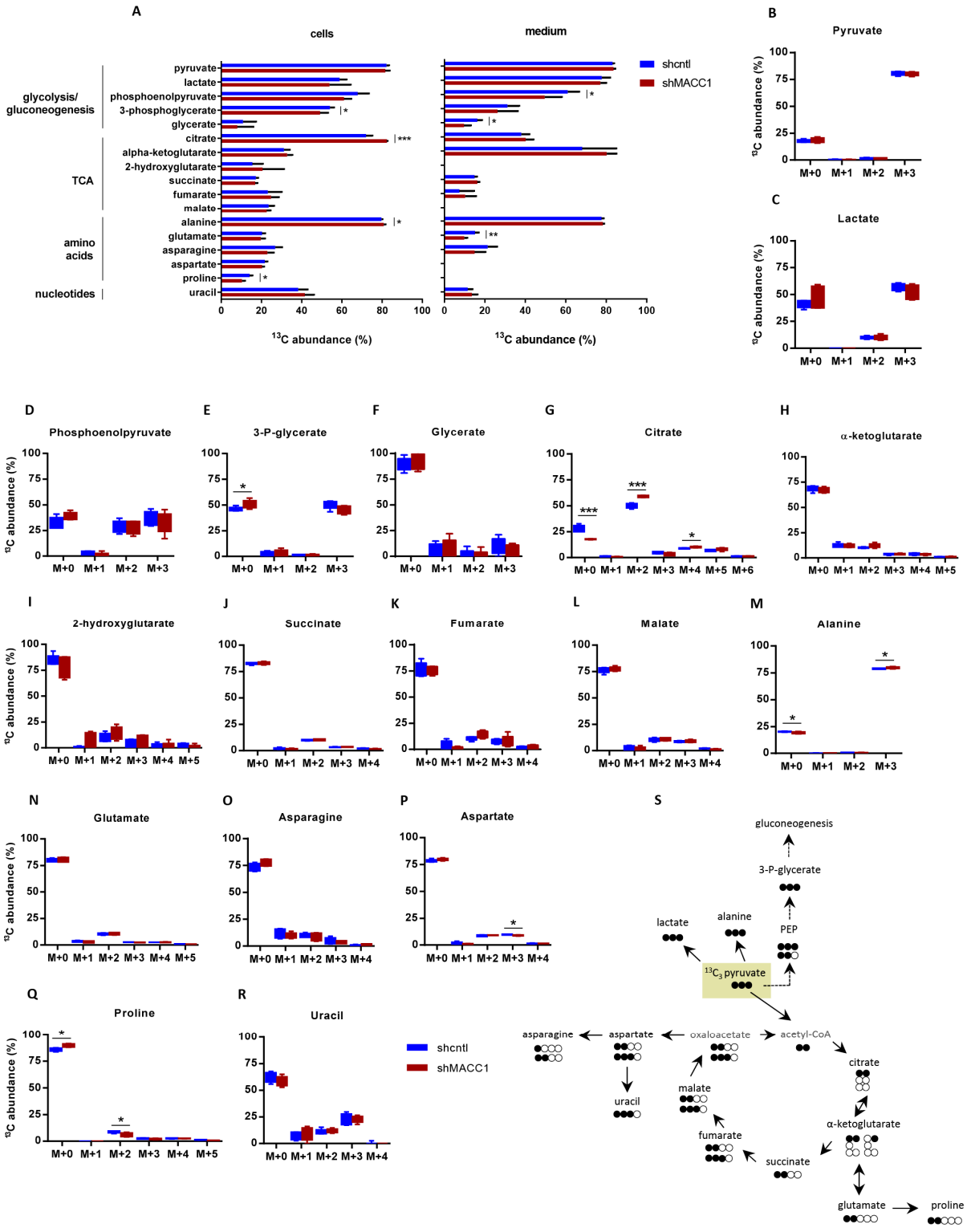

Fig. 9 Metabolic tracing of $^{13}C_3$ pyruvate. SW620 shcntl and shMACC1 cells were grown in glucose depleted conditions (0 mM glucose/2 mM glutamine) and treated with $^{13}C_3$ pyruvate for 24 hr. (A) The abundance of ^{13}C isotopologues in cells and cell growth medium. (B-R) Metabolite isotope distribution

within (B) pyruvate, (C) lactate, (D) phosphoenolpyruvate, (E) 3-P-glycerate, (F) glycerate, (G) citrate, (H) α-ketoglutarate, (I) 2-hydroxyglutarate, (J) succinate, (K) fumarate, (L) malate, (M) alanine, (N) glutamate, (O) asparagine, (P) aspartate, (Q) proline and (R) uracil metabolites measured in the cells. M plus consecutive number stands for mass shift on that number of atoms. (S) Scheme summarizing $^{13}C_3$ pyruvate distribution based on ^{13}C abundance within the cells. The most abundant ^{13}C containing isotopologues are shown. Each circle represents one carbon. Filled circles: ^{13}C carbon. Unfilled circles: ^{12}C carbon. Oxaloacetate and acetyl-CoA are not detected by GC-MS. *, $p<0.05$; **, $p<0.001$; ***, $p<0.0001$. Data are representative of a mean ±SD, n=5.

4.10 MACC1 enhances ^{18}F-FDG and ^{18}F-glutamate uptake *in vivo*

To prove *in vitro* findings that MACC1 increased glucose and glutamine depletion from cell growth medium *in vivo* metabolic substrate uptake studies were performed. Ten SCID/beige mice were intrasplenically injected with SW620 shnctl or SW620 shMACC1 cells (5 mice per group) and the tumor was grown for 21 days. For *in vivo* metabolic studies, positron emission tomography (PET) acquisitions were conducted and the glucose analog ^{18}F fluorodeoxyglucose (^{18}F-FDG) as well as ^{18}F-glutamate were used. Intravenous injection of ^{18}F-FDG into SCID/beige mice bearing primary tumors and liver metastases as confirmed by MRI (Fig. 10, A) revealed significantly higher ^{18}F-FDG uptake of 48% in primary tumor and 47% in liver metastases of SW620 shcntl group compared to SW620 shMACC1 group (primary tumor: p=0.025; liver metastases: p=0.008; Fig. 10, A-B). Cross-checking with the SUVratio (SUVtumor/SUVmuscle) revealed as well higher ^{18}F-FDG uptake of 35% for both primary tumor and liver metastases of SW620 shcntl group compared to SW620 shMACC1 group (primary tumor: p=0.02; liver metastases: p =0.022). Intravenous injection of ^{18}F-glutamate two days after ^{18}F-FDG imaging revealed an increase in ^{18}F-glutamate uptake of 32% in primary tumor and 168% in liver metastases of SW620 shcntl group compared to SW620 shMACC1 group (Fig. 10, C). The SUVratio showed an increase of 18% and 124% for primary tumor and liver metastases of SW620 shcntl group compared to SW620 shMACC1 group. Muscle uptake of the thigh served as control and showed no significant difference in ^{18}F-FDG and ^{18}F-glutamate uptake between SW620 shcntl and SW620 shMACC1 groups (p = 0.526 and p = 0.377, respectively). Analysis of primary tumors and liver metastases after removal from sacrificed mice of SW620 shcntl and SW620 shMACC1 groups revealed bigger primary tumor and multiple liver metastases in shcntl group compared to shMACC1 group (Fig. 10, D). Analysis of MACC1 expression in primary tumors and liver metastases confirmed MACC1 expression in SW620 shcntl group and MACC1 knockdown in SW620 shMACC1 group (Fig. 10, E). Similarly, analysis of human satellite DNA revealed

increased human cell load in the liver of SW620 shcntl group compared to SW620 shMACC1 group (Fig. 10, F). Immunohistochemical staining of livers for human cytokeratin 19 (CK19), a marker of human epithelial cells, showed larger areas of CK19 positivity in SW620 shcntl group compared to SW620 shMACC1 group (Fig. 10, G). This indicates more prominent metastasis formation and growth as shown by MRI and pictures of organs after sacrifice (Fig. 10, A and D).

In summary, our findings demonstrate that MACC1 enhances formation of liver metastases, what is in line with previous reports [42], and that this is accompanied with increased glucose and glutamate/glutamine uptake *in vitro* and *in vivo*, thus making MACC1 a novel regulator of cancer metabolism.

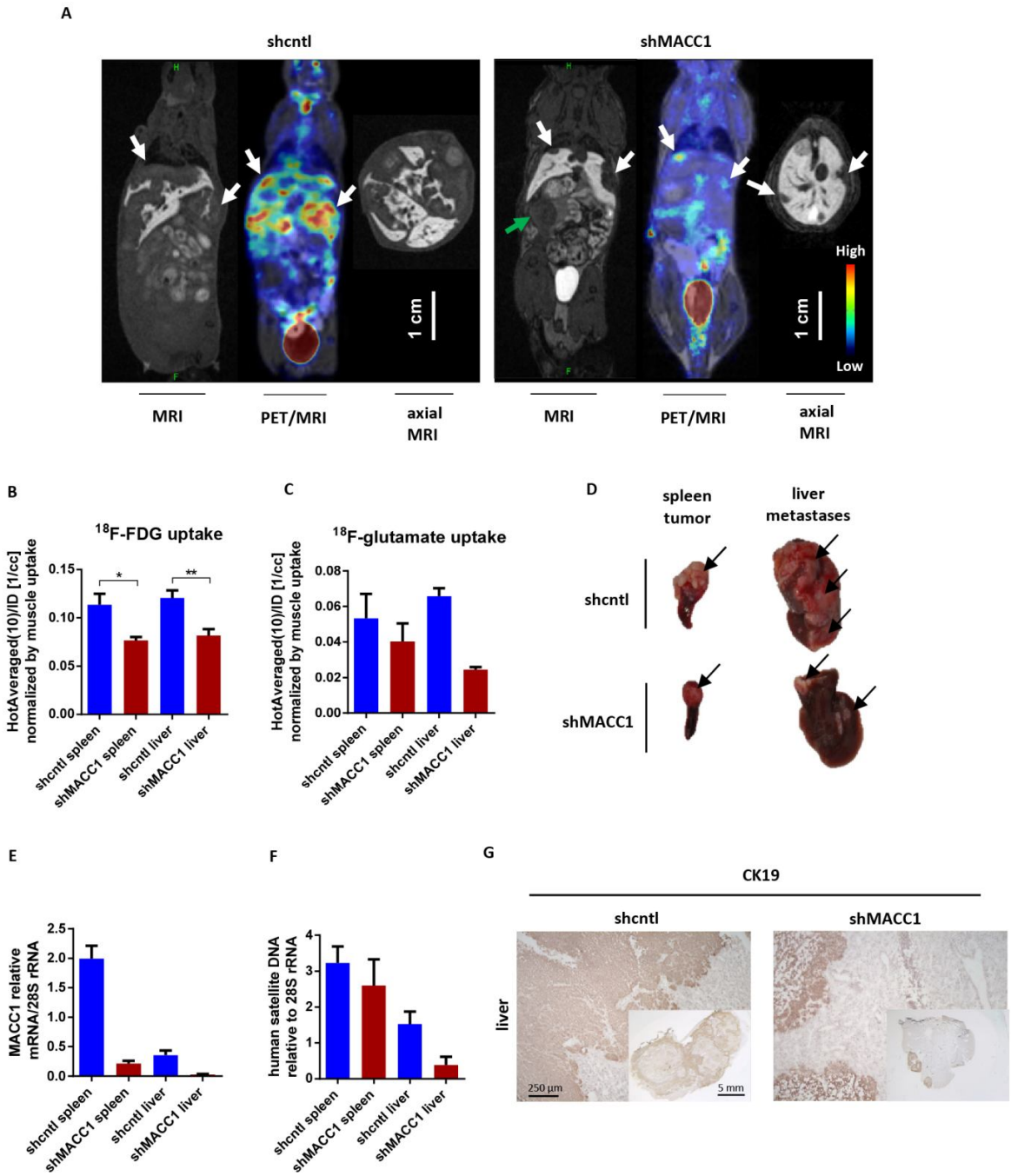

Fig. 10 MACC1 enhances ^{18}F-FDG and ^{18}F-glutamate uptake *in vivo*. (A) PET/MR images of liver metastases (white arrows) 60 min after intravenous injection of 9 MBq or 14 MBq ^{18}F-FDG to SCID/beige mice bearing tumors induced by SW620 shcntl or shMACC1 cells, respectively. T1 GRE EXT 3D coronal MRI shows the metastases (hypointensity) clearly surrounded by healthy liver tissue, represented by the hyperintensity of contrast agent Gadolinium™; fused MR and PET image; T1 GRE EXT 3D axial MRI of the liver. The green arrow indicates the primary tumor in the spleen. The scale bar is representative for MRI, PET/MRI and axial MRI images. In shcntl group 5 mice were imaged; in shMACC1 group 4 mice were

imaged. (B-C) Quantification of (B) ^{18}F-FDG and (C) ^{18}F-glutamate uptake in the primary tumor (spleen) and/or liver metastases. For ^{18}F-glutamate measurements 2 mice per group were analyzed. Data are representative of a mean ±SEM. (D) Pictures of primary tumor (spleen) and liver metastases after sacrifice. Arrows indicate primary tumor and liver metastases. Pictures are representative of 5 mice in shcntl group and 4 mice in shMACC1 group. (E-F) Expression of (E) MACC1 mRNA and (F) human microsatellite DNA in the primary tumor (spleen) and liver metastases. Data are representative of a mean ±SEM. (G) CK19 immunohistochemical staining of cryosections from liver metastases of SW620 shcntl or SW620 shMACC1 cells. Brown staining indicates human CK19 representing human tumor cells. Images taken with 10X magnification. Inset: images of whole tissue slice taken with 0.8X magnification. CK: cytokeratin 19. *, $p<0.05$; **, $p<0.001$; ***, $p<0.0001$.

PROJECT II: Identification of metabolic prognostic biomarkers for metachronous metastasis formation in the plasma of stage II CRC patients

4.11 Metabolic profiles are distinct between non-metastasized and metachronously metastasized CRC patients

Metabolic profiles of plasma samples and tumor tissues from non-metastasized (NON) and metachronously distantly metastasized (MET) CRC patients were retrospectively compared by gas/liquid chromatography coupled to high resolution mass spectrometry (GC/LC-MS). To identify a metabolic signature distinguishing non-metastasized from metachronously metastasized patients a threshold of fold change of 2 and $p<0.05$ (one-way ANOVA) was applied. In such a way, thirty seven metabolites were included into metabolic signature of plasma samples (Fig. 11, A), and thirteen metabolites were included into metabolic signature of CRC tumors (Fig. 11, B).

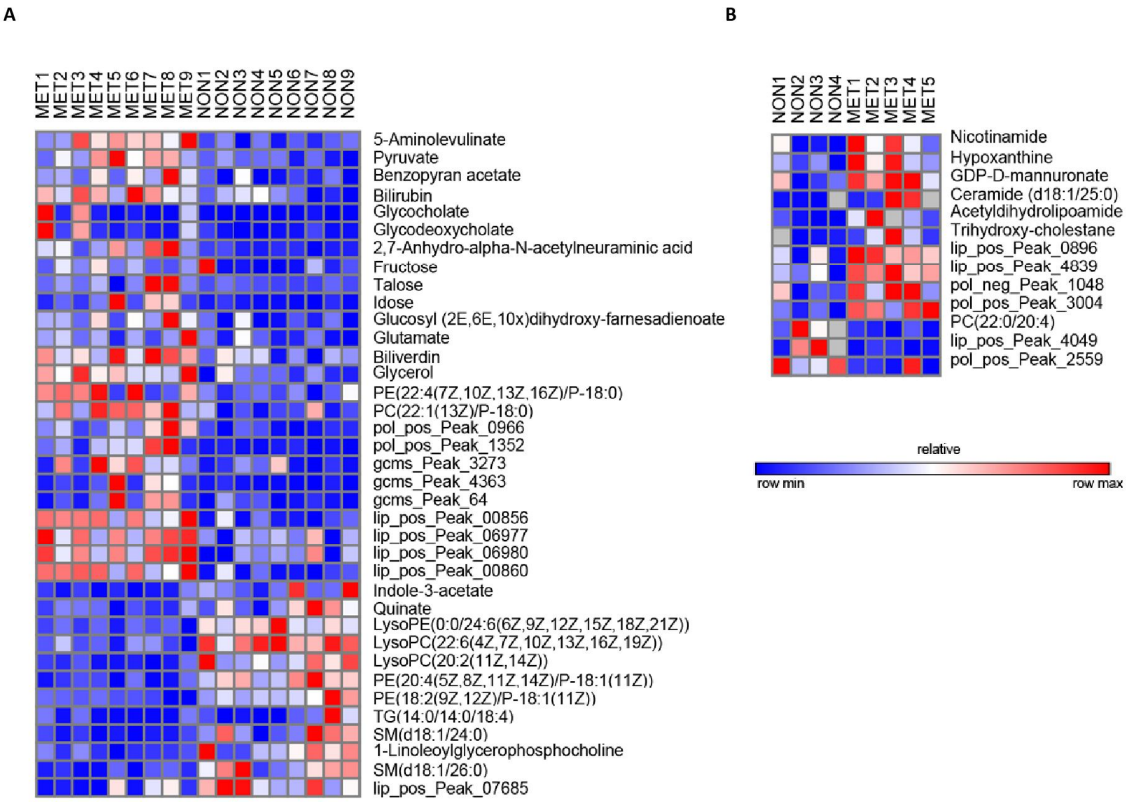

Fig. 11 Metabolic signature distinguishing non-metastasized vs metachronously metastasized stage II CRC patients. (A) Metabolic signature in the plasma samples and (B) tumor tissues. NON: non-metastasized. MET: metachronously metastasized. Not annotated metabolites are shown with internal names. Plasma samples: NON=9, MET=9. Tumor tissues: NON=4, MET=5.

4.12 Plasma metabolic profiles are predictive of metachronous metastasis in stage II CRC patients: the DACHS study

To investigate further the possibility of stratification of stage II CRC patients by plasma metabolic profiles the plasma samples from larger the DACHS (Darmkrebs: Chancen der Verhütung durch Screening; Colorectal cancer: chances for prevention through screening) study were analyzed. In total, 92 plasma samples (50 NON and 42 MET) of stage II CRC patients from the DACHS study were analyzed by LC (polar/non-polar)-MS. Detailed characteristics of patients are presented in Table 4.1.

Table 4.1 Clinical characteristics of patients: the DACHS study

	primary tumor without metachronous metastasis	primary tumor with metachronous metastasis	all patients
Plasma samples, n	50	42	92
UICC II, n	50	42	92
(neo)adjuvant therapy	-	-	-
Follow-up, median, months	65	34	44
Age, median (range), years	73 (45-87)	68 (52-86)	73 (45-87)
Sex, male/female	25/25	25/17	50/42
Tumor site, colon /rectum, n	colon 38/rectum 12	colon 34/rectum 8	colon 72/rectum 20

From here onwards all the data analysis was provided by collaborator Dr. Jan Lisec (Charité Metabolomics Core Facility). By LC-MS in total 590 non-redundant metabolic signals in the polar and non-polar fractions were determined. For each metabolite ANOVA multiple testing correction using Benjamini-Hochberg test to rule out the effect of analysis for group, sex, age, extraction batch, preparation set and measurement order was performed. In this way, significantly different metabolites between NON and MET groups ($p<0.05$) were found. Among significant metabolites (28 in total) eleven

metabolites were found in Human Metabolome Database (HMDB) (Table 4.2). Analysis of annotated metabolites with HMDB revealed that most of those metabolites constituted part of lipid metabolism (Table 4.2).

Table 4.2 Significant metabolites between NON and MET patients: the DACHS study

Metabolite ID	HMDB ID	Metabolic pathway	p-value
Monomenthyl succinate	HMDB36143	Monoterpenoid metabolism	4.77E-07
PE(18:0/18:2(9Z,12Z))	HMDB08994	Glycerophospholipid metabolism; Glycosylphosphatidylinositol(GPI)-anchor biosynthesis	7.16E-04
Polyethylene glycol (n=9-20)	-	-	3.08 E-04*
D-Erythrose 4-phosphate	HMDB01321	Phenylalanine, tyrosine and tryptophan biosynthesis; Pentose phosphate pathway; vitamin B6 metabolism	4.62E-03
PC(16:0/22:6(4Z,7Z,10Z,13Z,16Z,19Z))	HMDB07991	Linoleic acid metabolism; glycerophospholipid metabolism; alpha-Linolenic acid metabolism; Arachidonic acid metabolism	1.02E-02
13-L-Hydroperoxylinoleic acid	HMDB03871	Linoleic acid metabolism	1.19E-02
N-Nonanoylglycine	HMDB13279	Lipid metabolism	2.41E-02
L-Acetylcarnitine	HMDB00201	Lipid metabolism	2.59E-02
PC(16:1(9Z)/20:3(8Z,11Z,14Z))	HMDB08014	Linoleic acid metabolism; glycerophospholipid metabolism; alpha-Linolenic acid metabolism; Arachidonic acid metabolism	2.59E-02
2-O-(Z-p-Hydroxycinnamoyl)-(x)-glyceric acid	HMDB41195	Cinnamic acid ester metabolism	2.72E-02
Vaccenyl carnitine	HMDB06351	Lipid metabolism	3.07E-02
3-(2,3,4-Trimethoxyphenyl)propanoic acid	HMDB36226	Phenyl propane metabolism	3.65E-02

* Mean p-value is shown. ID: identifier.

PCA restricted to significantly different metabolites revealed separation of the NON and MET groups (Fig. 12, A), suggesting that plasma metabolic profiles from the DACHS study possess information about development of metachronous metastasis in stage II CRC patients. Significantly different individual metabolites had shown high variance within the NON and MET groups and moderate effect sizes (Fig. 12, B). Variance was defined as the average of the squared differences from the mean, whereas effect size was defined by the mean difference between analyzed groups divided by the pooled standard deviation for analyzed groups.

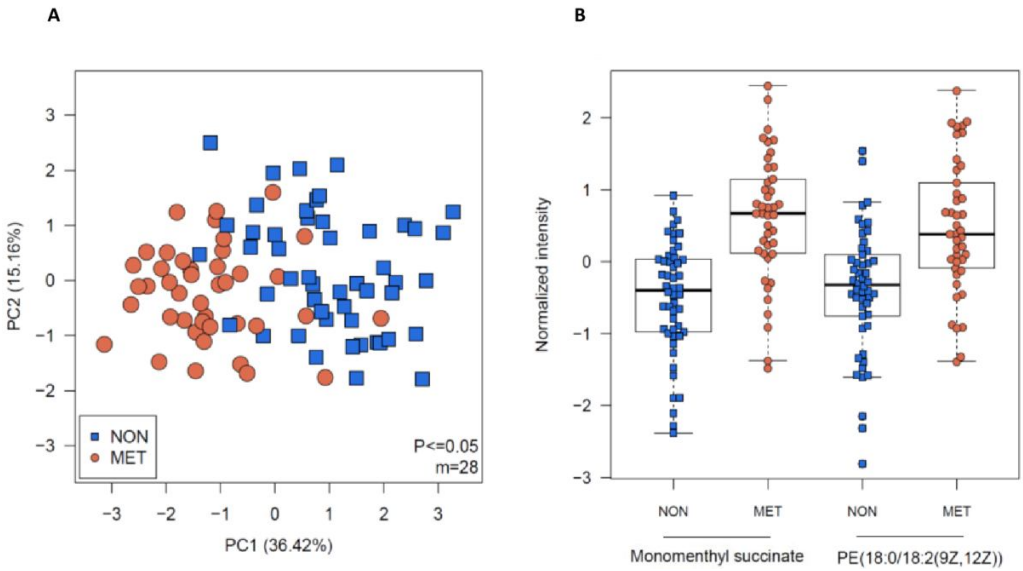

Fig. 12 Metabolic profiles distinguish non-metastasized vs metachronously metastasized stage II CRC patients. (A) PCA on significantly different metabolites between non-metastasized and metachronously metastasized groups. (B) Exemplarily, the levels of significantly different metabolites are shown. High within-group variance and moderate effect sizes are observed. Normalized intensity represents the intensity subtracted from mean within the group and divided by standard deviation. NON: non-metastasized. MET: metachronously metastasized. m: number of metabolites.

4.13 Classification approaches built on metabolic profiles identify prediction accuracies for prognosis of distant metastasis

To facilitate clinical use of metabolites as a biomarker both low metabolite number and clear cutoff values are of importance. Because the DACHS study contained sufficient number of samples to allow statistically robust classification several machine learning classification approaches, including decision trees (DTs) and support vector machines (SVMs) (Fig. 13), were performed on DACHS samples.

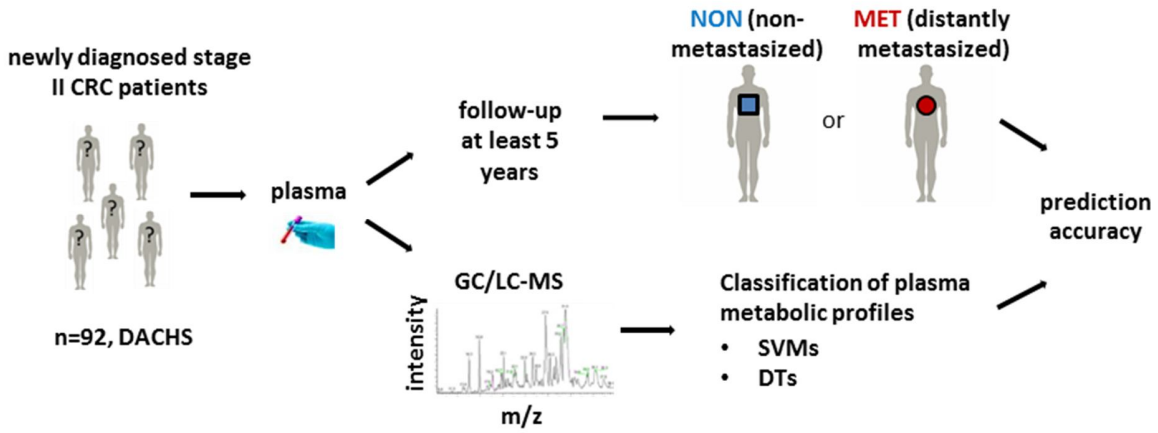

Fig. 13 Classification approach to predict metachronous distant metastasis. Outline of plasma metabolic profiling of non-metastasized vs metachronously metastasized stage II CRC patients. Plasma samples were taken from stage II CRC patients who participated in a DACHS study and who were followed up for at least 5 years to find out whether they developed metachronous metastasis or remained metastasis-free. Once the metastasis status of the patients was identified, their plasma samples (50 non-metastasized and 42 metachronously metastasized patients, 92 patients in total) were analyzed by (LC-MS). Plasma metabolic profiles were classified by support vector machines (SVMs) and decision trees (DTs), which yielded accuracies predicting metastasis formation. NON: non-metastasized. MET: metachronously metastasized.

To identify prognostic metabolites in the plasma samples of NON and MET patients from the DACHS study a classifier out of given metabolic profiles was built. A classifier represented a set of the rules which allowed to predict the formation of distant metastasis based on plasma metabolite levels. Classification performance was measured as an accuracy, a relative amount of samples correctly classified to NON or MET group based on a classification model.

DTs, in their principle, combine all samples in a node and evaluate every metabolite and possible metabolite combinations to identify cutoffs by which classes in successive nodes are represented at

maximal difference. Recursive partitioning is one possibility to calculate DTs, where the focus is to maximize separation while minimizing the number of metabolites within the tree. SVMs, another frequently used classification tool, often provide good results, while SVM models are less intuitive to interpret compared to DTs.

To assess the robustness of the classifier 10-fold cross validation on multiple replications (1000 replications in total) was applied and these results were compared against similarly obtained values for permuted data. Original data matrix (92 samples, 590 metabolites) was splitted into 10 equal folds, using 90% of samples as a training set and predicting the remaining 10% of samples as a validation set. This way, robust average prediction accuracies from DT and SVM models were obtained (0.75 and 0.82, respectively). These results were highly significant if compared with the respective control approach on permuted datasets, which resulted in average accuracies of 0.52 and 0.55 for DTs and SVMs, respectively, that is equal to chance as expected (Fig. 14). A t-test comparing both distributions of observed and permuted data had highly significant p value of less than 10^{-16} indicating the robustness of the classification approach.

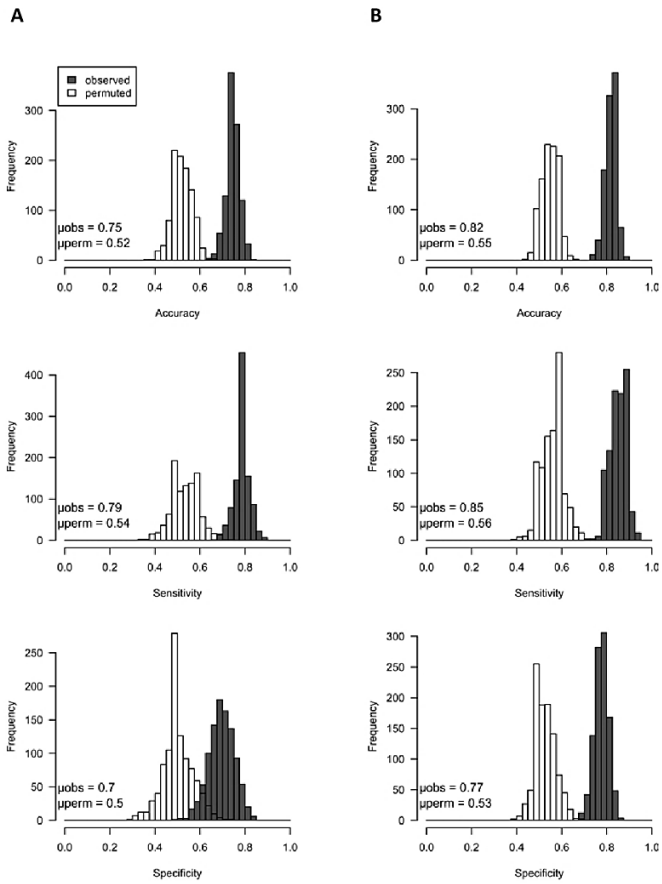

Fig. 14 Classification yields >80% accuracy on average. Using 10-fold cross validation and 1000 replications, the robustness of classification for metastasis prediction in plasma samples of stage II CRC patients was assessed. (A) Recursive partitioning (rpart, a DT method) allowed for an average accuracy of 0.75, which is highly significant compared to the 0.52 accuracy achieved for permuted data. (B) Alternative classification methods like SVMs allowed for higher average accuracy of 0.82 but are harder to interpret and transfer into clinical use. Frequency indicates the number of models which fall into 0.25 band on the x axis. μobs: mean of observed data distribution. μperm: mean of permuted data distribution.

4.14 A decision-tree based metabolite classifier for metastasis prognosis

Though SVM models had shown higher average prediction accuracy (0.82, Fig. 14, B) compared to DT models they are less intuitive to interpret [168,169]. Therefore, further the focus was on decision tree models.

To provide a robust example of a DT for metastasis prognosis feature selection by counting the frequency of metabolite occurrence in each DT model from cross-validation was performed. If in one replicate of a 10-fold cross-validation a metabolite was used once within DT models this was counted as one. With this approach metabolites which were used in more than 85% of all repetitions were considered to be the most important. In total, 32 metabolites were selected and were used as an input to calculate the representative DT shown in Fig. 15.

Naturally, a DT starts with one node containing all samples and ends with several (at least two) nodes where either samples are optimally distributed or cannot be separated further by any metabolite. Each metabolite within a DT has a cut-off value at which the samples are split. Depending on the cut-off rule (higher or lower than a cut-off) the samples are split to NON or MET bin.

The optimal DT for metastasis prognosis gave accuracy of 0.95 and consisted of four metabolites (polyethylene glycol (PEG) n=16, 1,4-D-xylobiose, and two unknown metabolites) correctly classifying 47 out of 50 NON patients and 40 out of 42 MET patients (Fig. 15). PEG (n=16), 1,4-D-xylobiose and unknown_pp_210 metabolites were found in polar metabolic fraction.

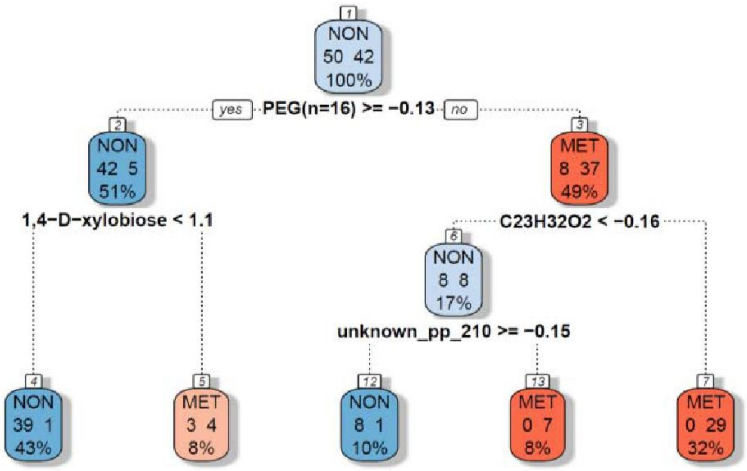

Fig. 15 The decision tree classification models for metastasis prognosis. A feature selected decision tree model consisting of four metabolites with cut-offs and yielding 0.95 accuracy. A decision tree consists of metabolites with cut-offs in the nodes (colored boxes). Each node is colored according to the majority of samples within the node (NON: blue; MET: red) and contains a number of samples within NON (left) and MET (right) group and percentage of all samples. The nodes serve to split samples. Metabolite peak cut-offs are used to split samples to NON or MET bin. In total 47 out of 50 NON and 40 out of 42 MET patients are correctly classified. PEG: polyethylene glycol. pp_210: internal ID for this metabolite.

4.15 Correlation between metastasis-free and overall survival assigned with clinical records or according to a decision tree based metabolite classifier

Using an optimal decision tree classifier (Fig. 15) the metastasis-free and overall survival of stage II CRC patients who were correctly classified as NON or MET patients with such survivals of all NON and MET patients according to their clinical records were correlated.

Because a metabolite-based decision tree classifier correctly classified 47 out of 50 NON samples and 40 out of 42 MET samples (Fig. 15) the metastasis-free survival based on prediction correlated with metastasis-free survival assigned with clinical records (Fig. 16, B), thus reflecting the high accuracy of the prediction. The overall survival of patients predicted as NON or MET correlated with patient overall survival assigned with clinical records (Figure 16, A).

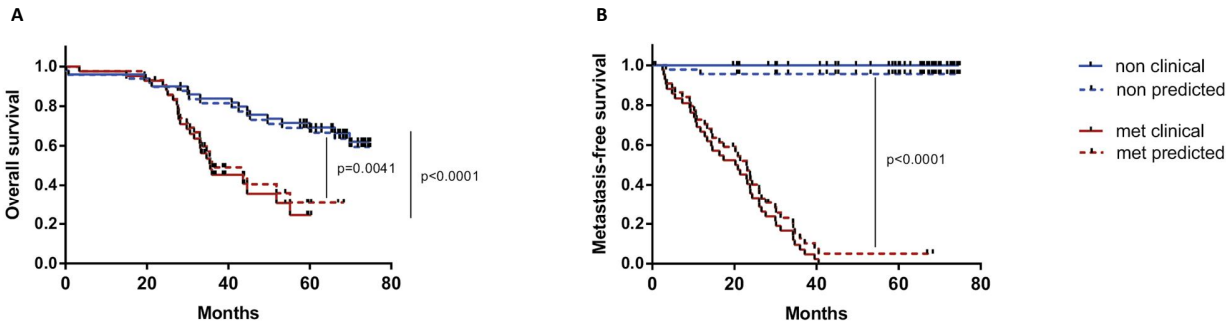

Fig. 16 Overall and metastasis-free survival according to a decision tree classification model. (A) Overall and (B) metastasis-free survival of stage II CRC patients based on clinical records (NON: blue, n=50; MET: red, n=42) or predicted assignment when a decision tree from Fig. 15 is applied (NON: blue dashed line, n=47, MET: red dashed line, n=40).

5. DISCUSSION

PROJECT I: Elucidation of MACC1 role in colorectal cancer metabolism

In the present study, a comprehensive systematic analysis aimed to elucidate MACC1-dependent metabolic processes through investigation of cell nutrient preferences, context dependent alterations of nutrient utilization and metabolic tracing using ^{13}C-labeled metabolic substrates had been performed. The results reveal that MACC1 exerts multiple effects on cancer cell metabolism, where most of them can be subdivided onto those which mediate increased nutrient depletion and those where MACC1 alters the intracellular nutrient fluxes by affecting metabolite production or turnover from metabolic substrates. In this context, the relation of MACC1 to the utilization of glucose, glutamine, pyruvate, lactate and palmitate was investigated. MACC1 was found to support context-dependently utilization of glucose, glutamine and pyruvate through their increased depletion or through altered distribution within downstream metabolic pathways. These results demonstrate that MACC1 is a novel potent regulator of cancer cell metabolism, and its targeting will affect metabolic pathways thus leading to disbalanced cell homeostasis and reduced cell survival.

Metabolic profiles are determined by multiple factors including cancer type and cell-of-origin, mutational and transcriptional profiles, expressed oncogenes and nutrient availability. All of this contributes to metabolic heterogeneity which is important in elucidation of metabolic preferences and in identification of metabolic vulnerabilities. The contribution of various nutrients to the survival of cancer cells and their dependency on a certain nutrient had been well recognized in the field of cancer metabolism and is well described in detail in [82]. Different oncogenes had been demonstrated to exert different metabolic profiles and studies of which profile attributes to which oncogene can help to personalized treatment. So, in prostate cancer Akt1 overexpression is associated with accumulation of glycolytic metabolites, while MYC overexpression results in dysregulated lipid metabolism [170]. In liver cancer, MYC increases catabolism of glucose and glutamine, while MET-driven tumors use glucose to produce glutamine. In the lung, MYC-driven tumors show increased expression of glutamine synthetase and glutaminase [86]. This suggests the importance of studying oncogene-dependent metabolic alterations in cancer cells.

Metastatic process is accompanied with the necessity to adapt to varying environmental conditions which migrating cells encounter on the way towards finding a suitable soil to attach, invade, adapt and

grow. PGC-1α, a well-established regulator of cancer metabolism, had been reported to promote metastasis, what is associated with increased bioenergetics capacity giving implications to resistance to metabolic drugs [171]. Similarly, the availability of certain nutrients in the environment had been shown to confer resistance to metabolic drugs [122,172]. This indicates the necessity in studying oncogene-dependent metabolic profiles with respect to various nutrients in order to elucidate the impact of an oncogene to cell metabolism, what may potentially open new avenues in personal treatment.

Out of available approaches and techniques to characterize cancer metabolism most of them were applied in this work to give insights into the role of MACC1 in CRC metabolism [173]. In this work, the data from cell viability related nutrient studies, nutrient transporter expression, nutrient depletion, nutrient distribution, metabolic pathway functionality and *in vivo* studies were integrated in order to better understand the impact of MACC1 into metabolic rewiring and metabolic adaptations under normal and stressed conditions. The integration of data from external (cell medium) and internal (cells) fluxes performed for various nutrients whose utilization as judged by cell viability was MACC1 dependent. Such data integration was performed for glucose, glutamine and pyruvate metabolic substrates. Contribution of MACC1 to the utilization of each of these nutrients will be discussed in detail below.

Effect of MACC1 on glucose metabolism

The regulation of MACC1 expression by glucose and its reciprocal effect on glucose uptake represents a positive feedback between MACC1 and glucose. MACC1 had been shown to enhance surface GLUT1 expression, which leads to increased glucose depletion and hence increased cell proliferation.

Sp1 binding site was found to be crucial for MACC1 promoter responsiveness to glucose availability. This finding is in line with published data, where Sp1 binding activity had been shown to be glucose regulated [174–176]. In addition, binding of Sp1 to MACC1 promoter had been shown to contribute the most to the regulation of MACC1 promoter activity in normal conditions [156]. This confirms and provides new insights into multiple levels of regulation of MACC1 expression.

Lin L. and colleagues found that in gastric cancer glucose depletion increased MACC1 expression [69]. The discrepancy between my findings and the findings of Lin L. and colleagues [69] lays in a different timepoint chosen as a reference to judge about effects of glucose on MACC1 expression. Lin L. and colleagues performed glucose treatment experiments for 12 hours, while in this work 48 hours timepoint

was used. Similar to their findings, I found that MACC1 expression was indeed increased by glucose depletion 12 hours after treatment. However, at 24 hours (data not shown) and 48 hours timepoints glucose depletion led to reduced MACC1 expression, i.e. increase in glucose concentration led to increased MACC1 expression (Fig. 1, B). Given the prolonged glucose starvation often observed 48 hours timepoint was selected as a basis for further experiments.

The MACC1-driven increase in glucose flux has multiple causes and consequences. The increase in surface GLUT1 expression leads to enhanced glucose depletion and therefore to enhanced cell proliferation. The ability of MACC1 to enhance surface GLUT1 expression presumes the potential of MACC1 to mediate translocation of GLUT1 from endosomal pool to the cell surface. PI3K/Akt signaling is a main trigger of GLUT1 release to the cell surface [177,178]. In gastric cancer, MACC1 is associated with increased PI3K/Akt signaling and pharmacological inhibition of Akt leads to reduced MACC1 expression [57], indicating that there is a feedback loop between MACC1 and PI3K/Akt signaling. This is in line with my findings, where I show that there is a positive feedback loop between MACC1 and glucose. The increase in glucose depletion by MACC1 in gastric cancer [57,69] and CRC suggests that MACC1-mediated effect on glucose depletion is common between gastric cancer and CRC.

The key finding of glucose flux experiment performed in this work was that MACC1 enabled serine synthesis from glucose. Though serine is normally present in the medium MACC1 wt cells used glucose to increase the serine availability to the cells, indicating that there is an increased demand for this metabolite in MACC1 wt cells. Serine is a big contributor of one-carbon metabolism, which is important for folate metabolism, biosynthetic processes, amino acid metabolism, epigenetic modifications and redox balance [179]. Metabolic flux studies revealed that cancer cells may use up to 50% of glucose-derived carbon for serine synthesis [180], and that serine is a big contributor to NADPH production [181]. The generation of a battery of one-carbon tetrahydrofolate species from serine is known to protect cells from hypoxia-induced oxidative stress [182]. Phosphoglycerate dehydrogenase (PHGDH) is the first enzyme in serine biosynthesis pathway. Its loss in PHGDH overexpressing breast cancer cells had been reported to reduce serine biosynthesis leading to a strong decrease in cell proliferation [183]. Treatment with small-molecule PHGDH inhibitors had been demonstrated to reduce production of glucose-derived serine and to inhibit growth of PHGDH-dependent cancer cells *in vitro* and in orthotopic xenograft tumors [184]. Together, this indicates that MACC1 provides metabolic advantage in rewiring of cell metabolism thus allowing to adapt to various metabolic and nutrient environments to ensure cell survival.

The analysis of ^{13}C-labeled glucose-derived metabolites in cell growth medium revealed the presence of multiple metabolites, which are either secreted or found as traces of dying cells. The presence of acidic metabolites such as lactate, citrate and alanine may serve for environment acidification thus facilitating destruction of extracellular matrix and promoting metastasis.

Increased glucose availability within the MACC1 wt cells compared to MACC1 knockdown cells may explain enhanced abundance of $^{13}C_6$-glucose-derived metabolites within glycolytic and TCA intermediates (Fig. 2). Another potential reason of glucose flux may be in enhanced enzymatic activity, enzyme protein expression, allosteric regulation or metabolite turnover. Though MACC1 had been shown as a transcription factor having c-MET, SPON2 and Nanog as transcriptional targets [42,185,186], analysis of mRNA expression of metabolism related genes (more than 23 genes tested) revealed that MACC1 does not increase expression of genes involved in metabolic processes, besides c-MYC whose expression was increased by MACC1 on 30% compared to the counterparts (Fig. 5, A). This excludes the possibility of transcriptional upregulation of metabolism related gene expression by MACC1 and opens a perspective of other mechanism involved in the regulation. It remains unclear whether MACC1-exerted effects are due to direct MACC1 actions or are manifested through a well-known regulator of cancer metabolism which acts downstream of MACC1. It seems very probable that the effects of MACC1 occur either through allosteric regulation of enzyme activity (c-MYC) or through altered cell signaling (Akt1).

Increased glucose depletion which leads to increased glucose availability within the cells logically resulted in enhanced glucose flux through glycolytic and TCA intermediates. However, the information about metabolite compartmentalization and hence their availability for metabolic pathways is missing. Measurement of mitochondrial respiration revealed the functionality of increased amount of glucose-derived TCA intermediates, where MACC1 surprisingly reduced mitochondrial respiration, while its effect on extracellular acidification was inconsistent. Reduced mitochondrial respiration by MACC1 may act as a compensation to increased glucose availability and hence reduced necessity to run the TCA. A potential explanation what TCA intermediates may be used for is epigenetic modifications. Succinate, fumarate and 2-hydroxyglutarate accumulation as a result of mutation in corresponding producing enzymes have impact on epithelial-to-mesenchymal transition and on epigenetic modifications [187–190]. This may provide additional advantage to MACC1 wt cells in metabolic reprograming compared to MACC1 knockdown in cells. One of the reasons of inconsistent effect of MACC1 on extracellular acidification may be that the acidification should not be treated as pure glycolysis readout because, besides glucose derived lactate, bicarbonate which is produced in high amounts by actively respiring mitochondria can

also contribute to it. Therefore, the contribution to acidification depends on the ratio between glycolytic activity and mitochondrial respiration. If the amount of bicarbonate produced by mitochondria is higher than the amount of lactate contributing to acidification the cells will show higher acidification without being glycolytic.

Effect of MACC1 on glutamine and pyruvate metabolism

MACC1 was found to have multiple effects on glutamine and pyruvate metabolism. This strongly depended on environmental context, demonstrating the role of MACC1 in metabolic adaptation to stress conditions.

In nutrient-replete conditions MACC1 had shown to be a modulator of glutamine utilization. Indeed, glutamine is important for cell survival as supported by multiple reports [77,84,103,105,191]. Yet, inhibition of glutamine metabolism did not result in MACC1 dependent effect on cell viability, suggesting that MACC1 modulates glutamine metabolism, however it does not lead to a rescue pathway with cell viability exerted phenotype.

Metabolic tracing with $^{13}C_5$ glutamine in nutrient-replete conditions revealed reduced relative abundance of ^{13}C containing glutamine-derived intermediates, while glutamine depletion remained unchanged. This may be explained by increased abundance of $^{13}C_6$ glucose-derived intermediates which may compensate the lack of glutamine-derived TCA intermediates. On the other hand, glutamine-derived glutamate is used for glutathione biosynthesis, leaving less glutamate to be used for α-ketoglutarate production and further in the TCA cycle.

One of the most astonishing findings is that most of glutamine-derived metabolites are exported to the medium, suggesting that glutamine is used to feed the TCA and to acidify the environment. Another possibility of metabolite usage in the medium may be that glutamate for example can be uptaken by nearby starving cells helping them this way to survive temporary nutrient insufficiency and demonstrating metabolic symbiosis between cells having sufficient nutrient supply and those cells which lack it and contributing to therapy resistance [114].

In glucose depleted conditions (0 mM glucose/1 mM glutamine) MACC1 had shown to support glutamine utilization providing an advantage to cell viability to resist nutrient stress. This increase in glutamine utilization in glucose depleted conditions was accompanied by increased glutamine depletion by MACC1 wt compared to MACC1 knockdown cells. Affecting nutrient depletion implies the ability of a molecule to affect one of the following: the transporter mRNA or protein expression, the transporter abundance in

plasma membrane or the transporter activity. Several reports have demonstrated that MACC1 increases the expression of plasma membrane transporters such as Na(+) /H(+) exchanger-1 (NHE1) [73] and MCT1 [61]. Although the expression of glutamine transporters was not checked in this study and given that MACC1 demonstrated to enhance surface GLUT1 expression it is hard to believe that MACC1 would have a direct impact on all affected transporters. It is more likely that MACC1 is involved in common mechanism, like endosomal regulation, transporter recycling or similar to control the amount of transporters in plasma membrane thus determining the cell nutrient preferences.

The effect of MACC1 on glutamine flux was independent of nutrient availability. In nutrient-replete conditions MACC1 did not affect glutamine depletion, while in nutrient depleted conditions MACC1 enhanced glutamine depletion and increased cell survival. Regardless of its effect on glutamine depletion MACC1 reduced glutamine flux. This demonstrates that despite various nutrient supply MACC1 exerts similar effects on metabolic substrate distribution within metabolic pathway. Interestingly, a lack of glucose and relatively insufficient supply of glutamine led to rewiring of metabolism in a way that pyruvate and alanine started to be produced from glutamine. This implemented altered gene expression since malate dehydrogenase 1, which is involved in malate-aspartate shuttle, is not expressed in nutrient-replete conditions. On the one hand, the synthesis of pyruvate and alanine from glutamine indicates rewiring of metabolism allowing to adapt to nutrient stress conditions and it demonstrates increased demand in these metabolites by the cells. On the other hand, the conversion of glutamine-derived malate to pyruvate allows to produce NADPH in a manner independent of glucose [84]. It remains unclear how exactly MACC1 provides more than 10-fold advantage in cell viability to the cells in nutrient depleted conditions, because increase in 20% in glutamine depletion while decrease of relative abundance of glutamine-derived metabolites in MACC1 wt compared to MACC1 knockdown cells can hardly explain this phenomena. It may be that the key metabolites involved in this process where not detected by GC-MS. Such metabolites may include glutathione, a tripeptide important for ROS scavenging, or complex membrane lipids.

Because pyruvate is a glycolytic intermediate it is not surprising that MACC1 supported pyruvate utilization only upon glucose depletion. In breast cancer, inhibition of MCT1 in cells which co-express MCT1 and MCT4 led to decreased pyruvate but not lactate export, demonstrating that besides lactate glycolytic cells also export pyruvate, thereby feeding starving nearby cells [123], a phenomenon known as metabolic symbiosis which contributes to resistance to targeted therapies [114,115]. The ability of MACC1 to support pyruvate but not lactate utilization demonstrates its ability to shape cell nutrient preferences. Unlike in breast cancer, where pyruvate is used through TCA [116] CRC cells have stronger

demand in glycolytic/gluconeogenic intermediates and therefore utilize pyruvate through both gluconeogenic and TCA pathways.

The studies of pyruvate depletion revealed that MACC1 increased pyruvate depletion from cell growth medium by 30%. Though metabolic tracing with $^{13}C_3$ pyruvate had demonstrated that pyruvate undergoes both gluconeogenic and TCA pathways treatment with cPEPCK inhibitor did not have pronounced effects on cell viability. This may be explained by dominancy of mitochondrial rather than cytoplasmic PEPCK isoform. In comparison to glucose and glutamine MACC1 had minor effects on pyruvate flux besides having significant effects on M+2 citrate, M+3 alanine, M+2 proline and M+3 aspartate. This and the findings that treatment with mitochondrial complex I inhibitor rotenone did not result in MACC1-dependent effects indicate that with respect to pyruvate MACC1 mainly affects its depletion, while having minor effects on its flux within the metabolic pathways.

Effect of MACC1 on nutrient uptake *in vivo*

The ability of an oncogene to affect nutrient uptake *in vivo* depends not only on its intrinsic property to alter transporter expression but also on nutrient availability in the microenvironment. Glucose remains to be the main fuel for cell growth and metastasis. However, owing to tumor heterogeneity other alternative metabolic fuels may be used by the tumors. In this work, the effect of MACC1 on ^{18}F-FDG uptake used as a proxy for glucose uptake, and the effect of MACC1 on ^{18}F-glutamate uptake used as a proxy for glutamine uptake had been demonstrated *in vivo*.

The findings that MACC1 increased ^{18}F-FDG uptake in CRC are in line with published data in gastric cancer, wherein MACC1 knockdown led to reduced ^{18}F-FDG uptake while MACC1 overexpression increased ^{18}F-FDG uptake [57,69]. As demonstrated in this work increased metastatic capacity by MACC1 expressing cells was accompanied with increased ^{18}F-FDG uptake *in vivo*. The previous findings of the induction of MACC1 expression by glucose and the fact that MACC1 expression is increased in tumor invasive front [195], where glucose availability is higher compared to necrotic tumor center, may explain increased invasiveness of MACC1 expressing cells.

While in cell culture conditions glutamine uptake was affected by MACC1 only by 20%, *in vivo* MACC1 had demonstrated to increase ^{18}F-glutamate uptake by 32% in primary tumor and by 168% in liver metastases. The discrepancy between *in vitro* and *in vivo* findings may be explained by several factors. First, the microenvironment is more complex *in vivo* than in culture experimental settings. Second, ^{18}F-glutamate tracer is uptaken by cystine/glutamate antiporter [192,193], meaning that for each molecule

of uptaken glutamate one molecule of cystine is exported. This puts a constraint on imaging with ^{18}F-glutamate tracer because it depends on cystine availability, however it was proven to be effective in imaging of cancer patients [192]. Interestingly, MACC1 shows different effects on ^{18}F-glutamate uptake in primary tumor vs liver metastases, what may be due to altered blood vessel supply between primary tumor and liver metastases, altered cystine availability or altered antiporter expression.

Though pyruvate depletion was also shown to be differentially regulated by MACC1 the imaging using hyperpolarized ^{13}C pyruvate probe is challenging since hyperpolarizers are not routinely available. In conclusion, MACC1 had shown its ability to alter glucose and glutamine uptake as demonstrated by ^{18}F-FDG and ^{18}F-glutamate imaging used as a proxy of glucose and glutamine uptake *in vivo*.

Overall, the findings of this work demonstrate that MACC1 is a novel regulator of cancer metabolism possessing various effects on multiple layers of metabolic regulation, ranging from determination of cell nutrient preferences to adaptation to their utilization in varying environmental conditions, thus providing metabolic flexibility to the cells to resist stress conditions and ensure cell survival.

PROJECT II: Identification of metabolic prognostic biomarkers for metachronous metastasis formation in the plasma of stage II CRC patients

In this work, plasma metabolic profiles were used to stratify stage II CRC patients according to their metastasis risk. For the first time, polar and non-polar metabolite fractions in order to identify the most relevant metabolites for metachronous metastasis prognosis and stratification of stage II CRC patients were compared. The majority of significantly different metabolites were found in the polar metabolic fraction, which can be readily analyzed by well-established reversed phase LC-MS. Using decision trees and support vector machines metabolite-based classification models with average accuracies of 0.75 and 0.82 for each of the methods, respectively, predicting metachronous metastasis were identified. Moreover, a low number of metabolites was generally sufficient to achieve such accuracies which simplifies their potential clinical use.

Metabolomics, and especially metabolic profiling of liquid biopsies, had long been proven to be effective in uncovering metabolic alterations of a tumor, including its interaction with the microenvironment and total host response, across various cancer types [194]. In lung cancer, serum metabolites had been reported to distinguish benign from malignant lesions [195], and contributed to early detection of lung

cancer[196]. In high-grade serous ovarian cancer hydroxybutyric acid had been reported to be a diagnostic and prognostic metabolite associated with tumor burden and patient survival [197]. In prostate cancer metabolites improved prediction of organ confinement and the 5-year recurrence rate [198]. In breast cancer, metabolic profiling predicted cancer subtypes [199], cancer occurrence [200], distinguished between early and metastatic disease [201], and even detected the recurrence before it was clinically diagnosed [202].

In this work it was demonstrated that plasma metabolic profiles of non-metastasized vs metachronously metastasized stage II CRC patients are significantly different, suggesting that metabolic changes significantly precede clinically detectable metastasis by a long period. This indicates that in CRC, similar to breast cancer [201], the capability of a tumor to metastasize is determined by alterations which appear already at early stages. These alterations can be detected in blood plasma sample, which reflect both tumor as well as systemic host alterations which are of prognostic value.

Multiple genomics [203,204], transcriptomics [205–207] and proteomics [208,209] studies on discovery of prognostic markers in CRC patients had been performed. Here, the potential of metabolomics and plasma metabolic profiles in predicting metastasis recurrence in stage II CRC patients was assessed. LC-MS is an accurate and sensitive analytical platform for targeted and non-targeted metabolite identification [210–212]. The analysis of plasma metabolic profiles of NON vs MET stage II CRC patients from the German population-based case-control multi-central DACHS study revealed that plasma metabolic profiles distinguish NON from MET patients. In a smaller study, serum metabolites measured at GC-MS platform had shown a trend towards separation of stage II CRC patients according to disease recurrence [213]. Similarly, in breast cancer serum metabolic profiles prognosticated disease relapse in early stage breast cancer patients [201]. These findings indicate that the capability of a tumor to metastasize is determined by alterations which appear already at early stages, and that these alterations can be detected in a blood sample.

Metabolites involved in lipid metabolism constituted a major part of identified metabolic signature distinguishing NON from MET patients. Bertini I. et al. in the study of serum metabolic profiles found that altered lipid levels were associated with reduced survival of synchronously metastasized CRC patients [214]. In breast cancer, altered membrane lipid metabolism had been reported to underlie disease progression [215]. Serum metabolomic analysis of esophageal squamous cell carcinoma revealed the dysregulated metabolsim of phosphatidylcholines [216]. In this study, several phosphatidylcholines and

phosphatidylethanolamine were found to be differentially abundant in NON vs MET plasma samples. In prostate cancer, the accumulation of cholesteryl ester induced by PTEN loss and PI3K/AKT activation had been reported to underlie the prostate cancer aggressiveness [217]. Overall, this indicates that lipid alterations are common between many tumor entities.

Besides differentially abundant lipids polyethylen glycols of various chain length also constituted part of metabolic signature distinguishing NON from MET patients. In the study of Farshidfar et al. [213] the monomeric unit of these compounds (ethylene glycol) was also found to be significantly different in the serum of CRC patients compared to healthy controls. While the blood-based assays for disease monitoring and prognosis are exciting the ability to determine the source of metabolites in the blood is limited. This is owned to the fact that multiple processes in the host contribute to blood metabolic profiles, including tumor metabolism, the gut microbiota, the host response to the disease as well as various environmental factors. Therefore, to determine the causality of altered metabolic profiles the studies of these factors will be further required. However, blood metabolic profiles have the advantage that they reflect systemic changes, which may be overseen when the primary tumor alone is studied. To further prove the potential of identified metabolic signature additional retrospective or prospective studies will be required. This work had demonstrated that plasma metabolites have the ability to stratify stage II CRC patients according to their metastasis risk.

Multiple supervised classification methods exist [168]. In this work, support vector machines and decision trees classification methods were selected due to their inherent property to build a classification model with defined cut-offs. An applicable metabolic classifier to be implemented in the clinics should possess several features. In particular, it should have high and robust accuracy and consist possibly of a small number of features. As demonstrated by 10-fold cross-validation the metabolite-based classification models are robust and allow to classify NON and MET patients with accuracy of 0.75 and 0.82 for decision trees and support vector machines models, respectively.

The optimal metabolite-based decision tree classification model had an accuracy of 0.95 in metastasis prognosis and consisted of four metabolites polyethylene glycol (n=16), 1,4-D-xylobiose, and two unknown metabolites. Polyethylene glycol (n=16) was found to be decisive in splitting NON vs MET patients. In study of Farshidfar et. al. it was also increased in serum of CRC patients compared to healthy controls [213], though its nature is unknown. 1,4-D-Xylobiose is a sugar and belongs to a class of disaccharides. It is a non-digestible disaccharide and is considered to be a prebiotic, having a beneficial

effect on human health [218]. Its research is mostly in conjunction with strains from *Bifidobacterium* and *Lactobacillus* genera [219,220]. The relation of xylobiose to gut microbiota and association with NON patients hints that metabolism of gut microbiota in NON patients is less altered compared to MET patients. Overall, classification of NON vs MET patients using a decision tree consisting of four metabolites could significantly reduce time and labor power necessary to assess the results in larger trials.

For several reasons, retrospective studies, similar to the current one, are difficult to perform. Firstly, long follow-up times of at least three, more convincingly five years with information on subsequent metastasis development is a mandatory pre-requisite. Secondly, to find metabolites of prognostic value, only samples from untreated patients can be analyzed. Thirdly, liquid biopsies are not routinely stored in biobanks compared to e.g. paraffin-embedded tissues. Therefore, considering all reasons described above the availability of suitable patient cohorts is limited. However, it was possible to show that plasma metabolic profiles are significantly different between non-metastasized and metachronously metastasized stage II CRC patients. For further validation of these findings larger, independent stage II CRC patient cohorts have to be analyzed retrospectively or prospectively.

In summary, the clinical need in biomarkers stratifying stage II CRC patients according to their metastasis risk was addressed by means of plasma metabolic profiling. Most of significantly different metabolites were found in the polar metabolic fraction, which can be readily analyzed by well-established reversed phase LC-MS. Moreover, optimal metabolite-based classification model included four metabolites what simplifies its potential use in larger trials. Overall, plasma metabolites were shown to have the potential to stratify stage II CRC patients according to their risk for metachronous metastasis linked to shorter overall and metastasis-free survival.

6. OUTLOOK

PROJECT I: Elucidation of MACC1 role in CRC metabolism

This work revealed that MACC1 is a novel regulator of CRC metabolism. It exerts multiple effects on metabolic processes ranging from altered nutrient depletion to metabolite conversion as demonstrated by nutrient depletion and ^{13}C studies, respectively. Yet, relatively recent discovery of MACC1 and its involvement in multiple cellular processes prones to think that it is very probable that most of its effects might own to well-established players rather than be governed through its direct actions. Therefore, it will be of interest to investigate whether MACC1-dependent metabolic program is unique to MACC1 or is a part of a program driven by other oncogenes such as MYC, MET, AKT, KRAS and/or HIF, which are well-established oncogenes known to rewire cancer metabolism in multiple tissue types. Similarly, the relation between MACC1 and other nutrient sensors such as AMPK, mTOR and TXNIP in regulation of nutrient uptake in environment-dependent context will have to be established. To address all of this, mechanistic studies on the role of MACC1 in cancer metabolism will be required.

PROJECT II: Identification of metabolic prognostic biomarkers for metachronous metastasis formation in the plasma of stage II CRC patients

In this work, prognostic metabolites in the plasma of stage II CRC patients were identified. Plasma metabolic profiles were demonstrated to distinguish non-metastasized from metachronously metastasized stage II CRC patients. To enable translation of these findings to the clinics further retrospective or prospective cohorts have to be analyzed. In addition, the nature, source and potentially functional relation to metachronous association with metastasis have to be elucidated. It is not clear whether identified prognostic metabolites, even in the optimal model incorporating four metabolites, are derived from tumor in itself, its microenvironment or from a host response to the disease. Also the nature of polyethylene glycol (n=16) metabolite which split non-metastasized from metachronously metastasized stage II CRC patients is very provocative. To exclude the human factor and the lab culture as potential sources of bias the analysis of further patient cohorts ideally has to be performed in independent labs by independent experts.

7. REFERENCES

[1] M. Arnold, M.S. Sierra, M. Laversanne, I. Soerjomataram, A. Jemal, F. Bray, Global patterns and trends in colorectal cancer incidence and mortality, Gut. 66 (2017) 683–691. doi:10.1136/gutjnl-2015-310912.

[2] Krebsdaten: Krebs in Deutschland Darm, (2015). http://www.krebsdaten.de/Krebs/DE/Content/Krebsarten/Darmkrebs/darmkrebs_node.html.

[3] D. Gingras, R. Béliveau, Colorectal Cancer Prevention Through Dietary and Lifestyle Modifications, Cancer Microenviron. 4 (2011) 133–139. doi:10.1007/s12307-010-0060-5.

[4] M. Karanikas, A. Esebidis, Increasing incidence of colon cancer in patients <50 years old: a new entity?, Ann. Transl. Med. 4 (2016) 164. doi:10.21037/atm.2016.04.13.

[5] C.M. Johnson, C. Wei, J.E. Ensor, D.J. Smolenski, C.I. Amos, B. Levin, D.A. Berry, Meta-analyses of Colorectal Cancer Risk Factors, Cancer Causes Control. 24 (2013) 1207–1222. doi:10.1007/s10552-013-0201-5.

[6] H. Brenner, M. Kloor, C.P. Pox, Colorectal cancer, Lancet. 383 (2014) 1490–1502. doi:10.1016/S0140-6736(13)61649-9.

[7] Y. Ma, P. Zhang, F. Wang, J. Yang, Z. Liu, H. Qin, Association Between Vitamin D and Risk of Colorectal Cancer: A Systematic Review of Prospective Studies, J. Clin. Oncol. 29 (2011) 3775–3782. doi:10.1200/JCO.2011.35.7566.

[8] R. Labianca, B. Nordlinger, G.D. Beretta, S. Mosconi, M. Mandalà, a Cervantes, D. Arnold, E.G.W. Group, Early colon cancer: ESMO Clinical Practice Guidelines for diagnosis, treatment and follow-up, Ann Oncol. 24 Suppl 6 (2013) vi64-72. doi:10.1093/annonc/mdt354.

[9] E. Van Cutsem, A. Cervantes, B. Nordlinger, D. Arnold, Metastatic colorectal cancer : ESMO Clinical Practice Guidelines for diagnosis, treatment and follow-up, Ann. Oncol. 25 (2014) iii1-iii9. doi:10.1093/annonc/mdu260.

[10] Web page. http://www.webmd.com/colorectal-cancer/ss/slideshow-colorectal-cancer-overview.

[11] S.B. Edge, C.C. Compton, The American Joint Committee on Cancer: the 7th Edition of the AJCC Cancer Staging Manual and the Future of TNM, Ann. Surg. Oncol. 17 (2010) 1471–1474. doi:10.1245/s10434-010-0985-4.

[12] B. Vogelstein, E.R. Fearon, S.R. Hamilton, S.E. Kern, A.C. Preisinger, M. Leppert, A.M.M. Smits, J.L. Bos, Genetic Alterations during Colorectal-Tumor Development, N. Engl. J. Med. 319 (1988) 525–532. doi:10.1056/NEJM198809013190901.

[13] M. Bettington, N. Walker, A. Clouston, I. Brown, B. Leggett, V. Whitehall, The serrated pathway to colorectal carcinoma: current concepts and challenges, Histopathology. 62 (2013) 367–386. doi:10.1111/his.12055.

[14] R. Ward, A. Meagher, I. Tomlinson, T. O'Connor, M. Norrie, R. Wu, N. Hawkins, Microsatellite instability and the clinicopathological features of sporadic colorectal cancer, Gut. 48 (2001) 821–

829. doi:10.1136/gut.48.6.821.

[15] J.M. Cunningham, C.-Y. Kim, E.R. Christensen, D.J. Tester, Y. Parc, L.J. Burgart, K.C. Halling, S.K. McDonnell, D.J. Schaid, C. Walsh Vockley, V. Kubly, H. Nelson, V. V Michels, S.N. Thibodeau, The Frequency of Hereditary Defective Mismatch Repair in a Prospective Series of Unselected Colorectal Carcinomas, Am. J. Hum. Genet. 69 (2001) 780–790. doi:http://dx.doi.org/10.1086/323658.

[16] M. Toyota, N. Ahuja, M. Ohe-Toyota, J.G. Herman, S.B. Baylin, J.-P.J. Issa, CpG island methylator phenotype in colorectal cancer, Proc. Natl. Acad. Sci. . 96 (1999) 8681–8686. doi:10.1073/pnas.96.15.8681.

[17] W.S. Samowitz, H. Albertsen, J. Herrick, T.R. Levin, C. Sweeney, M.A. Murtaugh, R.K. Wolff, M.L. Slattery, Evaluation of a Large, Population-Based Sample Supports a CpG Island Methylator Phenotype in Colon Cancer, Gastroenterology. 129 (2005) 837–845. doi:10.1053/j.gastro.2005.06.020.

[18] A. Walther, E. Johnstone, C. Swanton, R. Midgley, I. Tomlinson, D. Kerr, Genetic prognostic and predictive markers in colorectal cancer, Nat. Rev. Cancer. 9 (2009) 489–499. doi:10.1038/nrc2645.

[19] H. Andreyev, A. Norman, D. Cunningham, J. Oates, P. Clarke, Kirsten ras mutations in patients with colorectal cancer: the multicenter “RASCAL” study, J Natl Cancer Inst. 90 (1998) 675–84.

[20] D. Santini, F. Loupakis, B. Vincenzi, I. Floriani, I. Stasi, E. Canestrari, E. Rulli, P.E. Maltese, F. Andreoni, G. Masi, F. Graziano, G.G. Baldi, L. Salvatore, A. Russo, G. Perrone, M.R. Tommasino, M. Magnani, A. Falcone, G. Tonini, A. Ruzzo, High Concordance of KRAS Status Between Primary Colorectal Tumors and Related Metastatic Sites: Implications for Clinical Practice, Oncol. . 13 (2008) 1270–1275. doi:10.1634/theoncologist.2008-0181.

[21] F.A. Sinicrope, M.R. Mahoney, H.H. Yoon, T.C. Smyrk, S.N. Thibodeau, R.M. Goldberg, G.D. Nelson, D.J. Sargent, S.R. Alberts, Analysis of Molecular Markers by Anatomic Tumor Site in Stage III Colon Carcinomas from Adjuvant Chemotherapy Trial NCCTG N0147 (Alliance), Clin. Cancer Res. 21 (2015) 5294–5304. doi:10.1158/1078-0432.CCR-15-0527.

[22] C.S. Karapetis, S. Khambata-Ford, D.J. Jonker, C.J. O’Callaghan, D. Tu, N.C. Tebbutt, R.J. Simes, H. Chalchal, J.D. Shapiro, S. Robitaille, T.J. Price, L. Shepherd, H.-J. Au, C. Langer, M.J. Moore, J.R. Zalcberg, K-ras Mutations and Benefit from Cetuximab in Advanced Colorectal Cancer, N. Engl. J. Med. 359 (2008) 1757–1765. doi:10.1056/NEJMoa0804385.

[23] R.G. Amado, M. Wolf, M. Peeters, E. Van Cutsem, S. Siena, D.J. Freeman, T. Juan, R. Sikorski, S. Suggs, R. Radinsky, S.D. Patterson, D.D. Chang, Wild-Type KRAS Is Required for Panitumumab Efficacy in Patients With Metastatic Colorectal Cancer, J. Clin. Oncol. 26 (2008) 1626–1634. doi:10.1200/JCO.2007.14.7116.

[24] W. De Roock, B. Claes, D. Bernasconi, J. De Schutter, B. Biesmans, G. Fountzilas, K.T. Kalogeras, V. Kotoula, D. Papamichael, P. Laurent-Puig, F. Penault-Llorca, P. Rougier, B. Vincenzi, D. Santini, G. Tonini, F. Cappuzzo, M. Frattini, F. Molinari, P. Saletti, S. De Dosso, M. Martini, A. Bardelli, S. Siena, A. Sartore-Bianchi, J. Tabernero, T. Macarulla, F. Di Fiore, A.O. Gangloff, F. Ciardiello, P. Pfeiffer, C. Qvortrup, T.P. Hansen, E. Van Cutsem, H. Piessevaux, D. Lambrechts, M. Delorenzi, S. Tejpar, Effects of KRAS, BRAF, NRAS, and PIK3CA mutations on the efficacy of cetuximab plus chemotherapy in chemotherapy-refractory metastatic colorectal cancer: a retrospective

consortium analysis, Lancet Oncol. 11 (2010) 753–762. doi:http://dx.doi.org/10.1016/S1470-2045(10)70130-3.

[25] J.-Y. Douillard, K.S. Oliner, S. Siena, J. Tabernero, R. Burkes, M. Barugel, Y. Humblet, G. Bodoky, D. Cunningham, J. Jassem, F. Rivera, I. Kocákova, P. Ruff, M. Błasińska-Morawiec, M. Šmakal, J.L. Canon, M. Rother, R. Williams, A. Rong, J. Wiezorek, R. Sidhu, S.D. Patterson, Panitumumab–FOLFOX4 Treatment and RAS Mutations in Colorectal Cancer, N. Engl. J. Med. 369 (2013) 1023–1034. doi:10.1056/NEJMoa1305275.

[26] H. Rajagopalan, A. Bardelli, C. Lengauer, K.W. Kinzler, B. Vogelstein, V.E. Velculescu, Tumorigenesis: RAF/RAS oncogenes and mismatch-repair status, Nature. 418 (2002) 934. http://dx.doi.org/10.1038/418934a.

[27] T.S. Maughan, R.A. Adams, C.G. Smith, A.M. Meade, M.T. Seymour, R.H. Wilson, S. Idziaszczyk, R. Harris, D. Fisher, S.L. Kenny, E. Kay, J.K. Mitchell, A. Madi, B. Jasani, M.D. James, J. Bridgewater, M.J. Kennedy, B. Claes, D. Lambrechts, R. Kaplan, J.P. Cheadle, Addition of cetuximab to oxaliplatin-based first-line combination chemotherapy for treatment of advanced colorectal cancer: results of the randomised phase 3 MRC COIN trial, Lancet. 377 (2011) 2103–2114. doi:http://dx.doi.org/10.1016/S0140-6736(11)60613-2.

[28] A.F. Sobrero, J. Maurel, L. Fehrenbacher, W. Scheithauer, Y.A. Abubakr, M.P. Lutz, M.E. Vega-Villegas, C. Eng, E.U. Steinhauer, J. Prausova, H.-J. Lenz, C. Borg, G. Middleton, H. Kröning, G. Luppi, O. Kisker, A. Zubel, C. Langer, J. Kopit, H.A. Burris, EPIC: Phase III Trial of Cetuximab Plus Irinotecan After Fluoropyrimidine and Oxaliplatin Failure in Patients With Metastatic Colorectal Cancer, J. Clin. Oncol. 26 (2008) 2311–2319. doi:10.1200/JCO.2007.13.1193.

[29] K.M. Tveit, T. Guren, B. Glimelius, P. Pfeiffer, H. Sorbye, S. Pyrhonen, F. Sigurdsson, E. Kure, T. Ikdahl, E. Skovlund, T. Fokstuen, F. Hansen, E. Hofsli, E. Birkemeyer, A. Johnsson, H. Starkhammar, M.K. Yilmaz, N. Keldsen, A.B. Erdal, O. Dajani, O. Dahl, T. Christoffersen, Phase III Trial of Cetuximab With Continuous or Intermittent Fluorouracil, Leucovorin, and Oxaliplatin (Nordic FLOX) Versus FLOX Alone in First-Line Treatment of Metastatic Colorectal Cancer: The NORDIC-VII Study, J. Clin. Oncol. 30 (2012) 1755–1762. doi:10.1200/JCO.2011.38.0915.

[30] E. Van Cutsem, C.-H. Köhne, E. Hitre, J. Zaluski, C.-R. Chang Chien, A. Makhson, G. D'Haens, T. Pintér, R. Lim, G. Bodoky, J.K. Roh, G. Folprecht, P. Ruff, C. Stroh, S. Tejpar, M. Schlichting, J. Nippgen, P. Rougier, Cetuximab and Chemotherapy as Initial Treatment for Metastatic Colorectal Cancer, N. Engl. J. Med. 360 (2009) 1408–1417. doi:10.1056/NEJMoa0805019.

[31] G.A. McArthur, P.B. Chapman, C. Robert, J. Larkin, J.B. Haanen, R. Dummer, A. Ribas, D. Hogg, O. Hamid, P.A. Ascierto, C. Garbe, A. Testori, M. Maio, P. Lorigan, C. Lebbé, T. Jouary, D. Schadendorf, S.J. O'Day, J.M. Kirkwood, A.M. Eggermont, B. Dréno, J.A. Sosman, K.T. Flaherty, M. Yin, I. Caro, S. Cheng, K. Trunzer, A. Hauschild, Safety and efficacy of vemurafenib in BRAFV600E and BRAFV600K mutation-positive melanoma (BRIM-3): extended follow-up of a phase 3, randomised, open-label study, Lancet Oncol. 15 (2014) 323–332. doi:http://dx.doi.org/10.1016/S1470-2045(14)70012-9.

[32] S. Kopetz, G.J. Chang, M.J. Overman, C. Eng, D.J. Sargent, D.W. Larson, A. Grothey, J.-N. Vauthey, D.M. Nagorney, R.R. McWilliams, Improved Survival in Metastatic Colorectal Cancer Is Associated With Adoption of Hepatic Resection and Improved Chemotherapy, J. Clin. Oncol. 27 (2009) 3677–3683. doi:10.1200/JCO.2008.20.5278.

[33] R. Yaeger, A. Cercek, E.M. O\textquoterightReilly, D.L. Reidy, N. Kemeny, T. Wolinsky, M. Capanu, M.J. Gollub, N. Rosen, M.F. Berger, M.E. Lacouture, E. Vakiani, L.B. Saltz, Pilot Trial of Combined BRAF and EGFR Inhibition in BRAF-Mutant Metastatic Colorectal Cancer Patients, Clin. Cancer Res. 21 (2015) 1313–1320. doi:10.1158/1078-0432.CCR-14-2779.

[34] R.B. Corcoran, C.E. Atreya, G.S. Falchook, E.L. Kwak, D.P. Ryan, J.C. Bendell, O. Hamid, W.A. Messersmith, A. Daud, R. Kurzrock, M. Pierobon, P. Sun, E. Cunningham, S. Little, K. Orford, M. Motwani, Y. Bai, K. Patel, A.P. Venook, S. Kopetz, Combined BRAF and MEK Inhibition With Dabrafenib and Trametinib in BRAF V600–Mutant Colorectal Cancer, J. Clin. Oncol. 33 (2015) 4023–4031. doi:10.1200/JCO.2015.63.2471.

[35] A. Umar, C.R. Boland, J.P. Terdiman, S. Syngal, A. de la Chapelle, J. Rüschoff, R. Fishel, N.M. Lindor, L.J. Burgart, R. Hamelin, S.R. Hamilton, R.A. Hiatt, J. Jass, A. Lindblom, H.T. Lynch, P. Peltomaki, S.D. Ramsey, M.A. Rodriguez-Bigas, H.F.A. Vasen, E.T. Hawk, J.C. Barrett, A.N. Freedman, S. Srivastava, Revised Bethesda Guidelines for Hereditary Nonpolyposis Colorectal Cancer (Lynch Syndrome) and Microsatellite Instability, J. Natl. Cancer Inst. 96 (2004) 261–268. http://www.ncbi.nlm.nih.gov/pmc/articles/PMC2933058/.

[36] C.R. Boland, S.N. Thibodeau, S.R. Hamilton, D. Sidransky, J.R. Eshleman, R.W. Burt, S.J. Meltzer, M.A. Rodriguez-Bigas, R. Fodde, G.N. Ranzani, S. Srivastava, A National Cancer Institute Workshop on Microsatellite Instability for Cancer Detection and Familial Predisposition: Development of International Criteria for the Determination of Microsatellite Instability in Colorectal Cancer, Cancer Res. 58 (1998) 5248–5257. http://cancerres.aacrjournals.org/content/58/22/5248.

[37] A. Walther, R. Houlston, I. Tomlinson, Association between chromosomal instability and prognosis in colorectal cancer: a meta-analysis, Gut. 57 (2008) 941–950. doi:10.1136/gut.2007.135004.

[38] S. Popat, R. Hubner, R.S. Houlston, Systematic Review of Microsatellite Instability and Colorectal Cancer Prognosis, J. Clin. Oncol. 23 (2005) 609–618. doi:10.1200/JCO.2005.01.086.

[39] M. Guidoboni, R. Gafà, A. Viel, C. Doglioni, A. Russo, A. Santini, L. Del Tin, E. Macrì, G. Lanza, M. Boiocchi, R. Dolcetti, Microsatellite Instability and High Content of Activated Cytotoxic Lymphocytes Identify Colon Cancer Patients with a Favorable Prognosis, Am. J. Pathol. 159 (2001) 297–304. http://www.ncbi.nlm.nih.gov/pmc/articles/PMC1850401/.

[40] T. Ishikawa, T. Fujita, Y. Suzuki, S. Okabe, Y. Yuasa, T. Iwai, Y. Kawakami, Tumor-specific Immunological Recognition of Frameshift-mutated Peptides in Colon Cancer with Microsatellite Instability, Cancer Res. 63 (2003) 5564–5572. http://cancerres.aacrjournals.org/content/63/17/5564.

[41] K.M. Drescher, P. Sharma, P. Watson, Z. Gatalica, S.N. Thibodeau, H.T. Lynch, Lymphocyte recruitment into the tumor site is altered in patients with MSI-H colon cancer, Fam. Cancer. 8 (2009) 231–239. doi:10.1007/s10689-009-9233-0.

[42] U. Stein, W. Walther, F. Arlt, H. Schwabe, J. Smith, I. Fichtner, W. Birchmeier, P.M. Schlag, MACC1, a newly identified key regulator of HGF-MET signaling, predicts colon cancer metastasis., Nat. Med. 15 (2009) 59–67. doi:10.1038/nm.1889.

[43] Z. Wu, R. Zhou, Y. Su, L. Sun, Y. Liao, W. Liao, Prognostic Value of MACC1 in Digestive System Neoplasms: A Systematic Review and Meta-Analysis, Biomed Res. Int. 2015 (2015) 252043. doi:10.1155/2015/252043.

[44] G. Kim, J. Lee, M. Park, J. Yoon, Metastasis associated in colon cancer 1 predicts poor outcomes in patients with breast cancer, Anal Quant Cytopathol Histpathol. 37 (2015) 96–104.

[45] Z. Wang, Z. Li, C. Wu, Y. Wang, Y. Xia, L. Chen, Q. Zhu, Y. Chen, MACC1 overexpression predicts a poor prognosis for non-small cell lung cancer, Med. Oncol. 31 (2013) 790. doi:10.1007/s12032-013-0790-6.

[46] C. Hagemann, S. Fuchs, C.M. Monoranu, P. Herrmann, J. Smith, T. Hohmann, U. Grabiec, A.F. Kessler, F. Dehghani, M. Lo, R. Ernestus, G.H. Vince, U. Stein, Impact of MACC1 on human malignant glioma progression and patients' unfavorable prognosis, Neuro. Oncol. 15 (2013) 1696–1709.

[47] H. Li, H.U.I. Zhang, S. Zhao, Y.U.N. Shi, J. Yao, Y. Zhang, H. Guo, X. Liu, Overexpression of MACC1 and the association with hepatocyte growth factor/c-Met in epithelial ovarian cancer, Oncol. Lett. 9 (2015) 1989–1996. doi:10.3892/ol.2015.2984.

[48] L. Guo, W. Lu, X. Zhang, D. Luo, H. Zhang, Metastasis-associated colon cancer-1 is a novel prognostic marker for cervical cancer, Int. J. Clin. Exp. Pathol. 7 (2014) 4150–4155. http://www.ncbi.nlm.nih.gov/pmc/articles/PMC4129030/.

[49] Z. Jin, N. Xu, K. Guo, P. Xu, P. Li, Y. Zhang, X. Li, S. Zheng, C. Liu, A. Xu, P. Huang, Increased expression of metastasis-associated in colon cancer-1 in renal cell carcinoma is associated with poor prognosis, Int. J. Clin. Exp. Pathol. 8 (2015) 3857–3863. http://www.ncbi.nlm.nih.gov/pmc/articles/PMC4466956/.

[50] A. Lederer, P. Herrmann, D. Seehofer, M. Dietel, J. Pratschke, P. Schlag, U. Stein, Metastasis-associated in colon cancer 1 is an independent prognostic biomarker for survival in klatskin tumor patients, Hepatology. 62 (2015) 841–850. doi:10.1002/hep.27885.

[51] H. Hu, D. Tian, T. Chen, R. Han, Y. Sun, C. Wu, Metastasis-Associated in Colon Cancer 1 Is a Novel Survival-Related Biomarker for Human Patients with Renal Pelvis Carcinoma, PLoS One. 9 (2014) e100161. doi:10.1371/journal.pone.0100161.

[52] F. Schmid, S. Burock, K. Klockmeier, P.M. Schlag, U. Stein, SNPs in the coding region of the metastasis-inducing gene MACC1 and clinical outcome in colorectal cancer, Mol. Cancer. 11 (2012) 49. doi:10.1186/1476-4598-11-49.

[53] A.H. Lang, S. Geller-Rhomberg, T. Winder, N. Stark, K. Gasser, B. Hartmann, B. Kohler, I. Grizelj, H. Drexel, A. Muendlein, A common variant of the MACC1 gene is significantly associated with overall survival in colorectal cancer patients, BMC Cancer. 12 (2012) 20. doi:10.1186/1471-2407-12-20.

[54] A. Muendlein, M. Hubalek, S. Geller-Rhomberg, K. Gasser, T. Winder, H. Drexel, T. Decker, E. Mueller-Holzner, M. Chamson, C. Marth, A.H. Lang, Significant survival impact of MACC1 polymorphisms in HER2 positive breast cancer patients, Eur. J. Cancer. 50 (2017) 2134–2141. doi:10.1016/j.ejca.2014.05.007.

[55] U.P. Rohr, P. Hermann, K. Ilm, H. Zhang, S. Lohmann, A. Reiser, A. Muranyi, J. Smith, S. Burock, M. Osterland, Prognostic value of MACC1 and proficient mismatch repair status for recurrence risk prediction in stage II colon cancer patients: the BIOGRID studies, Ann Oncol. mdx207 (2017). doi:10.1093/annonc/mdx207.

[56] U. Nitsche, R. Rosenberg, A. Balmert, T. Schuster, J. Slotta-Huspenina, P. Herrmann, F.G. Bader, H. Friess, P.M. Schlag, U. Stein, K.-P. Janssen, Integrative Marker Analysis Allows Risk Assessment for Metastasis in Stage II Colon Cancer, Ann. Surg. 256 (2012). http://journals.lww.com/annalsofsurgery/Fulltext/2012/11000/Integrative_Marker_Analysis_Allows_Risk_Assessment.13.aspx.

[57] J. Liu, C. Pan, L. Guo, M. Wu, J. Guo, S. Peng, Q. Wu, Q. Zuo, A new mechanism of trastuzumab resistance in gastric cancer: MACC1 promotes the Warburg effect via activation of the PI3K/AKT signaling pathway, J. Hematol. Oncol. 2016 91. 9 (2016) E359–E386. doi:10.1186/S13045-016-0302-1.

[58] Z.M. Chen, H.R. Shi, X. Li, Y.X. Deng, R.T. Zhang, Downregulation of MACC1 expression enhances cisplatin sensitivity in SKOV-3/DDP cells, Genet. Mol. Res. 14 (2015) 17134–17144. doi:10.4238/2015.December.16.13.

[59] R. Zhang, H. Shi, F. Ren, X. Li, M. Zhang, W. Feng, Y. Jia, Knockdown of MACC1 expression increases cisplatin sensitivity in cisplatin-resistant epithelial ovarian cancer cells, Oncol. Rep. 35 (2016) 2466–2472. doi:10.3892/or.2016.4585.

[60] C. Shang, Y. Hong, Y. Guo, Y.H. Liu, Y.X. Xue, Influence of the MACC1 gene on sensitivity to chemotherapy in human U251 glioblastoma cells, Asian Pacific J. Cancer Prev. 16 (2015) 195–199. doi:10.7314/APJCP.2015.16.1.195.

[61] C. Wang, Z. Wen, J. Xie, Y. Zhao, L. Zhao, S. Zhang, Y. Liu, Y. Xue, M. Shi, MACC1 mediates chemotherapy sensitivity of 5-FU and cisplatin via regulating MCT1 expression in gastric cancer, Biochem. Biophys. Res. Commun. 485 (2017) 665–671. doi:https://doi.org/10.1016/j.bbrc.2017.02.096.

[62] L. Thorstensen, G.E. Lind, T. Løvig, C.B. Diep, G.I. Meling, T.O. Rognum, R.A. Lothe, Genetic and Epigenetic Changes of Components Affecting the WNT Pathway in Colorectal Carcinomas Stratified by Microsatellite Instability, Neoplasia. 7 (2005) 99–108. http://www.ncbi.nlm.nih.gov/pmc/articles/PMC1501125/.

[63] P.A.J. Muller, K.H. Vousden, Mutant p53 in cancer: New functions and therapeutic opportunities, Cancer Cell. 25 (2014) 304–317. doi:10.1016/j.ccr.2014.01.021.

[64] P.A.J. Muller, K.H. Vousden, J.C. Norman, p53 and its mutants in tumor cell migration and invasion, J. Cell Biol. 192 (2011) 209–218. doi:10.1083/jcb.201009059.

[65] A.J. Munro, S. Lain, D.P. Lane, P53 abnormalities and outcomes in colorectal cancer: a systematic review, Br J Cancer. 92 (2005) 434–444. http://dx.doi.org/10.1038/sj.bjc.6602358.

[66] A. Russo, V. Bazan, B. Iacopetta, D. Kerr, T. Soussi, N. Gebbia, The TP53 Colorectal Cancer International Collaborative Study on the Prognostic and Predictive Significance of p53 Mutation: Influence of Tumor Site, Type of Mutation, and Adjuvant Treatment, J. Clin. Oncol. 23 (2005) 7518–7528. doi:10.1200/JCO.2005.00.471.

[67] S. Popat, R.S. Houlston, A systematic review and meta-analysis of the relationship between chromosome 18q genotype, DCC status and colorectal cancer prognosis, Eur. J. Cancer. 41 (2005) 2060–2070. doi:http://dx.doi.org/10.1016/j.ejca.2005.04.039.

[68] H. Alazzouzi, P. Alhopuro, R. Salovaara, H. Sammalkorpi, H. Järvinen, J.-P. Mecklin, A. Hemminki, S.

Schwartz, L.A. Aaltonen, D. Arango, SMAD4 as a Prognostic Marker in Colorectal Cancer, Clin. Cancer Res. 11 (2005) 2606–2611. doi:10.1158/1078-0432.CCR-04-1458.

[69] L. Lin, H. Huang, W. Liao, H. Ma, J. Liu, L. Wang, N. Huang, Y. Liao, MACC1 supports human gastric cancer growth under metabolic stress by enhancing the Warburg effect., Oncogene. (2014) 1–11. doi:10.1038/onc.2014.204.

[70] Y. Li, Z. Lu, Z. Liang, D. Ji, P. Zhang, Q. Liu, X. Zheng, Y. Yao, Metastasis‐associated in colon cancer‐1 is associated with poor prognosis in hepatocellular carcinoma, partly by promoting proliferation through enhanced glucose metabolism, Mol. Med. Rep. (2015) 1–9. doi:10.3892/mmr.2015.3416.

[71] D. Ji, Z.T. Lu, Y.Q. Li, Z.Y. Liang, P.F. Zhang, C. Li, J.L. Zhang, X. Zheng, Y.M. Yao, MACC1 expression correlates with PFKFB2 and survival in hepatocellular carcinoma, Asian Pacific J. Cancer Prev. 15 (2014) 999–1003. doi:10.7314/APJCP.2014.15.2.999.

[72] J. Duan, L. Chen, M. Zhou, J. Zhang, L. Sun, N. Huang, J. Bin, Y. Liao, W. Liao, MACC1 decreases the chemosensitivity of gastric cancer cells to oxaliplatin by regulating FASN expression, Oncol. Rep. 37 (2017) 2583–2592. doi:10.3892/or.2017.5519.

[73] J. Xia, N. Huang, H. Huang, L. Sun, S. Dong, J. Su, J. Zhang, L. Wang, L. Lin, M. Shi, J. Bin, Y. Liao, N. Li, W. Liao, Voltage-gated sodium channel Nav1.7 promotes gastric cancer progression through MACC1-mediated upregulation of NHE1, Int. J. Cancer. 139 (2016) 2553–2569. doi:10.1002/ijc.30381.

[74] O. Warburg, K. Posener, E. Negelein, Über den Stoffwechsel der Carcinomzelle, Biochem Zeitschr. 152 (1924) 309–344.

[75] O.H. Warburg, K.-W.-I. für Biologie, Über den Stoffwechsel der Tumoren: , J. Springer, 1926. https://books.google.de/books?id=9K08AAAAIAAJ.

[76] P. Sonveaux, F. Végran, T. Schroeder, M.C. Wergin, J. Verrax, Z.N. Rabbani, C.J. De Saedeleer, K.M. Kennedy, C. Diepart, B.F. Jordan, M.J. Kelley, B. Gallez, M.L. Wahl, O. Feron, M.W. Dewhirst, Targeting lactate-fueled respiration selectively kills hypoxic tumor cells in mice, J. Clin. Invest. 118 (2008) 3930–3942. doi:10.1172/JCI36843.

[77] L. Yang, A. Achreja, T.-L. Yeung, L.S. Mangala, D. Jiang, C. Han, J. Baddour, J.C. Marini, J. Ni, R. Nakahara, S. Wahlig, L. Chiba, S.H. Kim, J. Morse, S. Pradeep, A.S. Nagaraja, M. Haemmerle, N. Kyunghee, M. Derichsweiler, T. Plackemeier, I. Mercado-Uribe, G. Lopez-Berestein, T. Moss, P.T. Ram, J. Liu, X. Lu, S.C. Mok, A.K. Sood, D. Nagrath, Targeting Stromal Glutamine Synthetase in Tumors Disrupts Tumor Microenvironment-Regulated Cancer Cell Growth, Cell Metab. 24 (2017) 685–700. doi:10.1016/j.cmet.2016.10.011.

[78] A.R. Diers, K.A. Broniowska, C.-F. Chang, N. Hogg, Pyruvate fuels mitochondrial respiration and proliferation of breast cancer cells: effect of monocarboxylate transporter inhibition, Biochem. J. 444 (2012) 561–571. doi:10.1042/BJ20120294.

[79] Z.T. Schug, B. Peck, D.T. Jones, Q. Zhang, S. Grosskurth, I.S. Alam, L.M. Goodwin, E. Smethurst, S. Mason, K. Blyth, L. McGarry, D. James, E. Shanks, G. Kalna, R.E. Saunders, M. Jiang, M. Howell, F. Lassailly, M.Z. Thin, B. Spencer-Dene, G. Stamp, N.J.F. van den Broek, G. Mackay, V. Bulusu, J.J. Kamphorst, S. Tardito, D. Strachan, A.L. Harris, E.O. Aboagye, S.E. Critchlow, M.J.O. Wakelam, A. Schulze, E. Gottlieb, Acetyl-CoA Synthetase 2 Promotes Acetate Utilization and Maintains Cancer

Cell Growth under Metabolic Stress, Cancer Cell. 27 (2015) 57–71. doi:10.1016/j.ccell.2014.12.002.

[80] K.M. Nieman, H.A. Kenny, C. V Penicka, A. Ladanyi, R. Buell-Gutbrod, M.R. Zillhardt, I.L. Romero, M.S. Carey, G.B. Mills, G.S. Hotamisligil, S.D. Yamada, M.E. Peter, K. Gwin, E. Lengyel, Adipocytes promote ovarian cancer metastasis and provide energy for rapid tumor growth, Nat Med. 17 (2011) 1498–1503. doi:doi.org/10.1038/nm.2492.

[81] S. Pavlides, D. Whitaker-Menezes, R. Castello-Cros, N. Flomenberg, A.K. Witkiewicz, P.G. Frank, M.C. Casimiro, C. Wang, P. Fortina, S. Addya, R.G. Pestell, U.E. Martinez-Outschoorn, F. Sotgia, M.P. Lisanti, The reverse Warburg effect: Aerobic glycolysis in cancer associated fibroblasts and the tumor stroma, Cell Cycle. 8 (2009) 3984–4001. doi:10.4161/cc.8.23.10238.

[82] U.E. Martinez-Outschoorn, M. Peiris-Pages, R.G. Pestell, F. Sotgia, M.P. Lisanti, Cancer metabolism: a therapeutic perspective, Nat Rev Clin Oncol. 14 (2017) 11–31. http://dx.doi.org/10.1038/nrclinonc.2016.60.

[83] A. Lehninger, L. Nelson, M. Cox, Lehninger Principles of Biochemistry, 6th ed., Worth Publishers, New York, 2000.

[84] J. Son, C. a Lyssiotis, H. Ying, X. Wang, S. Hua, M. Ligorio, R.M. Perera, C.R. Ferrone, E. Mullarky, N. Shyh-Chang, Y. Kang, J.B. Fleming, N. Bardeesy, J.M. Asara, M.C. Haigis, R. a DePinho, L.C. Cantley, A.C. Kimmelman, Glutamine supports pancreatic cancer growth through a KRAS-regulated metabolic pathway., Nature. 496 (2013) 101–5. doi:10.1038/nature12040.

[85] Z.E. Stine, Z.E. Walton, B.J. Altman, A.L. Hsieh, C. V Dang, MYC, Metabolism, and Cancer, Cancer Discov. 5 (2015) 1024–1039. doi:10.1158/2159-8290.CD-15-0507.

[86] M.O. Yuneva, T.W.M. Fan, T.D. Allen, R.M. Higashi, D. V. Ferraris, T. Tsukamoto, J.M. Matés, F.J. Alonso, C. Wang, Y. Seo, X. Chen, J.M. Bishop, The metabolic profile of tumors depends on both the responsible genetic lesion and tissue type, Cell Metab. 15 (2012) 157–170. doi:10.1016/j.cmet.2011.12.015.

[87] J.R. Mayers, M.G. Vander Heiden, Nature and Nurture: What Determines Tumor Metabolic Phenotypes?, Cancer Res. 77 (2017) 3131–3135. doi:10.1158/0008-5472.CAN-17-0165.

[88] M. Vander Heiden, L. Cantley, C. Thompson, Understanding the Warburg effect: The metabolic Requiremetns of cell proliferation, Science (80-.). 324 (2009) 1029–1033. doi:10.1126/science.1160809.Understanding.

[89] B. Thorens, M. Mueckler, Glucose transporters in the 21st Century, Am. J. Physiol. - Endocrinol. Metab. 298 (2010) E141–E145. doi:10.1152/ajpendo.00712.2009.

[90] M. V. Liberti, J.W. Locasale, The Warburg Effect: How Does it Benefit Cancer Cells?, Trends Biochem. Sci. 41 (2016) 211–218. doi:10.1016/j.tibs.2015.12.001.

[91] C.H. Chang, J. Qiu, D. O'Sullivan, M.D. Buck, T. Noguchi, J.D. Curtis, Q. Chen, M. Gindin, M.M. Gubin, G.J.W. Van Der Windt, E. Tonc, R.D. Schreiber, E.J. Pearce, E.L. Pearce, Metabolic Competition in the Tumor Microenvironment Is a Driver of Cancer Progression, Cell. 162 (2015) 1229–1241. doi:10.1016/j.cell.2015.08.016.

[92] A. Vazquez, J.J. Kamphorst, E.K. Markert, Z.T. Schug, S. Tardito, E. Gottlieb, Cancer metabolism at

a glance, J. Cell Sci. 129 (2016) 3367–3373. doi:10.1242/jcs.181016.

[93] M. Benej, S. Pastorekova, J. Pastorek, Carbonic Anhydrase IX: Regulation and Role in Cancer, in: S.C. Frost, R. McKenna (Eds.), Carbon. Anhydrase Mech. Regul. Links to Dis. Ind. Appl., Springer Netherlands, Dordrecht, 2014: pp. 199–219. doi:10.1007/978-94-007-7359-2_11.

[94] C. Muñoz-Pinedo, N. El Mjiyad, J.-E. Ricci, Cancer metabolism: current perspectives and future directions, Cell Death Dis. 3 (2012) e248. doi:10.1038/cddis.2011.123.

[95] I. Apostolova, F. Wedel, W. Brenner, Imaging of Tumor Metabolism Using Positron Emission Tomography (PET), in: Metab. Cancer, Springer International Publishing, 2016: pp. 177–205. doi:10.1007/978-3-319-42118-6.

[96] H. Jadvar, Prostate Cancer: PET with (18)F-FDG, (18)F- or (11)C-Acetate, and (18)F- or (11)C-Choline, J. Nucl. Med. 52 (2011) 81–89. doi:10.2967/jnumed.110.077941.

[97] R. Minamimoto, M. Senda, S. Jinnouchi, T. Terauchi, T. Inoue, Detection of prostate cancer by an FDG-PET cancer screening program: results from a Japanese nationwide survey, Asia Ocean. J. Nucl. Med. Biol. 2 (2014) 19–23. http://www.ncbi.nlm.nih.gov/pmc/articles/PMC4937707/.

[98] E.L. Rosen, W.B. Eubank, D.A. Mankoff, FDG PET, PET/CT, and Breast Cancer Imaging, RadioGraphics. 27 (2007) S215–S229. doi:10.1148/rg.27si075517.

[99] T. Yoshioka, K. Yamaguchi, K. Kubota, T. Saginoya, T. Yamazaki, T. Ido, G. Yamaura, H. Takahashi, H. Fukuda, R. Kanamaru, Evaluation of 18F-FDG PET in Patients with Advanced, Metastatic, or Recurrent Gastric Cancer , J. Nucl. Med. . 44 (2003) 690–699. http://jnm.snmjournals.org/content/44/5/690.abstract.

[100] M.M. Engelgau, K.M. Narayan, W.H. Herman, Screening for type 2 diabetes., Diabetes Care. 23 (2000) 1563–1580. doi:10.2337/diacare.23.10.1563.

[101] X. Liu, I.L. Romero, L.M. Litchfield, E. Lengyel, J.W. Locasale, Metformin Targets Central Carbon Metabolism and Reveals Mitochondrial Requirements in Human Cancers, Cell Metab. 24 (2016) 728–739. doi:10.1016/j.cmet.2016.09.005.

[102] W.W. Souba, Glutamine and cancer, Ann. Surg. 218 (1993) 715–728. doi:10.1097/00000658-199312000-00004.

[103] A.A. Cluntun, M.J. Lukey, R.A. Cerione, J.W. Locasale, Glutamine Metabolism in Cancer: Understanding the Heterogeneity, Trends in Cancer. 3 (2017) 169–180. doi:10.1016/j.trecan.2017.01.005.

[104] I. Marin-Valencia, C. Yang, T. Mashimo, S. Cho, H. Baek, X.-L. Yang, K.N. Rajagopalan, M. Maddie, V. Vemireddy, Z. Zhao, L. Cai, L. Good, B.P. Tu, K.J. Hatanpaa, B.E. Mickey, J.M. Matés, J.M. Pascual, E.A. Maher, C.R. Malloy, R.J. DeBerardinis, R.M. Bachoo, Analysis of Tumor Metabolism Reveals Mitochondrial Glucose Oxidation in Genetically Diverse Human Glioblastomas in the Mouse Brain In Vivo, Cell Metab. 15 (2012) 827–837. doi:http://dx.doi.org/10.1016/j.cmet.2012.05.001.

[105] C.T. Hensley, A.T. Wasti, R.J. DeBerardinis, Glutamine and cancer: cell biology, physiology, and clinical opportunities, J. Clin. Invest. 123 (2013) 3678–3684. doi:10.1172/JCI69600.

[106] A. Hirayama, K. Kami, M. Sugimoto, M. Sugawara, N. Toki, H. Onozuka, T. Kinoshita, N. Saito, A. Ochiai, M. Tomita, H. Esumi, T. Soga, Quantitative Metabolome Profiling of Colon and Stomach Cancer Microenvironment by Capillary Electrophoresis Time-of-Flight Mass Spectrometry, Cancer Res. 69 (2009) 4918–4925. doi:10.1158/0008-5472.CAN-08-4806.

[107] H.-S. Lai, J.-C. Lee, P.-H. Lee, S.-T. Wang, W.-J. Chen, Plasma free amino acid profile in cancer patients, Semin. Cancer Biol. 15 (2005) 267–276. doi:http://dx.doi.org/10.1016/j.semcancer.2005.04.003.

[108] H.F. Kung, K. Ploessl, D. Mankoff, L. Zhu, R. Zhou, Metabolic Imaging of Glutamine in Cancer, J. Nucl. Med. . (2017). doi:10.2967/jnumed.116.182345.

[109] R. Zhou, A.R. Pantel, S. Li, B.P. Lieberman, K. Ploessl, H. Choi, E. Blankemeyer, H. Lee, H.F. Kung, R.H. Mach, D.A. Mankoff, [18F] (2S, 4R)4-Fluoroglutamine PET Detects Glutamine Pool Size Changes in Triple-Negative Breast Cancer in Response to Glutaminase Inhibition, Cancer Res. 77 (2017) 1476 LP-1484. http://cancerres.aacrjournals.org/content/77/6/1476.abstract.

[110] M. Hassanein, M.R. Hight, J.R. Buck, M.N. Tantawy, M.L. Nickels, M.D. Hoeksema, B.K. Harris, K. Boyd, P.P. Massion, H.C. Manning, Preclinical Evaluation of 4-[18F]Fluoroglutamine PET to Assess ASCT2 Expression in Lung Cancer, Mol. Imaging Biol. 18 (2016) 18–23. doi:10.1007/s11307-015-0862-4.

[111] M.L. Schulte, M.R. Hight, G.D. Ayers, Q. Liu, Y. Shyr, M.K. Washington, H.C. Manning, Non-Invasive Glutamine PET Reflects Pharmacological Inhibition of BRAFV600E In Vivo , Mol. Imaging Biol. 19 (2017) 421–428. doi:10.1007/s11307-016-1008-z.

[112] S. Walenta, T.-V. Chau, T. Schroeder, H.-A. Lehr, L.A. Kunz-Schughart, A. Fuerst, W. Mueller-Klieser, Metabolic classification of human rectal adenocarcinomas: a novel guideline for clinical oncologists?, J. Cancer Res. Clin. Oncol. 129 (2003) 321–326. doi:10.1007/s00432-003-0450-x.

[113] T. Schroeder, H. Yuan, B.L. Viglianti, C. Peltz, S. Asopa, Z. Vujaskovic, M.W. Dewhirst, Spatial Heterogeneity and Oxygen Dependence of Glucose Consumption in R3230Ac and Fibrosarcomas of the Fischer 344 Rat, Cancer Res. 65 (2005) 5163–5171. doi:10.1158/0008-5472.CAN-04-3900.

[114] E. Allen, P. Miéville, C.M. Warren, S. Saghafinia, L. Li, M.-W. Peng, D. Hanahan, Metabolic Symbiosis Enables Adaptive Resistance to Anti-angiogenic Therapy that Is Dependent on mTOR Signaling, Cell Rep. 15 (2016) 1144–1160. doi:10.1016/j.celrep.2016.04.029.

[115] L. Pisarsky, R. Bill, E. Fagiani, S. Dimeloe, R.W. Goosen, J. Hagmann, C. Hess, G. Christofori, Targeting Metabolic Symbiosis to Overcome Resistance to Anti-angiogenic Therapy, Cell Rep. 15 (2016) 1161–1174. doi:10.1016/j.celrep.2016.04.028.

[116] S. Park, C.-Y. Chang, R. Safi, X. Liu, R. Baldi, J.S. Jasper, G.R. Anderson, T. Liu, J.C. Rathmell, M.W. Dewhirst, K.C. Wood, J.W. Locasale, D.P. McDonnell, ERR[alpha]-Regulated Lactate Metabolism Contributes to Resistance to Targeted Therapies in Breast Cancer, Cell Rep. 15 (2016) 323–335. doi:10.1016/j.celrep.2016.03.026.

[117] M. Yabu, H. Shime, H. Hara, T. Saito, M. Matsumoto, T. Seya, T. Akazawa, N. Inoue, IL-23-dependent and -independent enhancement pathways of IL-17A production by lactic acid, Int. Immunol. 23 (2011) 29–41. http://dx.doi.org/10.1093/intimm/dxq455.

[118] S. Walenta, T.S. and W. Mueller-Klieser, Lactate in Solid Malignant Tumors: Potential Basis of a

Metabolic Classification in Clinical Oncology, Curr. Med. Chem. 11 (2004) 2195–2204. doi:http://dx.doi.org/10.2174/0929867043364711.

[119] F. Hirschhaeuser, U.G.A. Sattler, W. Mueller-Klieser, Lactate: A Metabolic Key Player in Cancer, Cancer Res. 71 (2011) 6921–6925. doi:10.1158/0008-5472.CAN-11-1457.

[120] K.M. Kennedy, P.M. Scarbrough, A. Ribeiro, R. Richardson, H. Yuan, P. Sonveaux, C.D. Landon, J.-T. Chi, S. Pizzo, T. Schroeder, M.W. Dewhirst, Catabolism of Exogenous Lactate Reveals It as a Legitimate Metabolic Substrate in Breast Cancer, PLoS One. 8 (2013) e75154. https://doi.org/10.1371/journal.pone.0075154.

[121] J. Pérez-Escuredo, V.F. Van Hée, M. Sboarina, J. Falces, V.L. Payen, L. Pellerin, P. Sonveaux, Monocarboxylate transporters in the brain and in cancer, Biochim. Biophys. Acta. 1863 (2016) 2481–2497. doi:10.1016/j.bbamcr.2016.03.013.

[122] D.Y. Gui, L.B. Sullivan, A. Luengo, A.M. Hosios, L.N. Bush, N. Gitego, S.M. Davidson, E. Freinkman, C.J. Thomas, M.G. Vander Heiden, Environment Dictates Dependence on Mitochondrial Complex I for NAD+ and Aspartate Production and Determines Cancer Cell Sensitivity to Metformin, Cell Metab. 24 (2016) 716–727. doi:http://dx.doi.org/10.1016/j.cmet.2016.09.006.

[123] C.S. Hong, N.A. Graham, W. Gu, C. Espindola Camacho, V. Mah, E.L. Maresh, M. Alavi, L. Bagryanova, P.A.L. Krotee, B.K. Gardner, I.S. Behbahan, S. Horvath, D. Chia, I.K. Mellinghoff, S.A. Hurvitz, S.M. Dubinett, S.E. Critchlow, S.K. Kurdistani, L. Goodglick, D. Braas, T.G. Graeber, H.R. Christofk, MCT1 Modulates Cancer Cell Pyruvate Export and Growth of Tumors that Co-express MCT1 and MCT4, Cell Rep. 14 (2016) 1590–1601. doi:10.1016/j.celrep.2016.01.057.

[124] L.K. Boroughs, R.J. DeBerardinis, Metabolic pathways promoting cancer cell survival and growth, Nat. Cell Biol. 17 (2015) 351–359. doi:10.1038/ncb3124.

[125] Y.-A. Wen, X. Xing, J.W. Harris, Y.Y. Zaytseva, M.I. Mitov, D.L. Napier, H.L. Weiss, B. Mark Evers, T. Gao, Adipocytes activate mitochondrial fatty acid oxidation and autophagy to promote tumor growth in colon cancer, Cell Death Dis. 8 (2017) e2593. doi:10.1038/cddis.2017.21.

[126] J.D. Rabinowitz, E. White, Autophagy and Metabolism, Science (80-.). 330 (2010) 1344 LP-1348. http://science.sciencemag.org/content/330/6009/1344.abstract.

[127] M.T. Abreu, R.M. Peek, Gastrointestinal Malignancy and the Microbiome, Gastroenterology. 146 (2014) 1534–1546.e3. doi:10.1053/j.gastro.2014.01.001.

[128] J.C. Clemente, L.K. Ursell, L.W. Parfrey, R. Knight, The Impact of the Gut Microbiota on Human Health: An Integrative View, Cell. 148 (2012) 1258–1270. doi:10.1016/j.cell.2012.01.035.

[129] S.A. Comerford, Z. Huang, X. Du, Y. Wang, L. Cai, A.K. Witkiewicz, H. Walters, M.N. Tantawy, A. Fu, H.C. Manning, J.D. Horton, R.E. Hammer, S.L. McKnight, B.P. Tu, Acetate Dependence of Tumors, Cell. 159 (2014) 1591–1602. doi:http://dx.doi.org/10.1016/j.cell.2014.11.020.

[130] T. Mashimo, K. Pichumani, V. Vemireddy, K.J. Hatanpaa, D.K. Singh, S. Sirasanagandla, S. Nannepaga, S.G. Piccirillo, Z. Kovacs, C. Foong, Z. Huang, S. Barnett, B.E. Mickey, R.J. DeBerardinis, B.P. Tu, E.A. Maher, R.M. Bachoo, Acetate is a Bioenergetic Substrate for Human Glioblastoma and Brain Metastases, Cell. 159 (2014) 1603–1614. doi:10.1016/j.cell.2014.11.025.

[131] I. Grassi, C. Nanni, V. Allegri, J.J. Morigi, G.C. Montini, P. Castellucci, S. Fanti, The clinical use of

PET with (11)C-acetate, Am. J. Nucl. Med. Mol. Imaging. 2 (2012) 33–47. https://www.ncbi.nlm.nih.gov/pmc/articles/PMC3478117/.

[132] Z. Nie, G. Hu, G. Wei, K. Cui, A. Yamane, W. Resch, R. Wang, D.R. Green, L. Tessarollo, R. Casellas, K. Zhao, D. Levens, c-Myc is a universal amplifier of expressed genes in lymphocytes and embryonic stem cells, Cell. 151 (2012) 68–79. doi:10.1016/j.cell.2012.08.033.

[133] J. van Riggelen, A. Yetil, D.W. Felsher, MYC as a regulator of ribosome biogenesis and protein synthesis, Nat Rev Cancer. 10 (2010) 301–309. http://dx.doi.org/10.1038/nrc2819.

[134] D.R. Wise, R.J. DeBerardinis, A. Mancuso, N. Sayed, X.-Y. Zhang, H.K. Pfeiffer, I. Nissim, E. Daikhin, M. Yudkoff, S.B. McMahon, C.B. Thompson, Myc regulates a transcriptional program that stimulates mitochondrial glutaminolysis and leads to glutamine addiction, Proc. Natl. Acad. Sci. . 105 (2008) 18782–18787. doi:10.1073/pnas.0810199105.

[135] P. Gao, I. Tchernyshyov, T.-C. Chang, Y.-S. Lee, K. Kita, T. Ochi, K.I. Zeller, A.M. De Marzo, J.E. Van Eyk, J.T. Mendell, C. V Dang, c-Myc suppression of miR-23a/b enhances mitochondrial glutaminase expression and glutamine metabolism, Nature. 458 (2009) 762–765. http://dx.doi.org/10.1038/nature07823.

[136] F. Morrish, J. Noonan, C. Perez-Olsen, P.R. Gafken, M. Fitzgibbon, J. Kelleher, M. VanGilst, D. Hockenbery, Myc-dependent Mitochondrial Generation of Acetyl-CoA Contributes to Fatty Acid Biosynthesis and Histone Acetylation during Cell Cycle Entry, J. Biol. Chem. . 285 (2010) 36267–36274. doi:10.1074/jbc.M110.141606.

[137] S. Mannava, V. Grachtchouk, L.J. Wheeler, M. Im, D. Zhuang, E.G. Slavina, C.K. Mathews, D.S. Shewach, M.A. Nikiforov, Direct role of nucleotide metabolism in C-MYC-dependent proliferation of melanoma cells, Cell Cycle. 7 (2008) 2392–2400. doi:10.4161/cc.6390.

[138] J.R. Doherty, C. Yang, K.E.N. Scott, M.D. Cameron, M. Fallahi, W. Li, M.A. Hall, A.L. Amelio, J.K. Mishra, F. Li, M. Tortosa, H.M. Genau, R.J. Rounbehler, Y. Lu, C. V Dang, K.G. Kumar, A.A. Butler, T.D. Bannister, A.T. Hooper, K. Unsal-Kacmaz, W.R. Roush, J.L. Cleveland, Blocking Lactate Export by Inhibiting the Myc Target MCT1 Disables Glycolysis and Glutathione Synthesis, Cancer Res. 74 (2014) 908 LP-920. http://cancerres.aacrjournals.org/content/74/3/908.abstract.

[139] B. Li, M.C. Simon, Molecular Pathways: Targeting MYC-induced Metabolic Reprogramming and Oncogenic Stress in Cancer, Clin. Cancer Res. 19 (2013) 5835 LP-5841. http://clincancerres.aacrjournals.org/content/19/21/5835.abstract.

[140] F. Li, Y. Wang, K.I. Zeller, J.J. Potter, D.R. Wonsey, K.A. O'Donnell, J. Kim, J.T. Yustein, L.A. Lee, C. V Dang, Myc Stimulates Nuclearly Encoded Mitochondrial Genes and Mitochondrial Biogenesis, Mol. Cell. Biol. . 25 (2005) 6225–6234. doi:10.1128/MCB.25.14.6225-6234.2005.

[141] C. V Dang, MYC on the Path to Cancer, Cell. 149 (2012) 22–35. doi:10.1016/j.cell.2012.03.003.

[142] K.B. Pagnano, J. Vassallo, I. Lorand-Metze, F.F. Costa, S.T. Saad, p53, Mdm2, and c-Myc overexpression is associated with a poor prognosis in aggressive non-Hodgkin's lymphomas, Am J Hematol. 67 (2001) 84–92. doi:10.1002/ajh.1084.

[143] V.L. Dengler, M. Galbraith, J.M. Espinosa, Transcriptional Regulation by Hypoxia Inducible Factors, Crit. Rev. Biochem. Mol. Biol. 49 (2014) 1–15. doi:10.3109/10409238.2013.838205.

[144] M. Ema, S. Taya, N. Yokotani, K. Sogawa, Y. Matsuda, Y. Fujii-Kuriyama, A novel bHLH-PAS factor with close sequence similarity to hypoxia-inducible factor 1α regulates the VEGF expression and is potentially involved in lung and vascular development, Proc. Natl. Acad. Sci. . 94 (1997) 4273–4278. http://www.pnas.org/content/94/9/4273.abstract.

[145] Y. Gu, S. Moran, J. Hogenesch, L. Wartman, C. Bradfield, Molecular characterization and chromosomal localization of a third alpha-class hypoxia inducible factor subunit, HIF3alpha, Gene Expr. 7 (1998) 205–13.

[146] N. V Iyer, S.W. Leung, G.L. Semenza, The Human Hypoxia-Inducible Factor 1α Gene:HIF1AStructure and Evolutionary Conservation, Genomics. 52 (1998) 159–165. doi:https://doi.org/10.1006/geno.1998.5416.

[147] H. Zhang, P. Gao, R. Fukuda, G. Kumar, B. Krishnamachary, K.I. Zeller, C.V. Dang, G.L. Semenza, HIF-1 Inhibits Mitochondrial Biogenesis and Cellular Respiration in VHL-Deficient Renal Cell Carcinoma by Repression of C-MYC Activity, Cancer Cell. 11 (2007) 407–420. doi:http://dx.doi.org/10.1016/j.ccr.2007.04.001.

[148] C.M. Metallo, P. a. Gameiro, E.L. Bell, K.R. Mattaini, J. Yang, K. Hiller, C.M. Jewell, Z.R. Johnson, D.J. Irvine, L. Guarente, J.K. Kelleher, M.G. Vander Heiden, O. Iliopoulos, G. Stephanopoulos, Reductive glutamine metabolism by IDH1 mediates lipogenesis under hypoxia, Nature. 481 (2011) 380–384. doi:10.1038/nature10602.

[149] C.-J. Hu, L.-Y. Wang, L.A. Chodosh, B. Keith, M.C. Simon, Differential Roles of Hypoxia-Inducible Factor 1α (HIF-1α) and HIF-2α in Hypoxic Gene Regulation, Mol. Cell. Biol. . 23 (2003) 9361–9374. doi:10.1128/MCB.23.24.9361-9374.2003.

[150] Y. Makino, R. Cao, K. Svensson, G. Bertilsson, M. Asman, H. Tanaka, Y. Cao, A. Berkenstam, L. Poellinger, Inhibitory PAS domain protein is a negative regulator of hypoxia-inducible gene expression, Nature. 414 (2001) 550–554. http://dx.doi.org/10.1038/35107085.

[151] G.L. Semenza, HIF-1 mediates metabolic responses to intratumoral hypoxia and oncogenic mutations, J. Clin. Invest. 123 (2013) 3664–3671. doi:10.1172/JCI67230.

[152] T. Velasco-Hernandez, A. Hyrenius-Wittsten, M. Rehn, D. Bryder, J. Cammenga, HIF-1α can act as a tumor suppressor gene in murine acute myeloid leukemia, Blood. 124 (2014) 3597 LP-3607. http://www.bloodjournal.org/content/124/24/3597.abstract.

[153] B. Chiavarina, D. Whitaker-Menezes, G. Migneco, U.E. Martinez-Outschoorn, S. Pavlides, A. Howell, H.B. Tanowitz, M.C. Casimiro, C. Wang, R.G. Pestell, P. Grieshaber, J. Caro, F. Sotgia, M.P. Lisanti, HIF1-alpha functions as a tumor promoter in cancer-associated fibroblasts, and as a tumor suppressor in breast cancer cells, Cell Cycle. 9 (2010) 3534–3551. doi:10.4161/cc.9.17.12908.

[154] H. Radhakrishnan, K. Ilm, W. Walther, S. Shirasawa, T. Sasazuki, P.T. Daniel, B. Gillissen, U. Stein, MACC1 regulates Fas mediated apoptosis through STAT1/3 – Mcl-1 signaling in solid cancers, Cancer Lett. 403 (2017) 231–245. doi:https://doi.org/10.1016/j.canlet.2017.06.020.

[155] A. Pichorner, U. Sack, D. Kobelt, I. Kelch, F. Arlt, J. Smith, W. Walther, P.M. Schlag, U. Stein, In vivo imaging of colorectal cancer growth and metastasis by targeting MACC1 with shRNA in xenografted mice, Clin. Exp. Metastasis. 29 (2012) 573–583. doi:10.1007/s10585-012-9472-6.

[156] M. Juneja, K. Ilm, P.M. Schlag, U. Stein, Promoter identification and transcriptional regulation of

the metastasis gene MACC1 in colorectal cancer, Mol. Oncol. 7 (2013) 929–943. doi:10.1016/j.molonc.2013.05.003.

[157] Agilent Seahorse XF Cell Mito Stress Test Kit User Guide. http://www.agilent.com/cs/library/usermanuals/Public/XF_Cell_Mito_Stress_Test_Kit_User_Guide.pdf.

[158] J. Lisec, N. Schauer, J. Kopka, L. Willmitzer, A.R. Fernie, Gas chromatography mass spectrometry-based metabolite profiling in plants, Nat. Protoc. 1 (2006) 387–396.

[159] C. Smith, E. Want, G. O'Maille, R. Abagyan, G. Siuzdak, XCMS: processing mass spectrometry data for metabolite profiling using nonlinear peak alignment, matching, and identification., Anal Chem. 78 (2006) 779–87.

[160] C. Kuhl, R. Tautenhahn, C. Boettcher, T. Larson, S. Neumenn, CAMERA: an integrated strategy for compound spectra extraction and annotation of liquid chromatography/mass spectrometry data sets., Anal Chem. 84 (2012) 283–9.

[161] C. Jaeger, M. Meret, C. Schmitt, J. Lisec, Compound Annotation in LC-HRMS-based Metabolomics: Robust Adduct Ion Determination as a Prerequisite to Structure Prediction in Electrospray Ionization Mass Spectra, Rapid Comminucations Mass Spectrom. (2017). doi:10.1002/rcm.7905.

[162] J. Lisec, L. Römisch-Margl, Z. Nikoloski, H.-P. Piepho, P. Giavalisco, J. Selbig, A. Gierl, L. Willmitzer, Corn hybrids display lower metabolite variability and complex metabolite inheritance patterns, Plant J. 68 (2011) 326–336. doi:10.1111/j.1365-313X.2011.04689.x.

[163] W. Stacklies, H. Redestig, M. Scholz, D. Walther, J. Selbig, pcaMethods—a bioconductor package providing PCA methods for incomplete data, Bioinformatics. 23 (2007) 1164–1167. http://dx.doi.org/10.1093/bioinformatics/btm069.

[164] R Core Team, R: A language and environment for statistical computing. R Foundation for Statistical Computing, (2017). https://www.r-project.org/.

[165] T. Therneau, B. Atkinson, B. Ripley, rpart: Recursive Partitioning and Regression Trees. R package version 4.1-11., (2017). https://cran.r-project.org/package=rpart.

[166] D. Meyer, E. Dimitriadou, K. Hornik, A. Weingessel, F. Leisch, e1071: Misc Functions of the Department of Statistics, Probability Theory Group (Formerly: E1071)., (2017). https://cran.r-project.org/package=e1071.

[167] Y. Hao, Y. Samuels, Q. Li, D. Krokowski, B.-J. Guan, C. Wang, Z. Jin, B. Dong, B. Cao, X. Feng, M. Xiang, C. Xu, S. Fink, N.J. Meropol, Y. Xu, R.A. Conlon, S. Markowitz, K.W. Kinzler, V.E. Velculescu, H. Brunengraber, J.E. Willis, T. LaFramboise, M. Hatzoglou, G.-F. Zhang, B. Vogelstein, Z. Wang, Oncogenic PIK3CA mutations reprogram glutamine metabolism in colorectal cancer., Nat. Commun. 7 (2016) 11971. doi:10.1038/ncomms11971.

[168] A.L. Tarca, V.J. Carey, X. Chen, R. Romero, S. Drăghici, Machine Learning and Its Applications to Biology, PLoS Comput. Biol. 3 (2007) e116. doi:10.1371/journal.pcbi.0030116.

[169] A. Ben-Hur, C. Soon Ong, S. Sonnenburg, B. Schoelkopf, G. Raetsch, Support Vector Machines and Kernels for Computational Biology, PLoS Comput. Biol. 4 (2008) e1000173. doi:10.1371/journal.pcbi.1000173.

[170] C. Priolo, S. Pyne, J. Rose, E.R. Regan, G. Zadra, C. Photopoulos, S. Cacciatore, D. Schultz, N. Scaglia, J. McDunn, A.M. De Marzo, M. Loda, AKT1 and MYC induce distinctive metabolic fingerprints in human prostate cancer, Cancer Res. 74 (2014) 7198–7204. doi:10.1158/0008-5472.CAN-14-1490.

[171] S. Andrzejewski, E. Klimcakova, R.M. Johnson, D.J. Papadopoli, P.M. Siegel, J. St-pierre, PGC-1 a Promotes Breast Cancer Metastasis and Confers Bioenergetic Flexibility against Metabolic Drugs, Cell Metab. 26 (2017) 1–10. doi:10.1016/j.cmet.2017.09.006.

[172] S.M. Davidson, T. Papagiannakopoulos, B.A. Olenchock, J.E. Heyman, M.A. Keibler, A. Luengo, M.R. Bauer, A.K. Jha, J.P. O'Brien, K.A. Pierce, D.Y. Gui, L.B. Sullivan, T.M. Wasylenko, L. Subbaraj, C.R. Chin, G. Stephanopolous, B.T. Mott, T. Jacks, C.B. Clish, M.G. Vander Heiden, Environment Impacts the Metabolic Dependencies of Ras-Driven Non-Small Cell Lung Cancer, Cell Metab. 23 (2016) 517–528. doi:10.1016/j.cmet.2016.01.007.

[173] I. Zaimenko, J. Lisec, U. Stein, W. Brenner, Approaches and techniques to characterize cancer metabolism in vitro and in vivo, Biochim. Biophys. Acta - Rev. Cancer. 1868 (2017) 412–419. doi:https://doi.org/10.1016/j.bbcan.2017.08.004.

[174] S. Vaulont, M. Vasseur-Cognet, A. Kahn, Glucose Regulation of Gene Transcription, J. Biol. Chem. . 275 (2000) 31555–31558. doi:10.1074/jbc.R000016200.

[175] S. Daniel, S. Zhang, A.A. DePaoli-Roach, K.-H. Kim, Dephosphorylation of Sp1 by Protein Phosphatase 1 Is Involved in the Glucose-mediated Activation of the Acetyl-CoA Carboxylase Gene, J. Biol. Chem. . 271 (1996) 14692–14697. doi:10.1074/jbc.271.25.14692.

[176] S. Daniel, K.-H. Kim, Sp1 Mediates Glucose Activation of the Acetyl-CoA Carboxylase Promoter, J. Biol. Chem. . 271 (1996) 1385–1392. doi:10.1074/jbc.271.3.1385.

[177] A. Barthel, S.T. Okino, J. Liao, K. Nakatani, J. Li, J.P. Whitlock, R.A. Roth, Regulation of GLUT1 Gene Transcription by the Serine/Threonine Kinase Akt1 , J. Biol. Chem. . 274 (1999) 20281–20286. doi:10.1074/jbc.274.29.20281.

[178] H.L. Wieman, J.A. Wofford, J.C. Rathmell, Cytokine Stimulation Promotes Glucose Uptake via Phosphatidylinositol-3 Kinase/Akt Regulation of Glut1 Activity and Trafficking, Mol. Biol. Cell . 18 (2007) 1437–1446. http://www.molbiolcell.org/content/18/4/1437.abstract.

[179] G.S. Ducker, J.D. Rabinowitz, One-Carbon Metabolism in Health and Disease, Cell Metab. 25 (2017) 27–42. doi:10.1016/j.cmet.2016.08.009.

[180] J.W. Locasale, A.R. Grassian, T. Melman, C.A. Lyssiotis, K.R. Mattaini, A.J. Bass, G. Heffron, C.M. Metallo, T. Muranen, H. Sharfi, A.T. Sasaki, D. Anastasiou, E. Mullarky, N.I. Vokes, M. Sasaki, R. Beroukhim, G. Stephanopoulos, A.H. Ligon, M. Meyerson, A.L. Richardson, L. Chin, G. Wagner, J.M. Asara, J.S. Brugge, L.C. Cantley, M.G. Vander Heiden, Phosphoglycerate dehydrogenase diverts glycolytic flux and contributes to oncogenesis, Nat Genet. 43 (2011) 869–874. http://dx.doi.org/10.1038/ng.890.

[181] J. Fan, J. Ye, J.J. Kamphorst, T. Shlomi, C.B. Thompson, J.D. Rabinowitz, Quantitative flux analysis reveals folate-dependent NADPH production, Nature. 510 (2014) 298–302. doi:doi.org/10.1038/nature13236.

[182] J. Ye, J. Fan, S. Venneti, Y.-W. Wan, B.R. Pawel, J. Zhang, L.W.S. Finley, C. Lu, T. Lindsten, J.R. Cross,

G. Qing, Z. Liu, M.C. Simon, J.D. Rabinowitz, C.B. Thompson, Serine Catabolism Regulates Mitochondrial Redox Control during Hypoxia, Cancer Discov. 4 (2014) 1406 LP-1417. http://cancerdiscovery.aacrjournals.org/content/4/12/1406.abstract.

[183] R. Possemato, K.M. Marks, Y.D. Shaul, M.E. Pacold, D. Kim, K. Birsoy, S. Sethumadhavan, H.-K. Woo, H.G. Jang, A.K. Jha, W.W. Chen, F.G. Barrett, N. Stransky, Z.-Y. Tsun, G.S. Cowley, J. Barretina, N.Y. Kalaany, P.P. Hsu, K. Ottina, A.M. Chan, B. Yuan, L.A. Garraway, D.E. Root, M. Mino-Kenudson, E.F. Brachtel, E.M. Driggers, D.M. Sabatini, Functional genomics reveal that the serine synthesis pathway is essential in breast cancer, Nature. 476 (2011) 346. http://dx.doi.org/10.1038/nature10350.

[184] M.E. Pacold, K.R. Brimacombe, S.H. Chan, J.M. Rohde, C.A. Lewis, L.J.Y.M. Swier, R. Possemato, W.W. Chen, L.B. Sullivan, B.P. Fiske, S. Cho, E. Freinkman, K. Birsoy, M. Abu-Remaileh, Y.D. Shaul, C.M. Liu, M. Zhou, M.J. Koh, H. Chung, S.M. Davidson, A. Luengo, A.Q. Wang, X. Xu, A. Yasgar, L. Liu, G. Rai, K.D. Westover, M.G. Vander Heiden, M. Shen, N.S. Gray, M.B. Boxer, D.M. Sabatini, A PHGDH inhibitor reveals coordination of serine synthesis and one-carbon unit fate, Nat. Chem. Biol. 12 (2016) 452. http://dx.doi.org/10.1038/nchembio.2070.

[185] F. Schmid, Q. Wang, M.R. Huska, M.A. Andrade-Navarro, M. Lemm, I. Fichtner, M. Dahlmann, D. Kobelt, W. Walther, J. Smith, P.M. Schlag, U. Stein, SPON2, a newly identified target gene of MACC1, drives colorectal cancer metastasis in mice and is prognostic for colorectal cancer patient survival, Oncogene. 35 (2016) 5942–5952. doi:10.1038/onc.2015.451.

[186] C. Lemos, M.S. Hardt, M. Juneja, C. Voss, S. Förster, B. Jerchow, W. Haider, H. Bläker, U. Stein, MACC1 Induces Tumor Progression in Transgenic Mice and Colorectal Cancer Patients via Increased Pluripotency Markers Nanog and Oct4, Clin. Cancer Res. 22 (2016) 2812 LP-2824. http://clincancerres.aacrjournals.org/content/22/11/2812.abstract.

[187] J. Yun, J.L. Johnson, C.L. Hanigan, J.W. Locasale, Interactions between epigenetics and metabolism in cancers, Front. Oncol. 2 (2012) 163. doi:10.3389/fonc.2012.00163.

[188] M. Sciacovelli, E. Gonçalves, T. Isaac Johnson, V. Roberto Zecchini, A.S.H. da Costa, E. Gaude, A. Vercauteren Drubbel, S. Julian Theobald, S. Abbo, M. Tran, V. Rajeeve, S. Cardaci, S. Foster, H. Yun, P. Cutillas, A. Warren, V. Gnanapragasam, E. Gottlieb, K. Franze, B. Huntly, E. Richard Maher, P. Henry Maxwell, J. Saez-Rodriguez, C. Frezza, Fumarate is an epigenetic modifier that elicits epithelial-to-mesenchymal transition, Nature. 537 (2016) 544–547. doi:10.1038/nature19353.

[189] M. Yang, P. Pollard, Succinate: a new epigenetic hacker, Cancer Cell. 23 (2013) 709–711.

[190] E.-H. Shim, C.B. Livi, D. Rakheja, J. Tan, D. Benson, V. Parekh, E.-Y. Kho, A.P. Ghosh, R. Kirkman, S. Velu, S. Dutta, B. Chenna, S.L. Rea, R.J. Mishur, Q. Li, T.L. Johnson-Pais, L. Guo, S. Bae, S. Wei, K. Block, S. Sudarshan, L-2-Hydroxyglutarate: An Epigenetic Modifier and Putative Oncometabolite in Renal Cancer, Cancer Discov. 4 (2014) 1290–1298. doi:10.1158/2159-8290.CD-13-0696.

[191] G. a Turowski, Z. Rashid, F. Hong, J. a Madri, M.D. Basson, Glutamine modulates phenotype and stimulates proliferation in human colon cancer cell lines., Cancer Res. 54 (1994) 5974–5980.

[192] S. Baek, C.M. Choi, S.H. Ahn, J.W. Lee, G. Gong, J.S. Ryu, S.J. Oh, C. Bacher-Stier, L. Fels, N. Koglin, C. Hultsch, C.A. Schatz, L.M. Dinkelborg, E.S. Mittra, S.S. Gambhir, D.H. Moon, Exploratory clinical trial of (4S)-4-(3-[18F]fluoropropyl)-L- glutamate for imaging xC- transporter using positron emission tomography in patients with non-small cell lung or breast cancer, Clin. Cancer Res. 18

(2012) 5427–5437. doi:10.1158/1078-0432.CCR-12-0214.

[193] N. Koglin, A. Mueller, M. Berndt, H. Schmitt-Willich, L. Toschi, A.W. Stephens, V. Gekeler, M. Friebe, L.M. Dinkelborg, Specific PET imaging of xC- transporter activity using a ^{18}F-labeled glutamate derivative reveals a dominant pathway in tumor metabolism., Clin. Cancer Res. 17 (2011) 6000 LP-6011. http://clincancerres.aacrjournals.org/content/17/18/6000.abstract.

[194] J.L. Spratlin, N.J. Serkova, S.G. Eckhardt, Clinical Applications of Metabolomics in Oncology: A Review, Clin. Cancer Res. 15 (2009) 431–440. http://clincancerres.aacrjournals.org/content/15/2/431.abstract.

[195] J. Fahrmann, D. Grapov, B. DeFelice, S. Taylor, K. Kim, K. et al. Kelly, Serum phosphatidylethanolamine levels distinguish benign from malignant solitary pulmonary nodules and represent a potential diagnostic biomarker for lung cancer, Cancer Biomarkers. 16 (2016) 609–617.

[196] X. Zhang, X. Zhu, C. Wang, H. Zhang, Z. Cai, Non-targeted and targeted metabolomics approaches to diagnosing lung cancer and predicting patient prognosis, Oncotarget. 7 (2016) 63437–63448. http://www.impactjournals.com/oncotarget/index.php?journal=oncotarget&amp.

[197] M. Hilvo, I. de Santiago, P. Gopalacharyulu, W.D. Schmitt, J. Budczies, M. Kuhberg, M. Dietel, T. Aittokallio, F. Markowetz, C. Denkert, J. Sehouli, C. Frezza, S. Darb-Esfahani, E.I. Braicu, Accumulated Metabolites of Hydroxybutyric Acid Serve as Diagnostic and Prognostic Biomarkers of Ovarian High-Grade Serous Carcinomas, Cancer Res. 76 (2016) 796–804. http://cancerres.aacrjournals.org/content/76/4/796.abstract.

[198] J.E. McDunn, Z. Li, K.-P. Adam, B.P. Neri, R.L. Wolfert, M. V Milburn, Y. Lotan, T.M. Wheeler, Metabolomic signatures of aggressive prostate cancer., Prostate. 73 (2013) 1547–60. doi:10.1002/pros.22704.

[199] Y. Fan, X. Zhou, T.-S. Xia, Z. Chen, J. Li, Q. Liu, R.N. Alolga, Y. Chen, M.-D. Lai, P. Li, W. Zhu, L.-W. Qi, Human plasma metabolomics for identifying differential metabolites and predicting molecular subtypes of breast cancer, Oncotarget. 7 (2016) 9925–9938. http://www.impactjournals.com/oncotarget/index.php?journal=oncotarget&amp.

[200] S. Huang, N. Chong, N.E. Lewis, W. Jia, G. Xie, L.X. Garmire, Novel personalized pathway-based metabolomics models reveal key metabolic pathways for breast cancer diagnosis, Genome Med. 8 (2016). doi:10.1186/s13073-016-0289-9.

[201] L. Tenori, C. Oakman, P.G. Morris, E. Gralka, N. Turner, Serum metabolomic profiles evaluated after surgery may identify patients with oestrogen receptor negative early breast cancer at increased risk of disease recurrence. Results from a retrospective study, Mol Oncol. 9 (2015). doi:10.1016/j.molonc.2014.07.012.

[202] V.M. Asiago, L.Z. Alvarado, N. Shanaiah, G.A.N. Gowda, K. Owusu-Sarfo, R.A. Ballas, D. Raftery, Early Detection of Recurrent Breast Cancer Using Metabolite Profiling, Cancer Res. 70 (2010) 8309–8318. http://cancerres.aacrjournals.org/content/70/21/8309.abstract.

[203] Y. Deng, L. Wang, S. Tan, G.P. Kim, R. Dou, D. Chen, Y. Cai, X. Fu, L. Wang, J. Zhu, J. Wang, KRAS as a predictor of poor prognosis and benefit from postoperative FOLFOX chemotherapy in patients with stage II and III colorectal cancer, Mol. Oncol. 9 (2015) 1341–1347.

doi:10.1016/j.molonc.2015.03.006.

[204] M. Horvat, U. Potocnik, K. Repnik, R. Kavalar, V. Zadnik, S. Potrc, B. Stabuc, Single Nucleotide Polymorphisms in Genes MACC1, RAD18, MMP7 and SDF-1a As Prognostic Factors in Resectable Colorectal Cancer, Radiol. Oncol. 51 (2017) 151–159. doi:10.1515/raon-2016-0043.

[205] T. Ozawa, T. Matsuyama, Y. Toiyama, N. Takahashi, T. Ishikawa, H. Uetake, Y. Yamada, M. Kusunoki, G. Calin, A. Goel, CCAT1 and CCAT2 long noncoding RNAs, located within the 8q.24.21 “gene desert”, serve as important prognostic biomarkers in colorectal cancer, Ann. Oncol. 28 (2017) 1882–1888. http://dx.doi.org/10.1093/annonc/mdx248.

[206] J. Miyoshi, S. Toden, K. Yoshida, Y. Toiyama, S.R. Alberts, M. Kusunoki, F.A. Sinicrope, A. Goel, MiR-139-5p as a novel serum biomarker for recurrence and metastasis in colorectal cancer, 7 (2017) 43393. http://dx.doi.org/10.1038/srep43393.

[207] P.F. Lenehan, L.A. Boardman, D. Riegert-Johnson, G. De Petris, D.W. Fry, J. Ohrnberger, E.R. Heyman, B. Gerard, A.A. Almal, W.P. Worzel, Generation and external validation of a tumor-derived 5-gene prognostic signature for recurrence of lymph node-negative, invasive colorectal carcinoma, Cancer. 118 (2012) 5234–5244. doi:10.1002/cncr.27628.

[208] S.M. Álvarez-Fernández, M. Barbariga, L. Cannizzaro, C.V. Cannistraci, L. Hurley, A. Zanardi, A. Conti, F. Sanvito, A. Innocenzi, N. Pecorelli, M. Braga, M. Alessio, Serological immune response against ADAM10 pro-domain is associated with favourable prognosis in stage III colorectal cancer patients., Oncotarget. 7 (2016). doi:10.18632/oncotarget.11181.

[209] N. Snoeren, B.L. Emmink, M.J.G. Koerkamp, S.R. van Hooff, J.A.C.M. Goos, W.J. van Houdt, M. de Wit, A.M. Prins, S.R. Piersma, T. V Pham, E.J. Belt, H. Bril, H.B. Stockmann, G.A. Meijer, R. van Hillegersberg, F.C. Holstege, C.R. Jimenez, R.J.A. Fijneman, O.W. Kranenburg, I.H.M.B. Rinkes, Maspin is a marker for early recurrence in primary stage III and IV colorectal cancer, Br. J. Cancer. 109 (2013) 1636–1647. doi:10.1038/bjc.2013.489.

[210] S. Forcisi, F. Moritz, B. Kanawati, D. Tziotis, R. Lehmann, P. Schmitt-Kopplin, Liquid chromatography-mass spectrometry in metabolomics research: Mass analyzers in ultra high pressure liquid chromatography coupling, J. Chromatogr. A. 1292 (2013) 51–65. doi:10.1016/j.chroma.2013.04.017.

[211] B. Zhou, J.F. Xiao, L. Tuli, H.W. Ressom, LC-MS-based metabolomics, Mol Biosyst. 8 (2012) 470–481. doi:10.1007/s11103-011-9767-z.Plastid.

[212] P. Yin, G. Xu, Current state-of-the-art of nontargeted metabolomics based on liquid chromatography-mass spectrometry with special emphasis in clinical applications, J. Chromatogr. A. 1374 (2014) 1–13. doi:10.1016/j.chroma.2014.11.050.

[213] F. Farshidfar, A.M. Weljie, K. a Kopciuk, R. Hilsden, S.E. McGregor, W.D. Buie, A. MacLean, H.J. Vogel, O.F. Bathe, A validated metabolomic signature for colorectal cancer: exploration of the clinical value of metabolomics, Br. J. Cancer. 115 (2016) 1–10. doi:10.1038/bjc.2016.243.

[214] I. Bertini, S. Cacciatore, B. V Jensen, J. V Schou, J.S. Johansen, M. Kruhøffer, C. Luchinat, D.L. Nielsen, P. Turano, Metabolomic NMR Fingerprinting to Identify and Predict Survival of Patients with Metastatic Colorectal Cancer, Cancer Res. . 72 (2012) 356–364. doi:10.1158/0008-5472.CAN-11-1543.

[215] M. Hilvo, C. Denkert, L. Lehtinen, B. Müller, S. Brockmöller, T. Seppänen-Laakso, J. Budczies, E. Bucher, L. Yetukuri, S. Castillo, E. Berg, H. Nygren, M. Sysi-Aho, J.L. Griffin, O. Fiehn, S. Loibl, C. Richter-Ehrenstein, C. Radke, T. Hyötyläinen, O. Kallioniemi, K. Iljin, M. Orešič, Novel Theranostic Opportunities Offered by Characterization of Altered Membrane Lipid Metabolism in Breast Cancer Progression, Cancer Res. 71 (2011) 3236–3245. doi:10.1158/0008-5472.CAN-10-3894.

[216] S.A. Mir, P. Rajagopalan, A.P. Jain, A.A. Khan, K.K. Datta, S. V. Mohan, S.S. Lateef, N. Sahasrabuddhe, B.L. Somani, T.S. Keshava Prasad, A. Chatterjee, K.V. Veerendra Kumar, M. VijayaKumar, R. V. Kumar, S. Gundimeda, A. Pandey, H. Gowda, LC–MS-based serum metabolomic analysis reveals dysregulation of phosphatidylcholines in esophageal squamous cell carcinoma, J. Proteomics. 127 (2015) 96–102. doi:10.1016/j.jprot.2015.05.013.

[217] S. Yue, J. Li, S.-Y. Lee, H.J. Lee, T. Shao, B. Song, L. Cheng, T.A. Masterson, X. Liu, T.L. Ratliff, J.-X. Cheng, Cholesteryl Ester Accumulation Induced by PTEN Loss and PI3K/AKT Activation Underlies Human Prostate Cancer Aggressiveness, Cell Metab. 19 (2017) 393–406. doi:10.1016/j.cmet.2014.01.019.

[218] C. Manisseri, M. Gudipati, Prebiotic Activity of Purified Xylobiose Obtained from Ragi (Eleusine coracana, Indaf-15) Bran, Indian J. Microbiol. 52 (2012) 251–257. doi:10.1007/s12088-011-0176-4.

[219] G.C. van Zanten, A. Knudsen, H. Röytiö, S. Forssten, M. Lawther, A. Blennow, S.J. Lahtinen, M. Jakobsen, B. Svensson, L. Jespersen, The Effect of Selected Synbiotics on Microbial Composition and Short-Chain Fatty Acid Production in a Model System of the Human Colon, PLoS One. 7 (2012) e47212. doi:10.1371/journal.pone.0047212.

[220] L.D. Lasrado, M. Gudipati, Antioxidant property of synbiotic combination of Lactobacillus sp. and wheat bran xylo-oligosaccharides, J. Food Sci. Technol. 52 (2015) 4551–4557. doi:10.1007/s13197-014-1481-9.

ACKNOWLEDGEMENTS

I thank to my PI and direct supervisor Prof. Dr. Ulrike Stein for providing me the place to work on translationally related projects and for giving me a scientific freedom to realize my ideas. With her I realized that I am able to do science independently and ready for a career as a scientist. I express my gratitude to my supervisor for her continuous support and extremely high interest in my project. This is of high value for me.

I thank especially to Dr. Jan Lisec, head of core metabolomics platform at Charité University Medicine, for his creativeness, help and of course for analyzing the metabolomics data. Most if not all the results in my second project on identification of prognostic metabolites in plasma of stage II CRC patients were provided by Dr. Lisec.

I thank to all the collaborators for their interest in my projects and their willingness to shed more insights into them by any means through pursuing a collaborative research. Thank you to all those people who supported me in my work.

I thank to all the lab members for helping me with solving questions and for that nice and friendly working environment and atmosphere, especially valuable in times when someone had to patiently listen to me. Thank you, guys.

I thank to Prof. Clemens Schmitt for organizing such a graduate school, which I believe is unique in Germany, and which enables young scientists to perform innovative independent research, thus probing the potential of every student for a future scientific career. I am pleased to be part of such school. Thank you for organizing conceptually new educational paradigm.

I thank to my parents and family who taught me not to give up and who encouraged me to achieve more. Thank you, Mom and Dad, for your pushiness and care and for all you have done for me. Especially, I am extremely grateful to my Mom, who patiently and carefully listened to my experiment's descriptions and possible reasons of failure. Thank you that you love me so much!

Finally, I express my gratitude to all those people who were benchmarks for me and from whom I have learned how to do a good science. Many thanks to everyone who made this graduation possible. From the bottom of my heart – thank you.